U.PORTO

FEUP FACULDADE DE ENGENHARIA
UNIVERSIDADE DO PORTO

State Estimation: A Digital Twin approach for an Automated Tape Laying Process

Jhonny de Sá Rodrigues

Supervisor: Professor Dr. Fernando Gomes de Almeida

Co-Supervisor: PhD Luis Miguel Pereira Pina

Doctoral Program in Mechanical Engineering
January, 2023

inegi driving science & innovation

HORIZON 2020

LAY2FORM

Faculdade de Engenharia da Universidade do Porto

State Estimation: A Digital Twin approach for an Automated Tape Laying Process

Jhonny de Sá Rodrigues

Dissertation submitted to Faculdade de Engenharia da Universidade do Porto

to obtain the degree of

Doctor of Philosophy in Mechanical Engineering

January 2023

To my wife

Abstract

State Estimation: A Digital Twin approach for an Automated Tape Laying Process

by Jhonny de Sá Rodrigues

The pursuit of enhancing the automotive industry's performance has driven the advancement of composite materials manufacturing processes that are more efficient concerning time and energy consumption. Those points aim towards an out-of-autoclave solution. A possible path to address such a requirement is using an Automated Tape Laying process with In Situ consolidation. The main advantage of Automated Tape Laying with In Situ consolidation is allowing the manufacture of a composite material-based structure on top of a mould, conforming its final or nearly final shape.

The present thesis addresses the problem of an Automated Tape Laying process with In Situ consolidation by understanding the temperature distribution along the composite material where no sensors can be placed. This limitation has been identified as the process's main challenge. This thesis also focuses on the advantages of using the core concept derived from the Industry 4.0 tendency, the Digital Twin, to understand the composite temperature distribution and the challenges it rises along its implementation, as well as the development of a state estimation strategy for addressing the consequences of using a complex and non-linear system.

For the Automated Tape Laying process, are used Digital Twin's methods to understand the heat distribution, as well as their considerations and techniques to address the challenges encountered, are reviewed. Based on the gathered information, it is proposed a 1.5 dimension mathematical model representing the process, taking advantage of the larger dimensions of the heating element when compared with the material width, allowing to simplify the energy balance calculations. Also, analytical solutions gathered from the literature are used to obtain a reliable response related to view factors. Each one of the elements from the Automated Tape Laying assembly is analysed individually and mathematically described, including its parameter's variations with temperature, to compile the process Digital Twin. Attending to the concept of the Digital Twin, the composite material had to be characterized from a thermal point of view. This characterization required the use of standard procedures and in-house developed procedures for thermal conductivity and thermal-optical characterization.

Attending to the problem of being impossible to place a sensor at the nip point of the process, a state estimation technique is a proper approach. As the Digital Twin for the Automated Tape Laying processes solves a non-linear mathematical model, a state estimation

technique is required to handle such non-linearity. Recent literature proposes using an optimization technique to lower the gap between what is being calculated and what has been measured. A meta-heuristic algorithm based on swarm population was selected, the Artificial Bee Colony algorithm. This algorithm requires fewer hyper-parameters to be defined compared to similar algorithms, and does not depend on the problem.

The approaches developed in this thesis, are validated using a real Automated Tape Laying machine, available at INEGI's laboratories. The Digital Twin approach and the posterior integration with a state estimation strategy, were tested and validated using such equipment.

Keywords: Process Digital Twin, Non-linear State Estimation, Artificial Bee Colony, Polymer Matrix Composites.

Resumo

State Estimation: A Digital Twin approach for an Automated Tape Laying Process

by Jhonny de Sá Rodrigues

A procura pela melhoria do desempenho da indústria automóvel tem impulsionado o avanço dos processos de fabrico de materiais compósitos que sejam mais eficientes em termos de tempo e consumo de energia. Isso aponta para uma solução fora da autoclave e um possível caminho para atender a essa exigência é o uso de um processo de *Automated Tape Laying* com consolidação In Situ. A principal vantagem do processo *Automated Tape Laying* com consolidação In Situ é ser possível o fabrico de uma estrutura de material compósito sobre um molde, sendo que o material é depositado com uma forma muito mais próxima da sua forma final.

A presente tese aborda o problema de um processo de *Automated Tape Laying* com consolidação In Situ, para compreender a distribuição de temperatura do material compósito onde não é possível colocar sensores, o que foi identificado como seu principal desafio. Esta tese também se concentra nas vantagens do uso do conceito central derivado da tendência da Indústria 4.0, o *Digital Twin*, e nos desafios que surgem ao longo de sua implementação, bem como no desenvolvimento de uma estratégia de estimação de estados para abordar as consequências do uso de um sistema complexo e não-linear.

Relativamente ao *Digital Twin* do processo, é realizada uma revisão aos métodos utilizados para compreender a distribuição de calor, bem como suas considerações e técnicas para abordar os desafios encontrados. Com base nas informações reunidas, é proposto um modelo matemático de 1.5 dimensões que representa o processo, aproveitando o facto de o elemento de aquecimento ser consideravelmente maior quando comparado com a largura do material, o que permite a simplificação dos cálculos de balanço de energia. Além disso, são utilizadas soluções analíticas da literatura para obter uma resposta confiável relacionada aos fatores de visão. Cada um dos elementos do conjunto de *Automated Tape Laying* é analisado individualmente e descrito matematicamente, incluindo a variação dos seus parâmetros com a alteração da temperatura, de forma a compilar o *Digital Twin* do processo. De acordo com o conceito de Digital Twin, o material compósito teve que ser caracterizado do ponto de vista térmico. Isso exigiu o uso de procedimentos padrão e procedimentos desenvolvidos internamente para caracterização da condutividade térmica e das propriedades ópticas do material.

Face ao problema da impossibilidade de colocar um sensor no *nip point* do processo, uma técnica de estimação de estados é uma abordagem adequada. Uma vez que o *Digital Twin*

para os processos de *Automated Tape Laying* resolve um modelo matemático não linear, a técnica de estimação de estados precisa lidar com essa não-linearidade. A literatura recente propõe o uso de técnicas de otimização para reduzir a diferença entre o que é calculado e o que é medido, assim, um algoritmo meta-heurístico baseado em população de enxambre foi selecionado, o algoritmo *Artificial Bee Colony*. Esse algoritmo requer que menos hiperparâmetros sejam definidos em comparação com outros algoritmos similares e não depende da complexidade do problema.

As abordagens desenvolvidas nesta tese foram validadas utilizando uma máquina de *Automated Tape Laying* real, localizada nos laboratórios do INEGI. A abordagem de *Digital Twin* e a integração posterior com a estratégia de estimação de estados foram testadas e validadas utilizando esse equipamento.

Palavras chave: *Process Digital Twin, Non-linear State Estimation, Artificial Bee Colony, Polymer Matrix Composites.*

Acknowledgements

This thesis was developed between 2018 and 2022 at INEGI - Institute of Science and Innovation in Mechanical and Industrial Engineering, which financed the entire research duration. I also acknowledge the financial support provided by Horizon 2020 from 2018 until 2021, under the scope of the European Union's Horizon 2020 research and innovation programme under grant agreement No 768710. Developing this research at INEGI allowed for my contact with the different partners involved in the LAY2FORM project, who have indirectly contributed with this thesis.

I would like to express my gratitude to the supervisors of this research, for their support, guidance and more important, for the patience to answer my questions along this time. In particular, to Professor Dr. Fernando Gomes de Almeida for giving me advices and the encouragement to develop the thesis. To Dr. Luís Miguel Pereira Pina for giving me the confidence, and the opportunity to start and pursue this journey from the beginning.

I would like to thank my friend overseas, Eng. Jose David Muñoz, Eng. Miguel Vallejo and Eng. Israel Herrara for their support along those years. Also, to my colleagues from INEGI, and particularly, the Unit of Composite Materials and Structures (UMEC). A special thanks to Fernando Silva, Tiago Rodrigues, Tiago Silva, for their support during those long days at the laboratory to figure out how to develop experimental work. Another very special thanks to the team formed by a group of colleagues and friends for their support along this journey, Paulo Teixeira, Alejandro Goldar, Pedro Fernandes, João Machado, that as PhD candidate colleagues, were always giving me strength to continue even in the most difficult times. To my former Master's degree supervisor, Dr. Joaquin Santos, for its friendship and support from the beginning, allowing me to find a path since then.

I won't let pass the friendships created along this journey to Carolina Borges, PhD candidate Beatriz Maia and Dr. Federico Danzi, that even our research topics were different, those encouragements given were valuable and appreciated, specially in difficult times while being nervous during a conference, or simply giving any advice on how to expose my topics.

A final, and warm word of gratitude goes to my supporting wife, without I could not finish this journey, to understand all those long days and nights being apart, carrying our marriage and making it even stronger. It has been a pleasure to share this journey with all of you.

Jhonny de Sá Rodrigues

Contents

List of Figures

List of Tables

List of Abbreviations

Acronyms

Acronym	Meaning
ABC	Artificial Bee Colony
ACO	Ant Colony Optimization
AS	Simulated Annealing
ATL	Automated Tape Laying
Al	Aluminium
C	Carbon
CM	Composite Material
CPS	Cyber-Physical System
DT	Digital Twin
EKF	Extended Kalman Filter
GA	Genetic Algorithm
I4.0	Industry 4.0
IT	Information Technology
KF	Kalman Filter
LAY2FORM	Layup and Forming of Metals and Composites
MPC	Model Predictive Control
NASA	National Aeronautics and Aerospace Administration
ODE	Ordinary Differential Equation
PA6	Polyamide 6
PEEK	PolyEther Ether Ketone
PSO	Particle Swarm Optimization
PTFE	Polytetrafluoroethylene
hABC	hybrid Artificial Bee Colony
q	Quartz
w	Tungsten

Symbols

Symbol	Meaning
A_i	Area of surface i
A_q	Quartz glass surface area
D_{roll}	Compaction roll diameter
E_b	Black body radiation energy
$E_{\lambda,i}$	Radiation of wavelength λ for surface i
F_{j-i}	View factor from surface j to surface i
G_i	Irradiation of element i
J_i	Radiosity of element i
L_m	Composite material thickness
L_{Mould}	Mould thickness
L_{PTFE}	Polytetrafluoroethylene thickness
Nu	Nusselt number
P_{el}	Electric power
Pr	Prandalt number
$Q_{c,n}$	Neon conductivity heat
$Q_{r,f}$	Tungsten filament radiation heat
$Q_{r,q}$	Quartz radiation heat
R_w	Tungstene electrical resistance
R_{Mould}	Mould equivalent thermal resistance
Re	Reynolds number
T_f	Tungstene filament temperature
T_m	Composite material temperature
T_n	Neon mean temperature
T_q	Quartz lamp temperature
T_r	Reflector temperature
T_w	Tungstene temperature
T_∞	Environmental temperature
T_{film}	Film temperature
U	Process velocity
U_e	Voltage
V_m	Composite material cell volume
W_m	Composite material thickness
W_r	Reflector plate width
ϵ	Material permitivity
ϵ_0	Vacuum permitivity
λ	Wavelength

Continued on next page

Symbol	Meaning
ν	Dynamic viscosity
ϕ	Volume fraction of fibres
ρ_m	Composite material density
ρ_r	Reflector material density
σ	Stefan-Boltzmann Constant
$\tau_{\lambda,i}$	Transmissivity of wavelength λ for surface i
$\varepsilon_{\lambda,i}$	Emissivity of wavelength λ for surface i
c_0	Light speed in vacuum
cp_f	Tungstene filament heat capacity
cp_m	Composite material specific heat
cp_q	Quartz glass specific heat
cp_r	Reflector specific heat
d_f	Filament diameter
d_l	Lamp diameter
d_{coil}	Filament coil diameter
g	Gravitational acceleration
h	Universal Plank constant
h_f	Internal fluid convection coefficient
h_q	Quartz envelope convection coefficient
k_b	Boltzmann constant
k_c	Thermal conductivity of matrix
k_d	Thermal conductivity of fibres
k_e	Equivalent thermal conductivity
k_m	Composite material thermal conductivity
k_m	Composite material thermal conductivity
k_n	Neon thermal conductivity
k_r	Reflector thermal conductivity
k_{Al}	Aluminium shell thermal conductivity
k_{air}	Thermal conductivity of air
k_{sil}	Rubber layer thermal conductivity
l_q	Lamp length
l_r	Tungsten filament length
m_f	Tungstene filament mass
m_q	Quartz glass envelope mass
$q''_{\mathrm{cond},m}$	Composite material conduction heat
$q''_{\mathrm{conv},m}$	Composite material convection heat
$q''_{\mathrm{rad},m}$	Composite material radiation heat
$q_{\mathrm{conv,r}}$	Reflector convection heat
$q_{\mathrm{rad,r}}$	Reflector radiation heat

Continued on next page

Symbol	Meaning
r_w	Tungstene electrical resistivity
$r_{\lambda,i}$	Reflectivity of wavelength λ for surface i
t_r	Reflector plate thickness
t_{rubber}	Rubber layer thickness
v_{output}	Output disturbance
w_{input}	Input distrubances
SN	Source Number
d	Dimension

Chapter 1

Introduction

The present chapter introduces the control problem of composite material manufacturing processes, specifically when using an Automated Tape Laying process. The relevance of defining an appropriate modelling strategy, using a Digital Twin of the process, to support a model-based control scheme is also discussed. The control scheme is focused on the manufactured structure quality.

This chapter is organized as follows: section 1.1 provides a brief overview of the project scope in which this thesis is developed and the fields of research involved, section 1.2 refers to the problem statement to be developed along this work, section 1.3 provides the scientific objectives, section 1.4 highlights contributions, and Section 1.5 gives an overall structure of the thesis.

1.1. Motivation and background

The need of the automotive industry to develop high quality structures for performance applications promoted the search for new materials. Recently, the automotive industry has identified advantages of using composite materials-based structures. The goal is to implement structural reinforcements to replace sections of non-critical structures, typically manufactured from metal, for structures manufactured using composite materials. The replacement reflects in the overall weight reduction and enhancement of mechanical properties of the vehicle structure.

This trend is made evident in a project proposed to the Horizon 2020 program and the European Union funding for Research & Innovation, named Efficient Material Hybridization by Unconventional Layup and Forming of Metals and Composites for Fabrication of Multifunctional Structures project, LAY2FORM [1]. This project proposes the design and build of a manufacturing platform to produce composite structures with embedded metal reinforcements for the automotive industry. To manufacture these structures, the project proposes the use of an Automated Tape Laying (ATL) process machine with in-situ consolidation. The ATL process is here identified as a relevant industrial composite material manufacturing process, not only due to its flexibility to work with thermoplastic-based composites but also due to its adaptability to produce structures directly on top of a mould, avoiding the use of autoclave-based processes, which requires a significant amount of time and energy.

The main difficulty of using an ATL process is replicating the manufactured structure quality compared to autoclave-based processes, where its temperature could be precisely controlled. The ATL machine then requires a suitable temperature control strategy. The goal of the control strategy is to ensure the composite material reaches the required temperature conditions at the nip point, which is the point where the heated incoming material meets the mould or the substrate and consolidates the polymeric structure. Knowing the nip point temperature also allows a detailed characterization of the composite material bonding and consolidation levels, its matrix chemical degradation, and residual stresses by using temperature-dependent models [2–6].

Knowing the nip point temperature represents a challenge for quality control due to the impossibility of placing a temperature sensor at that location. To address this problem, researchers have presented strategies based on a trial-and-error approach. They propose to adjust the process parameters to manufacture structures samples, and then, perform mechanical tests to correlate the combination of parameters with the quality of the produced sample. The results of the mechanical tests are used to fine-tune a combination of the heating power and process velocity until a set of appropriate process parameters is found and the structure satisfies defined quality requirements [7–10].

In a different approach to deal with the same challenge, some authors proposed a strategy involving the use of mathematical heating models, in 3D, 2D, and 1D configurations. The goal of those models is to predict the thermal distribution along the composite material as a function of the incident heating power and the process velocity [11–17]. Those mathematical

models have been used to analyse the problem on a steady state regime, neglecting the transient stage. On the other hand, those models assume constant thermal properties for the composite material and the machine elements, relying only on the amount of energy sent by the heating element, usually a laser beam, which affects not only the temperature distribution along the composite material but the uncertainty of the temperature estimation.

Those control strategies are conceived as an open loop approach where, as no online decision is made, then, no change in the actuation is performed to deal with material non-linearities and their variations, process conditions and disturbances. Thereby, to guarantee the quality of the composite material structure, it is relevant to close the control loop by implementing a suitable control strategy capable of handling not only the impossibility of placing a temperature sensor at the nip point, but also to be able of dealing with complex heating and transport phenomena estimations, due to non-linearities and properties variations over time.

To close the control loop for the ATL process, a model-based control seems to be an adequate strategy [18–26]. Regardless of the selected model-based control strategy, it requires developing a state estimator for the ATL process, which includes the complex heat transfer phenomena involved and the non-linear properties of the machine assembly.

This work addresses the development of an ATL process model based on the concept of Digital Twin (DT), that is a recent field of interest for industrial processes [27–30], which goal is to mathematically replicate all the involved phenomena and dynamical interactions, obtaining its digital representation. To create a DT for the ATL process involves a detailed understanding of the thermal dynamics, and heat energy transfer, for all machine assembly elements involved in the process. The developed DT is intended to represent the main process model, acting as part of a state estimation strategy. On the other hand, the state estimator requires a suitable optimization algorithm to handle not only the non-linearity of the DT but measurement uncertainties and system constraints, leading to understand the temperature dynamics at the nip point of the ATL process.

1.2. Problem Statement

Regarding the amount of available literature about ATL processes, limited research and study are available on how infrared radiation affects composite material's temperature. Similarly, information about how the thermal properties of composite materials change along a range of temperatures is scarce. In addition, due to the complex heat transfer phenomena of an ATL process, researchers have neglected the study of the interaction among the elements conforming an ATL process machine assembly, focusing on the application of a fixed amount of thermal energy over the composite material and predicting the temperature distribution in a permanent regime. This method has been applied to 3D, 2D and 1D models, without including the effect of the surroundings, which influence the overall composite material temperature and hence, the nip point temperature.

It is the scope of this research project to review and address the technical challenges

associated with creating a DT for an ATL process, leading to satisfy the control requirement of having an effective state estimation. The state estimator requires a detailed thermal characterization of the composite material and the machine assembly components, to identify how the ATL machine elements interact among themselves and with their surroundings, as well as a generalized optimization technique, based on a zero-order approach, which gives support to the state estimator for overcoming the uncertainties related to the measurements of process variables and the characterized composite material properties.

Throughout this thesis, an ATL machine located at INEGI's laboratories will be used. This machine will determine the physical constraints of the actuators and establish the spatial disposition of the elements comprising the assembly.

1.3. Scientific Objectives

With this project, the following scientific and technical aims are defined:

- The development and evaluation of a suitable modelling strategy to define a Digital Twin for a composite material manufacturing process, Automated Tape Laying, which allows predicting the temperature dynamics along the composite material.
- The development and evaluation of an optimization strategy, as support for a state estimation methodology, suitable for handling non-linear systems, constraints, and uncertainties derived from measurements and the process Digital Twin.

1.4. Contributions

Beyond the scientific objectives that have been fully achieved, the following methodological contributions are also proposed:

- A 1.5-dimensional model for an Automated Tape Laying process, based on the Digital Twin definition, capable of predicting the composite material temperature along its length.
- An optimization methodology based on the Artificial Bee Colony algorithm, resulting from the hybridization of a zero-order and a first-order methods, improving both the exploration and exploitation phases of the original Artificial Bee Colony algorithm.
- The development of a methodology for measuring and modelling the thermal conductivity of a composite material as a function of its temperature.
- The development of a methodology for measuring and modelling the general hemispherical thermal-optical properties of a composite material as function of its temperature.

1.5. Thesis Structure

This thesis is constituted by a total of six chapters. This first Chapter introduces the performed scientific work. Chapter 2 summarizes the state-of-the-art on the topics relevant to this thesis. The topics reviewed are the digitalization of the physical world as an implemen-

tation of the Industry 4.0 tendency, where its base subject is the creation of processes Digital Twins. This chapter also discusses different approaches to how researchers address and study the thermal distribution of an Automated Tape Laying process. As a fundamental parameter for estimating thermal distribution is the material thermal conductivity, this chapter also presents different approaches, both theoretical and practical, researchers have used to estimate such parameters. As the main challenge in the Automated Tape Laying process is concerning to know the temperature at the nip point, the main used estimation filters are discussed, mentioning the relevance of having a proper process model to provide information for a control or supervision system to close the control loop. This chapter also discusses different population-based optimization algorithms, that are used in highly non-linear systems.

Chapter 3 presents a detailed modelling and validation procedure for the proposed ATL process DT, based on the modelling strategies identified for each machine assembly element. The process model, assembly elements and spatial disposition, are based on the ATL machine located at INEGI's laboratories for processing thermoplastic-based composite materials, in this case Polyamide 6, with reinforced uni-directional carbon fibres. The process DT is developed using phenomenological equations and an energy balance for radiation exchange. Also, are modelled all the elements involved and their interactions. The presented DT proved to handle and replicate different dynamical responses for randomly imposed conditions. The work described in this chapter has been published on the following journal article:

- Jhonny de Sá Rodrigues, Paulo Teixeira Gonçalves, Luis Pina, and Fernando Gomes de Almeida. **Modelling the Heating Process in the Transient and Steady State of an In Situ Tape-Laying Machine Head**. *Journal of Manufacturing and Materials Processing*, 6(1):8, January 2022. ISSN 2504-4494. doi: 10.3390/jmmp6010008

and the following conference papers:

- J Rodrigues, F Silva, and J Santos. **Automated in situ consolidation process for pre-impregnated carbon fibers : a cyber physical approach**. *Materiales Compuestos*, 3(3):80–89, 2019. ISSN 2531-0739. URL `https://revista.aemac.org/`
- Jhonny de Sá Rodrigues and Paulo Teixeira. **Model for an Automated Tape Laying Process: Heat source Identification**. In *DCE21: Symposium on Mechanical Engineering: Book of Abstracts and Invited Lectures*, pages 29–31. FEUP Edições, 2021. ISBN 978-972-752-286-6
- Jhonny Rodrigues, Paulo Gonçalves, and Susana Sousa. **Composite material thermal characterization with conventonal and non-conventional tests**. In *5th Meeting of the Young Researchers of LAETA*, Lisbon, May 2022. IDMEC, Instituto Superior Técnico, Universidade de Lisboa. ISBN 978-989-53-5991-2. URL `https://5ejil.tecnico.ulisboa.pt/papers/`

Chapter 4 proposes a state estimation strategy for handling non-linear processes, that can be useful for cases when the linearization approach is not feasible or is not computationally

convenient. The algorithm uses the ATL process as a case of study, allowing to estimate the temperature of the composite material at the nip point. Section 4.3 describes the original Artificial Bee Colony optimization technique, while its modification and hybridization are presented in Section 4.4. Section 4.5 presents the materials and methods used for validating the proposed state estimation strategy and its results are presented in Section 4.6. The work described in this chapter is intended to be published on the following journal article:

- Jhonny de Sá Rodrigues, Luís Pina, and Fernando Gomes de Almeida. **State Estimation using a Hybrid Artificial Bee Colony Algorithm for an Automated Tape Laying Process**. *Applied Soft Computing Journal*, 2022. (To be submitted)

and the following conference papers:

- Jhonny Rodrigues and Paulo Teixeira Gonçalves. **Design of an Optimal Automated Tape Laying Process Using Digital Twin and Artificial Bee Colony Algorithms**. In *Composites Meet Sustainability – Proceedings of the 20th European Conference on Composite Materials, ECCM20*, volume 2, pages 44–50, Lausanne, Switzerland, July 2022. Ecole Polytechnique Fédérale de Lausanne. ISBN 978-2-9701614-0-0. doi: doi.org/10.5075/epfl-298799_978-2-9701614-0-0

- Jhonny Rodrigues and Alejandro Goldar. **Computational Use of an Artificial Bee Colony approach for Model Predictive Control**. In *41st Benelux Meetings on Systems and Control*, volume 1, pages 193–194, Brussels, July 2022. Université libre de Bruxelles. URL `https://beneluxmeeting.nl/2022/uploads/images/2022/boa_BeneluxMeeting2022_Web_betaV12_withChairs.pdf`

Chapter 5 discusses the results obtained in the previous chapters and the implications of using detailed models for control techniques based on quality control. Finally, Chapter 6 summarizes the thesis conclusions and proposes future work to be developed enabling the implementation of a suitable control strategy that takes into account constrains of the ATL process.

Along the course of this thesis, some work has been done collaborating with other researchers in the field of composite materials related to the design and optimization of structures and defects analysis at the micro-scale level, which is related to the subjects addressed in this thesis and is reflected on the following conference papers:

- Pedro Fernandes, Rui Marques, Ricardo Pinto, Pedro Mimoso, Jhonny Rodrigues, and Nuno Correia. **Design and optimization of a self-deployable composite structure**. *Materiales Compuestos*, 3(3):15–23, 2019. ISSN 2531-0739. URL `https://revista.aemag.org/`

- Paulo Gonçalves, Albertino Arteiro, Nuno Rocha, and Jhonny Rodrigues. **Numerical analysis of cure induced stress in polymeric composite materials using a**

micromechanics approach. In *5th Meeting of the Young Researchers of LAETA*, Lisbon, May 2022. IDMEC, Instituto Superior Técnico, Universidade de Lisboa. ISBN 978-989-53-5991-2. URL `https://5ejil.tecnico.ulisboa.pt/papers/`

Chapter 2

State of the Art review

The present chapter presents a state-of-the-art review on the topics addressed in this thesis. The introduction of the Digital Twin concept in industrial processes as a digital representation of the physical world, concept derived from the Cyber-Physical Systems approach, its implementation in different industrial sectors, as well as the improvements achieved. Different configurations for the Automated Tape Laying machine are also presented, and different approaches for understanding the heat flow distribution. This distribution implies to perform material thermal characterizations, allowing to predict the dynamical response for the elements involved. The use of state estimation techniques for handling linear and non-linear estimation problems is presented. This chapter also presents an introduction of population based optimization algorithms as a decision making strategy for maximization and minimization problems.

This chapter is divided into seven sections. Section 2.1, introduces the concept of Cyber-Physical Systems. Section 2.2, reviews the Digital Twin definition. Section 2.3 presents different configurations for the Automated Tape Laying machine and common used mathematical models. Section 2.4, briefly describes different techniques researchers have developed to characterize composite materials from a thermal point of view. Section 2.5 shows common state estimation strategies for linear and non-linear systems. Section 2.6 reviews population-based optimization algorithms. Section 2.7 presents the final remarks for this chapter.

2.1. Introduction

In terms of industrial manufacturing, technological advances have a relevant role by supporting the industrialization phenomena. No agreement stands on what constitutes an Industrial Revolution but, the general point of view establishes that merging existing technologies with current production processes to improve or create new manufacturing proceedings, becomes a revolution when those changes become a global tendency, in that sense and according to Vaidya et al. [30], and Liao et al. [40], three revolutions happened.

Those three revolutions took around two centuries, and they were the result of particular needs for each period to improve manufacturing processes towards mass and quality production. In what is defined as the first revolution, the introduction of water and steam-powered machines at industrial facilities seems to be the crucial factor. For the second revolution, the introduction and use of electrical-powered machines allowed a mass production approach and, the third industrial revolution happened with the introduction of electronic-based components for control systems and Information Technology (IT) [28, 30, 40, 41].

have been identified and presented in Table 2.1. Regardless the application of the CPS, the core that enables the bridge between the digital and the real world is the concept of Digital Twin.

Even though authors have not yet agreed on the milestone that marked the beginning of the fourth industrial revolution, according to Jazdi [42], the most relevant change that the majority of researchers agree with is the implementation of the Cyber-Physical Systems (CPS) concept into the production process. This concept is intended to digitally replicate a production process, to not only know its current state but, to simulate possible scenarios and apply actions that could mitigate them [43]. Being the CPS the focus of attention, its implementation represents a challenge in terms of technical and specialized knowledge [44–47]. Some of those challenges have been identified and presented in Table 2.1. Regardless of the application of the CPS, the core that enables the bridge between the digital and the real world is the concept of Digital Twin.

2.2. Digital Twin

The concept of the Digital Twin (DT) has been around for a long time but, it was put to test by the National Aeronautics and Space Administration (NASA) [54], claiming that a DT is a multi-physics and multi-scale simulation that, supported in historical data, can reproduce with high accuracy a process. As stated by Tao et al. [27] and, Tao and Zhang [55], this simulation is intended to become a digital mirror of a physical system allowing it to perform a wide range of simulations so, the main objective of the DT is to replicate the physical operation process, to be analysed, predicted and optimized using advanced mathematical techniques, during the design stage or even at the working phase, to ensure the best set of operational parameters [28, 49, 50, 52, 56–58].

The concept of DT not only includes the digital representation of an object, but also its integration with the dynamics of other objects in its surroundings [29, 59–61]. Such

Table 2.1: Challenges found when implementing the Industry 4.0 technologies [27, 30, 44, 48–53]

Challenges	Business	Knowledge	Applications
1. CPS-based manufacturing. Plant control	Service based.Short lead-time to market. Data-driven performance management systems.	Transformation in manufacturing. Digitalization of production processes	Mass customization. Big-data analytics. CPS-based human interactions. Simulated models for CPS-based manufacturing control.
2. Resilient digital manufacturing networks, collaborative control for Industry 4.0 and cyber-physical supply chains	Business and strategy models. Strategic risk management. Customized supply network control. Customized flexible process-based services.	Business process and operations in supply chains. Core competences in the supply chains. Sharing principles and operation rules.	Collaborative software solutions. Simulation software for resilient and data-driven manufacturing systems. Tools for monitoring and control of disruptions in the supply chain.
3. Cyber-Physical Systems of systems interoperability	Integration of business information. Ontology mapping and matching. Consistent enterprise-wide decision-making structure.	Interoperability and process. Shared ontology. Explicit knowledge. Knowledge management system.	Modular and reconfigurable systems. Symbolic artificial intelligence and software agents. Agent-based simulation software. Cobots and new human-machine interaction with robots.
4. Interdependent networked systems and data analytics for decision support.	New networked model of business. Artificial Intelligence and data-driven business. Risk and operations management through analytics from big-data.	Modelling of interdependencies. Dynamical analysis. Behavioural pattern identification.	Tools for monitoring and control. Building resilient systems. Perspective and predictive modelling. Risk and control.

concept, has been applied in complex systems such as cooling towers. The aim was to guarantee operational reliability, energy and resource efficiency as well as minimize the impact on health and environment [62]. This DT allowed to create a decision-making algorithm for analysis and performance prediction, monitoring the dynamic cooling tower system behaviour and calculating key performance indicators related to its operational performance. The DT allowed to lower the cooling tower water demand by 7% and the energy demand by 27%.

The DT concept has been applied not only to industrial processes, but also as virtual sensors [63] and [64], to other non-industrial areas such as vehicle handling, guarantee the activity of critical infrastructures, and for health care purposes. Table 2.2 summarizes examples of those applications.

Table 2.2: DT applications in different fields

Application	Aims	Improvements	Source
Industrial. Smart Factory	Management and resources handling. Robotics	Handle production turbulences using real-time data to optimize resources	[65–69]
Networked unmanned air vehicles	Design of an appropriate control strategy for guidance system	System stability improvement and uncertainties handling	[70]
Services. Critical infrastructure operation	Providing a constant power source for critical infrastructure such as health and defence centres	Model-based energy distribution grid which controls the power distribution to priority locals	[61, 71]
Health care and Medicine	Monitor the patient health and alert about possible occurrences and treatments	Fast and accurate response from the medical services	[72–75]

2.3. Automated Tape Laying Process

As the use of composite materials increases, the search for automated processes gains relevance for guaranteeing production standards. Those processes need to guarantee uniformity, minimize the amount of scrap material, and reduce time and energy consumption. Limitations on production by traditional means such as hand lay-up, vacuum bagging, and in-autoclave methods, tend not to be as efficient when the size and shape complexity of the structure being produced increases, motivating the search for alternative processes such as Automated Tape Laying (ATL).

This process requires a machine which is mainly composed of a heating source in order to raise the composite temperature and a compaction mechanism for mechanically ensuring the contact between the heated material and a substrate. The quality of the manufactured structure is built by ensuring that all the laid composite layers have been welded among themselves [76]. According to the works of Saenz-Castillo et al. [77], and Khan et al. [78], the main parameters that affect the quality of the final structure in ATL processes are the composite material temperature and the compaction roll pressure at the nip point, being

temperature the most critical parameter.

Reaching the necessary composite temperature ensures a good bonding condition between the structure layers [79, 80]. The exposure of the thermoplastic matrix to inadequate high temperatures may cause the degradation of the material, as mentioned in the works of Yassin and Hojjati [4], and Martín et al. [5], decreasing the structure quality. Another consequence of those high temperatures is the induction of residual thermal stresses [6, 15, 81]. On the other hand, underheating the material may cause defects associated with void formation and further structure delamination due to a bad bonding [78], turning the final structure defective and unable to meet the required performance.

As the composite material matrix has a relevant role in structural integrity, its integrity has been subject of study under the effects of heat transfer, Sonmez and Hahn [16], which reinforces the heating process as the most critical stage. To control the temperature at the nip point, authors have centred their study on the temperature distribution caused by the use of different heat sources. The most common heat sources used in ATL process, are summarized in Table 2.3.

Table 2.3: Types of heat sources for the ATL process

Heat source type	Advantages	Disadvantages	References
Hot gas	Easy to implement. Relatively high temperatures. Inexpensive.	High uncertainties with respect to the heating power delivery. High sensitivity to disturbances. Can interfere with other machine elements.	[17, 82–87]
Infra-red lamp	Easy to implement. Easy to change its state. Inexpensive.	Lower power rates compared to other sources. Relevant heat losses to surroundings.	[88–90]
Laser-beam	Capability of focusing the heating power. Easy to control delivered power.	Expensive implementation.	[9, 77, 78, 88, 91–93]

The work of Kim et al. [17], studied the effects of different process parameters of using a torch of hot gas to heat the incoming composite material. Figure 2.1 shows a general schematic of the ATL process studied.

The authors modelled the heat transfer as a two-dimensional problem, assumed anisotropy of the thermal conductivity, and the governing equation was defined as Equation 2.1 [94]. Also, the authors considered the variation of the thermal conductivity and the heat capacity as a function of the temperature.

$$\rho\, c\, U \frac{\partial T}{\partial x} = \nabla \left(\bar{K} \cdot \nabla T \right), \tag{2.1}$$

where ρ stands for the material density, c the specific heat and U the process velocity. The challenge in this work was concerning the boundary conditions. The authors assumed the

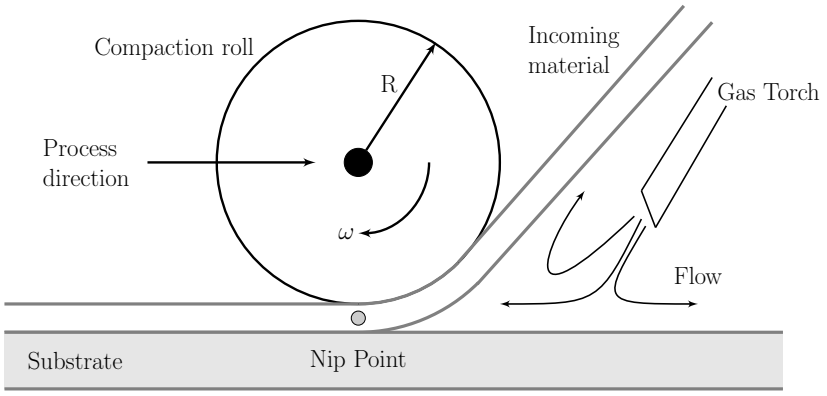

Figure 2.1: General scheme of an ATL process using a hot gas torch as main heating source.

heat-transfer coefficient value as a constant along the process for the gas torch, validating later those values with mechanical tests. On the other hand, this type of heating process is sensitive to external disturbances, requiring a controlled environmental conditions. A similar work, also using a hot air torch, was performed by Khan et al. [78], the authors defined a one-dimensional model that faced the same challenges related to the boundary conditions. Even though the main goal of this work was the study of the effects of the process parameters on void formations, the final correlation proceeds from an empirical approach.

The hot gas torch model studied by Khan et al. [86], and Pitchumani et al. [87], also established a high dependency on the convection coefficient, computed using empirical correlations, which is sensible to environmental conditions. The authors implied that for a proper estimation of the heating energy delivered, measuring the flow of the gases and the temperature of the ignition is relevant.

Another heat source for the ATL process and the most works are focused on, is laser-beams [78, 91–93]. Those heat sources have the advantage of being controllable in terms of power deliver towards a defined heating area, also in some cases, control of the emitted wavelength is possible, which simplifies calculations in terms of boundary conditions regardless the dimension of the heat equation used.

The use of a laser beam has two main approaches with respect to its use. The approach described by Chinesta et al. [13], using a laser beam for an ATL process, proposes to heat the substrate ahead of the compaction roll path. The authors used a three-dimensional model to estimate the heat distribution between a previously laid composite material layer and the newer laid layer. The goal of this approach is to generate enough heat to melt together the two composite layers as the laser beam passes through, without increasing too much the composite temperature to avoid damage. Figure 2.2a shows a general schematic of the proposed ATL strategy, where the solid blue line between the substrate layers represents the fused zone of the structure and the blue dashed line, represents the zone to be heated and fused.

The authors focused the research on how to quantify the contact resistance between layers as a function of temperature to ensure the matrix fusion. Using a trial and error approach, the

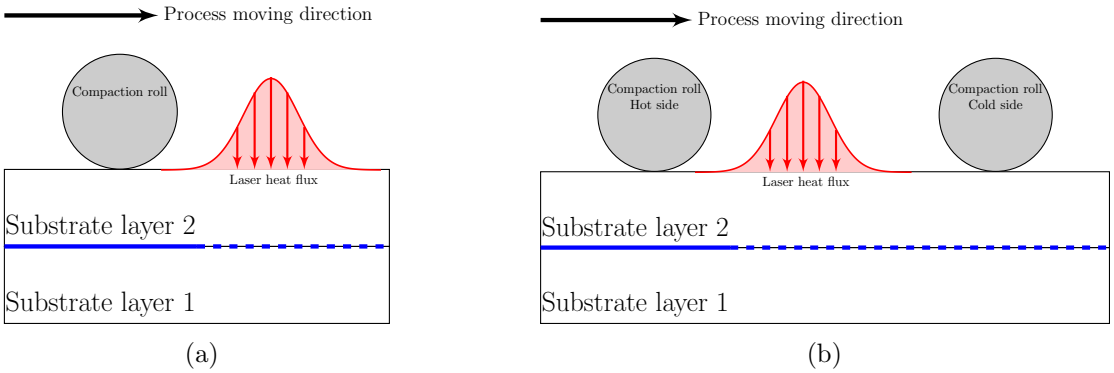

Figure 2.2: Laser-beam as heating element. **(a)** Strategy proposed by Chinesta et al. [13]. **(b)** Strategy proposed by Barasinski et al. [95].

researchers could empirically correlate the numerical simulated data, and the used parameters while producing structures, with its quality by performing mechanical delamination tests. For the numerical simulations, the authors assumed constant properties for the composite materials and for the heat losses due to convection effects. The work of Barasinski et al. [95], uses a similar approach, considering constant parameters for the composite material but, adding a second compaction roll to the cold side of the non-welded structure to improve the thermal distribution.

The other approach when using laser beams as heat sources, is to heat simultaneously the incoming composite material and the substrate, as close as possible to the nip point location, as presented in Figure 2.3, in an attempt to achieve a heat distribution that ensures the composite temperature when the incoming material enters in contact with the substrate [12, 81, 92, 96].

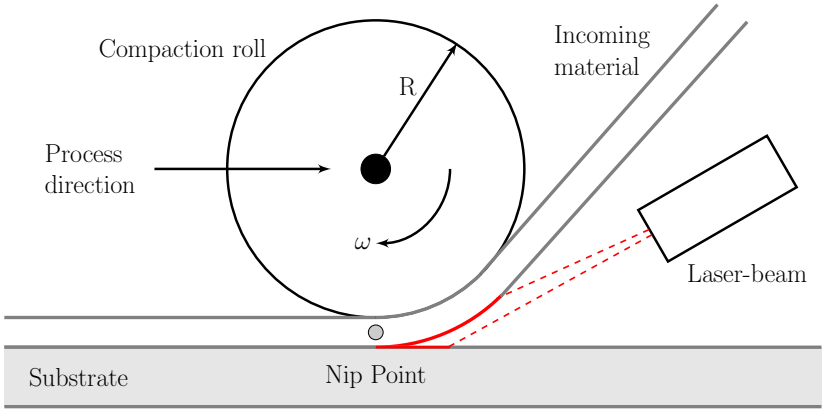

Figure 2.3: General schematic for the second laser-beam heating strategy

Another proposal for controlling the nip point temperature of the ATL process is reflected in the work of Di Francesco et al. [11], where the authors created an empirical correlation between the heater power and the process speed with the residual temperature, using a thermal camera, measured after the compaction roll. The described empirical model included the incidence angle in which the laser beam is pointed towards the zone where the incoming composite material meets the substrate, as well as a parameter defined as “The visible nip

point". This parameter intends to compensate for a shadow effect, caused by the compaction roll deformation, on the laser beam incidence upon the composite material.

The position of the heat source relative to the composite tape is one of the most relevant parameters, as presented by Stokes-Griffin et al. [91], claiming that the heating process depends on the optical reflectivity of the incident laser beam, which may reduce the absorptivity of the composite material, due to surface irregularities. The work of Stokes-Griffin and Compston [92], included those irregularities into the ATL process heat equation, by studying the impact of pointing the laser-beam towards the incoming composite material, Figure 2.4a, or towards the substrate, Figure 2.4b, with the goal of understanding how the reflections caused by the surface irregularities and, fibres alignments, affected the overall temperature.

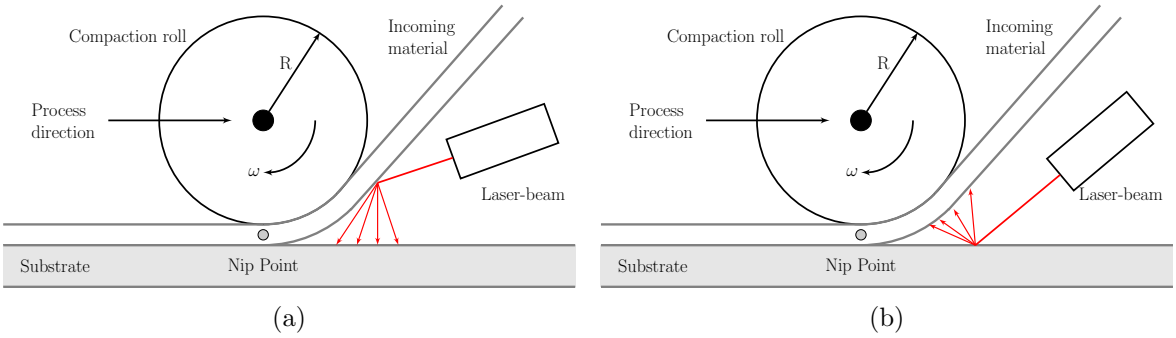

Figure 2.4: General schematic of the study of Stokes-Griffin and Compston [92]. **(a)** Laser-beam pointed towards the incoming material. **(b)** Laser-beam pointed towards the substrate.

In an attempt to control the heat distribution of the composite material in ATL process, other studies, using laser beams as heat sources, study the temperature distribution by measuring the temperature just before the nip point using thermal cameras [97], and analysing the results for several laser-beam power values. The collected data allowed to reverse engineer the mathematical model to understand the effects of the process parameters over the nip point temperature. A similar approach was used by Barakat and Tannous [3], to study the influence of the geometrical characteristics of the composite material on the overall heating process when the machine has to follow a non-straight path.

A non-related study about the manufacturing of composite materials discusses the topic of infra-red heat sources. It was carried out by [88, 98, 99]. This work series present a strategy to model a radiation heat source, using infrared lamps, for a continuous paper drying process. This work suggests that an energy balance between the process machine parts involved is relevant to understand the overall heat distribution.

2.4. Material Thermal characterization

Composite material characterization allows engineers to simulate more accurately the interaction of the material with the elements for a specifc manufacturing process. In the case of thermoplastic composites, the thermal characterization becomes relevant.

The first steps for predicting the thermal conductivity on composite materials are pre-

sented in the work of Progelhof et al. [100], where are summarized some of the most relevant theoretical approaches for predicting an equivalent the thermal conductivity, based on Equation 2.2 and Equation 2.3.

$$k_e = (1 - \phi) \cdot k_c + \phi \cdot k_d \tag{2.2}$$

$$\frac{1}{k_e} = \frac{1 - \phi}{k_c} + \frac{\phi}{k_d} \tag{2.3}$$

being k_e the equivalent thermal conductivity of the composite material, k_c the thermal conductivity of the reinforcements, k_d the thermal conductivity of the matrix and ϕ the matrix proportion that is present into the composite.

The research states that for a specific combination of fibre and matrix, there is a correlation that describes the equivalent thermal conductivity for such particular composite.

Another approach to estimate the thermal conductivity as a temperature-dependent property, was proposed by Yang [101], where using a single temperature measurement, and two well-known sources of heat, imposes a heat flux through a material and, by solving Equation 2.4, obtain a correlation between the material temperature and is thermal conductivity [94].

$$\frac{\partial}{\partial x}\left[k(T)\frac{\partial T}{\partial x}\right] = \frac{\partial T}{\partial t} \tag{2.4}$$

The work of Betta et al. [102], although not related to composite materials but applied to the food industry, proposes an approach for measuring the thermal diffusivity of several prepared types of foods, this implies its thermal conductivity, as food could be considered as a composite material. The relevance of this work is to understand the process of conservation minimizing the effects of fast, or slow, changes in temperature in quality control. The method proposed by the authors is to solve, by finite differences, Equation 2.5, using a set of three, equally separated Δx temperature sensors.

$$\frac{T_j^{p+1} - T_j^p}{\Delta t} = \alpha \cdot \frac{T_{j+1}^p - 2T_j^p + T_{j-1}^p}{(\Delta x)^2}, \tag{2.5}$$

where the term α stands for the diffusivity term, that is function of the thermal conductivity in the j direction. Equation 2.5 allows calculating the thermal conductivity as a function of the temperature u_j^p at each sampling time p.

A similar approach for determining the thermal conductivity of a thin ply of thermoplastic composite was performed by Villière et al. [103]. Where the authors created a mould to place a composite sample, in order to force the heat flux in one direction. The work used the same approach of measuring at time intervals p, in order to solve the one-dimensional Equation 2.5. One of the objectives of this work was to compare the error impact between measuring the temperature of the composite at its surface and at a point inside the ply, concluding that even there is a difference, it can be neglected.

A more detailed study of the thermal conductivity of composite materials was performed using finite elements simulations at a micro-scale level. Such is the work of Cong et al. [104], where it was developed an empirical correlation estimating the thermal conductivity of the composite material, as a function of its temperature, according to its fibre volume fraction. The method proposes an analogy with electric circuits, where using probabilistic methods, it simulates an array of connected resistors in series and parallel. The method implies that the thermal conductivity for each component of the composite material is known.

A more theoretical approach for estimating an equivalent thermal conductivity of composite materials can be found in literature, such as the M-G model Nan [105], the Fricke model Fricke [106], the H-J model Benveniste [107], among others, which takes into account not only uni-directional materials but, for woven made and for materials that use different direction combinations [108–110]. Those models also take into account added particles to the composite matrix to improve its overall thermal conductivity.

2.5. State estimation

In industrial processes is relevant to have enough information to ensure the control quality. This information is achieved by reading as many physical variables as possible. However, the measurement of those variables is not possible due to the cost it represents, the lack of availability of the required sensor or simply because the location of the variable that should be measured is physically unreachable. A strategy to deal with those restrictions has been to develop estimation strategies, which have gained industrial relevance, allowing system trajectory estimation, control, data merging and signal processing [111].

One of the most used state estimators is the Kalman Filter (KF) [112], being an optimal recursive estimator of the state of a dynamic system. It has a simple and effective formulation that has been implemented in areas such as econometric theory, as presented in the work of Blundell et al. [113], and to the control theory for aerospace applications [114].

The KF, as a model-based algorithm, has been well implemented for linear applications [115–117], this means the state equation and the observation equations are analytically defined and linear. For applications where the equation describing the system is not linear, it has been developed the Extended Kalman Filter (EKF) [117–121], where the main idea is to linearize the system, using the first-order term of a Taylor expansion to be able to implement the procedure of a linear KF.

As systems become more complex, their mathematical model also tends to become more complex, and even non-linear, which difficult the implementation of a traditional KF. The alternative, the EKF, has been object of research, to lower the computational demand while computing the solutions. The computational load of a KF has two main reasons: the number of mathematical operations to be executed at each sampling period, the nature of the operations such as sum and matrix multiplications, and the most relevant of all, the matrix inversion. Therefore, researchers have naturally tried to reduce the computing load by taking advantage of some aspects of the matrices involved like symmetries or sparsity [111, 122].

Other types of filters have been developed to handle non-linear systems, such as the Minimum Variance Estimator [123–126], the Least Square Filter [127]. Those methods, including the KF and the EKF, consider the uncertainty in the obtained data, otherwise, the computed estimates lose significance.

To avoid complex system linearization, some researchers proposed the use of Big Data based models and interactive multiple-model strategies to improve the computational performance of the state estimation process [128–130]. On the other hand, to avoid losing precision while handling highly non-linear models, researchers tend to use numerical methods to compute the system states, such is the case of the Moving Horizon Estimation algorithm [131–133]. This algorithm requires minimizing an objective function, which leads to implementing an appropriate optimization technique capable of handling not only the non-linear mathematical model but also their respective constraints [134–137].

Regardless of the selected state estimation method, the general objective is to provide enough information to a control and supervision system about the required process variable, to perform the proper control actions.

2.6. Population-based optimization

Optimization is a concept used in a wide range of applications such as economic sciences, engineering, technology and industrial sectors, due to their pursuit of minimizing input values and maximizing the outputs, frequently associated with quality [138].

Population-based algorithms have been used in the field of composite materials, like the work of Rongrong et al. [139] that used Genetic Algorithms for material orientation for maximizing a structure performance by lowering its weight. A review from [140–142], confirmed the efficiency of heuristic meta-methods such as Genetic Algorithms (GA), Simulated Annealing (AS), Particle Swarm Optimization (PSO) and Ant Colony Optimization (ACO), with respect to gradient-based methods, that in spite of having a fast convergence, require a significative high amount of simulations per iteration to compute all the required gradients per variable involved, which can be very time-consuming according to the complexity of the model [143].

Another population-based optimization algorithm is the Artificial Bee Colony (ABC). First proposed by Karaboga [144], has been the main optimization algorithm of areas from agriculture, as presented in the work of Kumar and Nagabhooshanam [145] to position and operate agricultural vehicles, to the oil industry to determine the optimal position of well placements in fracturing reservoirs as presented in the work of Nozohour-leilabady and Fazelabdolabadi [146], to improve the work-flow at shop-floor level [147–149], to route planning for a swarm of Unmanned Aerial Vehicles to avoid collisions [150].

As the original ABC algorithm depends on a random population for initialize and, explore the search domain, some authors have implemented variations to minimize the slow convergence effect caused by the randomness [151–153]. The main goal of the original ABC algorithm is to randomly explore the search domain, as a normal swarm of honeybees should

do in nature. When a honeybee finds a source of food, it communicates that information to the rest of the hive. With this information, a new swarm of honeybees goes to randomly explore the food source surroundings in search of more or a better food source. The surroundings of the ABC algorithm could be defined as constrained or unconstrained. The constraints could represent physical limitations of systems, as already implemented in the work of Vanchinathan and Selvaganesan [154], where the algorithm was included in a self tunning strategy for a fractional order Proportional Integral Derivative (PID) controller.

2.7. Concluding remarks

As production systems have increased in complexity due to the implementation of the Cyber-Physical Systems approach, using the concept of Digital Twin has proven to be advantageous by digitally represent the physical world, allowing to better understand system dynamics leading to the possibility of design better control algorithms as stated by Sztipanovits et al. [70]. Those improved control algorithms require information about all the system states, which in some complex cases those states cannot be measured directly, requiring the implementation of a state estimation strategy.

For the ATL process, the most common control strategy researchers have used, for achieving a desired temperature at the nip point, is mostly based on performing trial and error tests in an open loop configuration. The majority of authors in this field have focused their efforts on numerical and experimental studies of the problem, fixing process parameter values, and studying the steady state condition while neglecting the transient stage of the process. They also neglected the effects from the surroundings and the disturbances the composite material may introduce to the process due to variation in the amount of resin and fibre along its length.

To implement a proper control strategy, it is required to close the control loop. The control strategy implementation represents a challenge due to the impossibility of placing a sensor at the required location. Nevertheless, it can be achieved by computing the heat distribution along the composite material using a state estimation strategy.

For the state estimation strategy to be effective it requires a detailed process mathematical model, in which the DT concept brings advantages to compute the dynamics of a system. The ATL models share a similar phenomenological problem that is, understanding the temperature response of the composite material during the heating and cooling process.

Defining the mathematical model for an ATL process highly depends on the heat source, namely hot gas, infra-red lamp or laser beam. Regardless of the heat source type, all face the same challenge which is understanding the heat transfer phenomena occurring, for the hot gas heat source, is relevant to understand the convective phenomena and for the other two sources, the radiation heat exchange is imposed.

On the other hand, for the DT to be effective to predict the composite material temperature, the handled composite material requires a full thermal characterization as a function of its temperature [17]. As stated by researchers [91, 97], a proper characterization of the

composite material, as a function of temperature, improves the temperature estimation and minimizes uncertainties.

It is required to know the composite material density as well as its specific heat as a function of temperature, which can be measured using standard methods such as ASTM D 792-07 [155] and ASTM E 1269-99 [156] respectively.

Another required parameter to know about the composite material is its thermal conductivity as a function of its temperature. The main challenge for characterizing the thermal conductivity of the composite material resides on guarantee two main aspects, first, the one-dimensional heat flux and second, minimizing any external disturbances. The most common method for determining the thermal conductivity in solids is the Flash method ASTM E 1461-13 [157].

The state estimation problem requires using the best model of the system, and analysing all the information gathered so far, coming from the available inputs and outputs from the system. The used system model has to be submitted to a trade-off between reliability and computational load.

The computational load depends on the complexity of the used model. So, a linear, or linearisable solution cannot be obtained to be used as the state estimator, it is required to implement a different approach, such as numerical simulations. The numerical simulation must guarantee the stability of the prediction. This approach implies the use of an optimization algorithm to minimize a convex cost function. For this scenario, a population-based algorithm could be the best choice as the optimization technique for the state estimator. The selected algorithm is intended to be efficient, from a computational point of view, while looking for convergence improvement, as well as capable of handling the imposed constraints, that could be time dependant [158, 159].

Chapter 3

Automated Tape Laying Process modelling: Digital Twin

This chapter presents a detailed modelling and validation procedure for the ATL process DT based on the modelling strategies identified in Chapter 2 Section 2.3. The relevance for a proper thermal characterization of all the elements involved in the machine assembly. The understanding of how the heat flows according to the type of heating element involved and the radiative response of the machine assembly.

This chapter is divided as follows, Section 3.1 introduces the relevance of developing a detailed mathematical model for an ATL process. The ATL process is briefly described in Section 3.2 then, the machine assembly is presented and their respective mathematical models are described in detail from Section 3.3 through Section 3.7. Section 3.8 presents the energy flux balance involving all the assembly elements described in the previous sections. As part of the composite material modelling, Section 3.9 presents the characterization procedure for the composite material, including an in-house designed procedure for characterising its thermal conductivity and thermo-optical properties, based on the reviewed literature presented in Section 2.4. Section 3.10 briefly describes the time integration scheme used, the converge analysis performed and the variables measurement procedure. Section 3.11 describes the Digital Twin assembly and validation process whose results are presented in Section 3.12. Finally, in Section 3.13 are presented concluding remarks for this chapter.

3.1. Introduction

The search for more efficient and automated manufacturing processes to manufacture composite materials structures has identified the Automated Tape Laying (ATL) process with in situ consolidation as an alternative for out-of-autoclave processes, contributing to reduced material scrap and increasing the manufacturability of complex geometries by conforming structures directly on top of a mould [3, 9, 77, 81]. The main challenge of using an ATL machine is to measure the composite material temperature at the nip point, where no sensor can be placed due to an overlapping between the composite material, the compaction element and the mould. This chapter focuses on describing the strategy for developing a process model, from the perspective of a Digital Twin (DT) definition, for an existing ATL machine process. The physical machine is located at INEGI's laboratory as part of the LAY2FORM project [1]. The DT considers the heat source, the composite material, the compaction roll and the surroundings as an enclosure, to predict the temperature distribution along the composite material under different process conditions. The developed DT uses a 1.5-dimensional mathematical model, as the material thickness is modelled with only one element in such direction. The thermo-optical properties of the elements, as temperature dependant, were considered within the infrared range, as well as the composite material thermal properties variations, also as a function of temperature, to obtain an accurate description of the process response.

3.2. Process Machine Description

The ATL machine assembly is composed mainly by an infrared lamp as a heating element, an aluminium backplate as a radiation reflector element, and a consolidation roll for pressing down the heated composite material against a mould. There are another required components for the ATL machine assembly, which are numbered in Figure 3.1a as: (1) material feeder, (2) material tensioner, (3) compaction roll, (4) heating element, (5) reflector, (6) primary pyrometer, (7) nip point and (8) mould. The real assembly is presented in Figure 3.1b.

Figure 3.1b presents the layout of the machine head assembly. This assembly moves horizontally to the x direction according to Figure 3.1a, parallel to the heated mould. The material is fed vertically to the compaction roll and changes its orientation to horizontal when the nip point is reached. This assembly configuration makes the material feed velocity to match the machine head assembly velocity. The other assembly elements such as the infrared lamp, the reflector, the compaction roll and the optical temperature sensor move horizontally along with the machine head.

Figure 3.2 shows a schematic for the model of the ATL. The curved path that the composite material is imposed to follow, as consequence of the compaction roll, is simplified to a straight line, where $y_{\text{convection}}$ corresponds to the region before reaching the roll, y_{roll} corresponds to the curved path in contact with the roll with its equivalent length and y_{mould} corresponds to the region after the nip point.

Understanding the relative movements between the machine head components and the

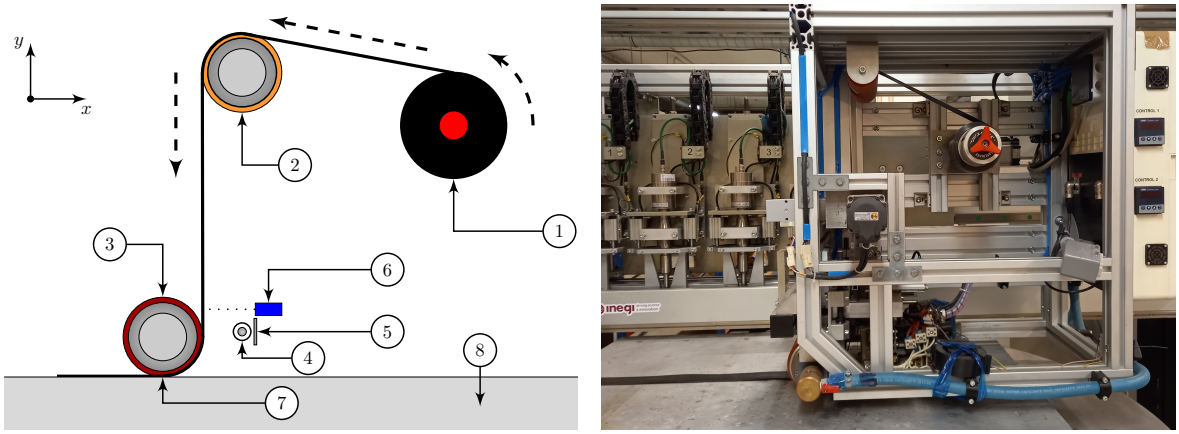

(a) (b)

Figure 3.1: Machine head assembly. **(a)** (1) material feeder, (2) material tensioner, (3) compaction roll, (4) heating element, (5) reflector, (6) primary pyrometer, (7) nip point, (8) mould. **(b)** physical assembly.

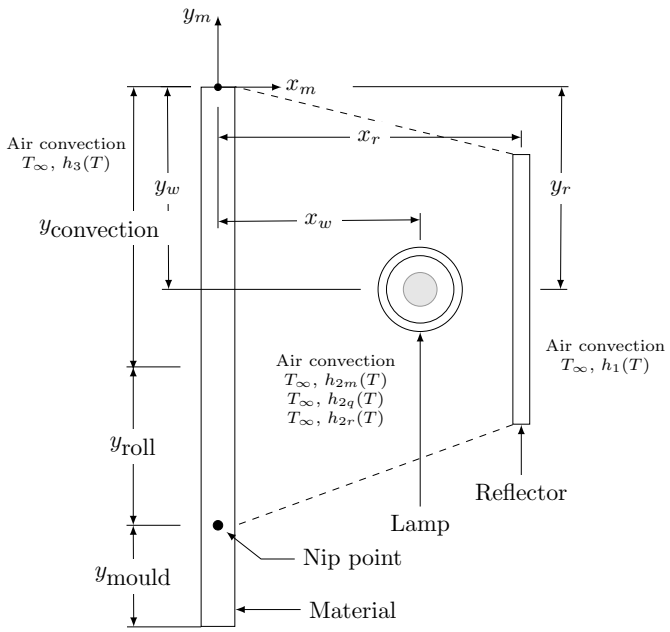

Figure 3.2: 1.5D model schematic

material is relevant as it determines the selection of an appropriate correlation to estimate the convection coefficients.

The ATL model involves an open cavity radiation problem where the heat emitted by the lamp and reflected by the reflector is used to increase the temperature of the entering material tape before it reaches the nip point. Heat loss to the ambient by convection and radiation also takes place and will be considered in the modelling.

Figure 3.2 shows three different zones of heat exchange over the material. The first one, delimited by $y_{\text{convection}}$ has radiation from the lamp at the right-hand side and convection to the surrounding air at the left-hand side, which convection coefficient depends on air temperature, airflow velocity and direction. The second one, delimited by y_{roll} involves heat exchange

from radiation and convection at the right-hand side, and conduction to the compaction roll at the left-hand side. The third zone, delimited by y_{mould} involves only conduction to both compaction roll and mould, at the left and right-hand sides respectively.

To study the component's dynamics, it is required to analyse each one individually, to obtain the governing equation and the corresponding finite differences schemes. Once all the equations and schemes are defined, a model can be developed to understand the influence of the assembly elements over the composite material, allowing to assemble the process DT.

The process involves two main phenomena, namely: the heating process to raise the temperature of the incoming material, and the consolidation process itself. The focus is given to the heating process of the incoming material because it is the most critical for ensuring the structure quality [10, 13, 16, 80].

Both the reflector and the material will be modelled using a single element along its thickness. For the reflector, as its main function is to redirect the heating energy towards the material, it is not relevant to know the temperature distribution along its thickness. A compensation factor is implemented for heat losses due to convection at the surface facing the composite material and at the opposite surface. For the material, as its thickness is significantly smaller than its length, the temperature gradient along its thickness is negligible. On the other hand, even though the incoming radiation heat reaches the composite material at its larger surface, coming from different sources, it is considered just as an input value in terms of the mathematical model.

This consideration comes from an energy balance that takes into account the spatial distribution of the assembly for computing the radiation distribution, whose intensity is also affected by the alignment of the surfaces. As the radiation intensity has already been considered, it allows to propose a 1.5D heat transfer model of the ATL machine head to develop the process DT. The DT will serve to run process simulations, describing as detailed as possible, all the heat transfer due to the interaction among the assembly elements, enabling to implement a proper control strategy to ensure the quality of the manufactured structure.

3.3. Heating element

The used heating element for the ATL assembly is an infrared heater. The infrared heater consists of a tungsten filament coil, heated by an electric current, that serves as the energy emitter. This emitter is surrounded by a quartz glass envelope for protection from the environment. This quartz glass also acts as an enclosure containing an inert gas to prevent filament oxidation at high temperatures as well as small amounts of halogen to inhibit the evaporation of tungsten via the halogen cycle.

To maintain the atmosphere inside the quartz envelope, the current is passed through a pair of Molybdenum foil pads ensuring the gas chamber is sealed to the outside atmosphere, this is done to ensure a proper service life. Figure 3.3 shows a schematic of the heating element assembly.

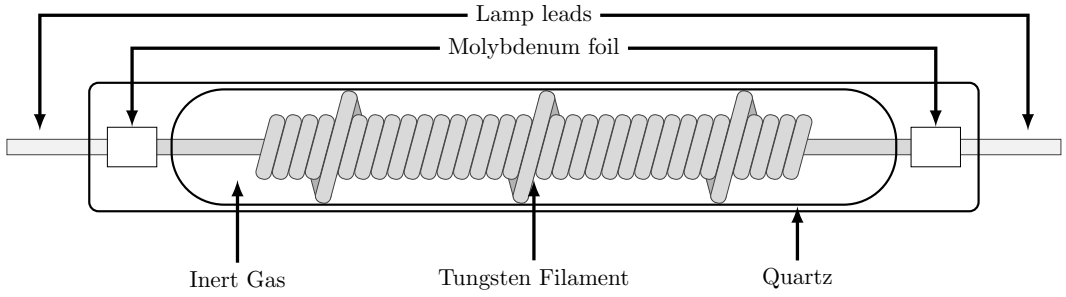

Figure 3.3: Heating element and its cross section

3.3.1 Heating element mathematical model

The heater element is composed of 3 main elements, namely: a tungsten filament shaped as a cylindrical coil, an atmosphere filled with neon gas, and an enclosure made by a cylindrical quartz envelope containing the neon gas atmosphere. A simplification of the lamp geometry is presented in Figure 3.4 where a concentric arrangement of the components, as initially proposed by Pettersson and Stenström [160] for a similar heating element of a paper drying mechanism. Figure 3.4a presents a front view of the lamp model as the tungsten is modelled as a solid cylinder of length l_w and diameter d_{coil} as a simplification of its spiral construction, as shown in Figure 3.4c, and the quartz envelope as a hollow cylinder of length l_q, thickness t_q as presented in Figure 3.4a and external diameter d_l, as shown in Figure 3.4b.

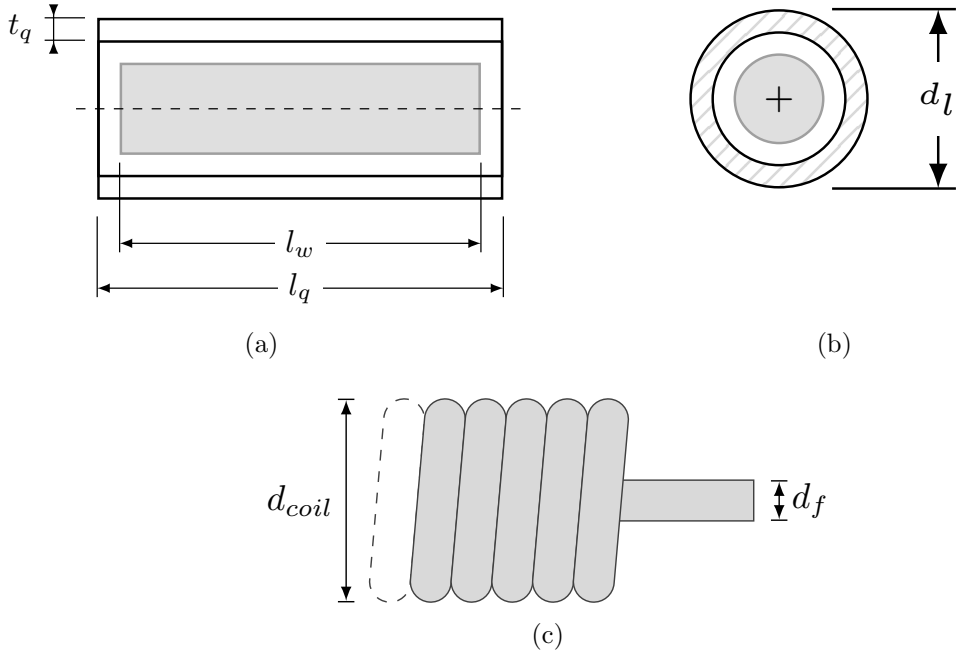

Figure 3.4: Lamp model. **(a)** Lamp model front view. **(b)** Lamp model cross section. **(c)** Filament model

Tungsten filament

The tungsten filament is considered as a homogeneous cylindrical element with an internal heat generation, the internal generation is given by the material electrical resistance which is a function of its temperature T_f and the applied voltage. The cylindrical-shaped tungsten exchanges heat with the neon by conduction and with the inner face of the quartz lamp by radiation. No convection between the filament and the neon is considered because of the low value for the Grashof number, as suggested by Pettersson and Stenström [160], which indicates the conduction as the predominant phenomenon for this particular heat exchange process. Then, the heat transfer model used for the tungsten filament is the energy balance given in Equation 3.1 [94, 161],

$$m_f \; cp_f(T_f) \; \frac{dT_f}{dt} = \left(P_{el} - Q_{r,f} - Q_{c,n}\right), \tag{3.1}$$

where:

m_f: Filament mass, [kg]
T_f: Filament temperature, [K]
$cp_f(T_f)$: Filament specific heat, temperature dependent, $\left[\frac{\mathrm{J}}{\mathrm{kg \cdot K}}\right]$
P_{el}: Electric power, [W]
$Q_{r,f}$: Radiation heat, [W]
$Q_{c,n}$: Conduction heat (Neon gas), [W]

The electric power delivered to the tungsten filament can be expressed using Equation 3.2, as a function of the voltage applied and its resistance.

$$P_{el} = \frac{U_e^2}{R\left(T_f\right)}, \tag{3.2}$$

where U_e stands for the applied voltage to the filament, and $R\left(T_f\right)$ is the electrical resistance, which is a function of the filament temperature, and can be expressed as a function of its resistivity $r_f\left(T_f\right)$, the filament length l_f and the filament cross sectional area a_f, as shown in Equation 3.3.

$$R\left(T_f\right) = r_f\left(T_F\right) \frac{l_f\left(T_f\right)}{a_f\left(T_f\right)} \tag{3.3}$$

The thermal property for the tungsten filament, such as specific heat, is taken from literature [160, 162, 163] and summarized in Equation 3.4 and Equation 3.5 for a tungsten temperature between 298 K $< T_w \leq$ 1900 K and 1900 K $< T_w \leq$ 3680 K respectively.

$$cp_w\left(T_w\right) = \frac{\left[23.9593 + 2.63968\left(\frac{T_w}{10}\right) + 1.25775\left(\frac{T_w}{10}\right)^2 - 0.25364\left(\frac{T_w}{10}\right)^3 - \frac{0.048407}{\left(\frac{10}{T_w}\right)^2}\right]}{183.84 \times 10^{-3}} \tag{3.4}$$

$$cp_w\left(T_w\right) = \frac{\left[-22.5764 + 90.2798\left(\frac{T_w}{10}\right) - 44.2715\left(\frac{T_w}{10}\right)^2 + 7.1766\left(\frac{T_w}{10}\right)^3 - \frac{24.0974}{\left(\frac{T_w}{10}\right)^2}\right]}{183.84 \times 10^{-3}} \tag{3.5}$$

For the resistivity of the tungsten filament, Equation 3.6 [160], describes the correlation between the tungsten filament temperature and its electrical resistivity.

$$r_w\left(T_w\right) = -5.0134 \times 10^{-9} + 7.3070759 \times 10^{-11} \cdot T_w^{1.1796583} \tag{3.6}$$

Neon gas

As the neon gas has a low thermal capacitance compared with the tungsten filament and the quartz envelope, the capacitance is hence neglected. Accordingly, the neon gas transfers heat from the tungsten filament to the quartz envelope's internal surface by conduction. Taking advantage of the cylindrical configuration of the heating element, the heat conducted by the neon can be approximated using the cylindrical solution for radial conduction expressed in Equation 3.7, as suggested by Pettersson and Stenström [160] and Incropera et al. [94].

$$Q_{c,n} = 2 \cdot \pi \cdot l_q \cdot k_n\left(T_n\right) \cdot \frac{\left(T_f - T_q\right)}{ln\left(\frac{d_L}{d_{coil}}\right)}, \tag{3.7}$$

where:

$Q_{c,n}$: Conduction heat (Neon gas), [W]

k_n: Neon thermal conductivity, temperature dependent $\left[\frac{\mathrm{W}}{\mathrm{m \cdot K}}\right]$

T_n: Neon mean temperature $\left(\frac{T_f + T_q}{2}\right)$, [K]

T_q: Quartz lamp temperature, [K]

d_L: Lamp diameter, [m]

d_{coil}: Filament coil diameter, [m]

l_q: Lamp length, [m]

The neon gas thermal conductivity can be computed using Equation 3.8 for a temperature range of 250 K $< T_n <$ 2500 K [160].

$$k_n\left(T_n\right) = -3.601821 \times 10^{-3} + 1.4290623 \times 10^{-3} \cdot T_n^{0.63362378} \tag{3.8}$$

Quartz glass envelope

The quartz glass envelope is considered to have a constant temperature T_q across its thickness because of its small thickness compared with its length. The energy balance for the quartz glass envelope is given in Equation 3.9 as suggested by Pettersson and Stenström [160].

$$m_q \cdot cp_q\left(T_q\right) \cdot \frac{\mathrm{d}T_q}{\mathrm{d}t} = \left(Q_{r,f} + q_{c,n} - Q_{r,q} - h_q A_q \left(T_q - T_\infty\right)\right), \tag{3.9}$$

where:

m_q: Quartz glass envelope, [m]
$cp_q\left(T_q\right)$: Quartz glass specific heat, $\left[\frac{\mathrm{J}}{\mathrm{J \cdot K}}\right]$
$Q_{r,f}$: Incoming radiation heat, [W]
$Q_{r,q}$: Outgoing radiation heat, [W]
$Q_{c,n}$: Conduction heat, [W]
h_q: Convection coefficient, $\left[\frac{\mathrm{W}}{\mathrm{m^2 \cdot K}}\right]$
A_q: Quartz glass surface area, $\left[\mathrm{m^2}\right]$
T_∞: Environmental temperature, [K]

The physical characteristics of the heating element, which are required for the heating element simulation, were measured and are reported in Table 3.1.

Table 3.1: Measurements for the heating element characteristics

Characteristic	Measurement
Lamp length l_q	189.02 mm ± 0.34 mm
Lamp diameter d_l	10.01 mm ± 0.19 mm
Lamp resistance R_w (at 23 °C)	9.6 Ω ± 6.41 $\times 10^{-6}$ Ω
Filament diameter d_f	0.410 mm ± 0.004 mm
Filament coil diameter d_{coil}	2.890 mm ± 0.004 mm
Filament coil length l_r	290.04 mm ± 0.37 mm
Filament mass m_f	5.2019 g ± 0.0005 g
Quartz glass mass m_q	13.8780 g ± 0.0005 g

The specific heat for the quartz glass can be computed from Equation 3.10 as suggested by Pettersson [88] and by Pettersson and Stenström [160], as a function of the quartz glass temperature in a range of 298 K $< T_q <$ 2000 K.

$$cp_q\left(T_q\right) = \frac{\left[55.98 + 15.4 \times 10^{-3} \cdot T_q - \frac{14.1 \times 10^5}{T_q^2}\right]}{60.085 \times 10^{-3}} \tag{3.10}$$

The convection term in Equation 3.9, h_q, is computed using the Morgan correlation [94, 164], suitable for a long cylinder with free convection. The free convection phenomenon is assumed due to the relative position of the heating element with respect to reflector element inside the machine head assembly, the reflector blocks direct air to flow towards the heating element while the machine head assembly is moving.

To estimate the convection coefficient h_q, Churchill and Chu [165] establish a correlation for the Rayleigh number and the average Nusselt number, Equation 3.11.

$$\overline{Nu_q} = \left\{ 0.60 + \frac{0.387 \cdot Ra_q^{1/6}}{\left[1 + \left(0.559/Pr_{\text{air}}\left(T_{\text{film}}\right)\right)^{9/16}\right]^{8/27}} \right\}^2, \tag{3.11}$$

where the Rayleigh number is computed using Equation 3.12.

$$Ra_q = \frac{g \cdot \left(1/T_{\text{film}}\right) \cdot \left(T_q - T_\infty\right) \cdot d_L^3}{\nu\left(T_{\text{film}}\right) \cdot \alpha\left(T_{\text{film}}\right)}, \tag{3.12}$$

then, the average convection coefficient for free convection of a long cylinder is computed using Equation 3.13.

$$\overline{h_q} = \frac{\overline{Nu_q} \cdot k_{\text{air}}\left(T_{\text{film}}\right)}{d_L} \tag{3.13}$$

The properties of the air for Equation 3.11, Equation 3.12 and Equation 3.13 such as Pr, ν, α and k_{air}, can be found in literature [94], and taken at atmospheric pressure and film temperature $T_{film} = 0.5 \cdot (T_q + T_\infty)$. In Equation 3.12 the value of the gravity acceleration is defined as $g = 9.81$ m/s^2.

3.4. Reflector

The reflector is considered as a vertically oriented flat thin surface, with a homogeneous thickness t_r and width of W_r. The reflector is made from polished aluminium alloy 6061, and its main objective is to reflect the incoming energy from the heating element towards the composite material.

3.4.1 Reflector mathematical model

The reflector is modelled as a 1.5D finite volume problem along its width W_r, Figure 3.5. Due to the convection effect, the reflector transfers heat to the ambient air at both surfaces of length W_r. An energy balance over a reflector cell of volume V_r is given in Equation 3.14, taking into account its surfaces S_r for heat exchange.

$$\frac{\partial}{\partial t}\int_{V_r} \rho_r \cdot cp_r(T_r) \cdot T_r \cdot dV_r = \int_{\partial V_r} k_r(T_r) \cdot (\nabla T_r \cdot \hat{n}) \cdot dS_r + \int_{\partial V_r} q''_{\text{rad,r}} \cdot dS_r + \int_{\partial V_r} q''_{\text{conv,r}} \cdot dS_r \tag{3.14}$$

where:

ρ_r: Reflector material density, $\left[\frac{\text{kg}}{\text{m}^3}\right]$
T_r: Reflector temperature, [K]
$cp_r\left(T_r\right)$: Reflector specific heat, temperature dependent, $\left[\frac{\text{J}}{\text{kg·K}}\right]$
$k_r\left(T_r\right)$: Reflector thermal conductivity, temperature dependent, $\left[\frac{\text{W}}{\text{kg·K}}\right]$

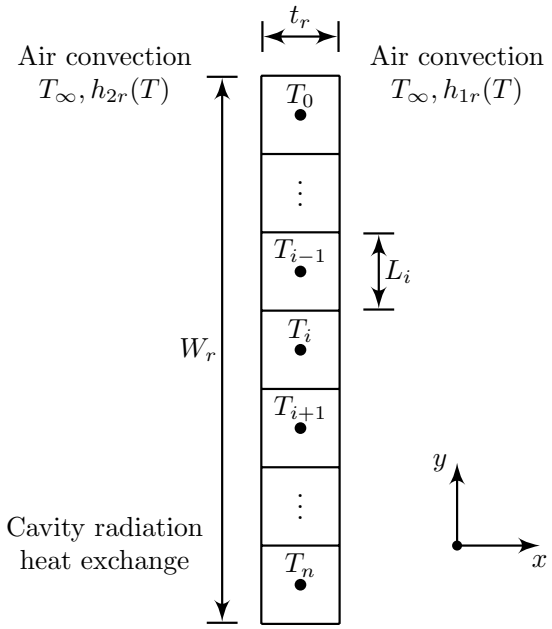

Figure 3.5: 1.5D finite volume discretization for the reflector model

$q''_{\mathrm{rad,r}}(T_r)$: Radiation heat, $\left[\frac{\mathrm{W}}{\mathrm{m^2 \cdot K}}\right]$
$q''_{\mathrm{conv,r}}(T_r, T_\infty)$: Convection heat, $\left[\frac{\mathrm{W}}{\mathrm{m^2 \cdot K}}\right]$

The aluminium properties, required in Equation 3.14, are well documented in the literature. For the case of the specific heat of the reflector, $cp_r(T_r)$, the expression is presented in Equation 3.15 for a temperature range of 298 K $< T <$ 933 K, which is documented in [162, 166, 167]; the reflector thermal conductivity, $k_r(T_r)$, expressed in Equation 3.16 for a temperature range of 250 K $< T <$ 800 K is documented by Lide [168].

$$cp_r(T_r) = \frac{4.186 \cdot \left(4.94 + 2.96 \times 10^{-3} \cdot T_r\right)}{26.98154} \tag{3.15}$$

$$k_r(T_r) = 186.0219 + 0.327088 \cdot T_r - 6.069629 \times 10^{-4} \cdot T_r^2 + 3.101227 \times 10^{-7} \cdot T_r^3 \tag{3.16}$$

A finite volume technique is used to discretize the reflector geometry as shown in Figure 3.5. The application of an energy balance to each reflector cell gives a cell equation, Equation 3.17, for the unknown cell temperature.

$$\begin{aligned} \dot{T_r} = &\left(A_r\right) T_{r-1} - \left(2A_r + B_{r,1} + B_{r,2}\right) T_r + \left(A_r\right) T_{r+1} \\ &+ \left(B_{r,1}\right) T_{\infty,1} T_{\infty,1} + \left(R_{r,2}\right) T_{\infty,2} + \left(C_r\right) q''_{\mathrm{rad,r}}\left(T_r\right) \end{aligned} \tag{3.17}$$

which coefficients are defined as presented in Equation 3.18, Equation 3.19, Equation 3.20 and Equation 3.21.

$$A_r = \frac{k_r\left(T_r\right)}{\rho_r \cdot cp_r\left(T_r\right) \cdot L_r^2} \tag{3.18}$$

$$B_{r,1} = \frac{h_{1r}}{\rho_r \cdot cp_r\left(T_r\right) \cdot t_r} \tag{3.19}$$

$$B_{r,2} = \frac{h_{2r}}{\rho_r \cdot cp_r\left(T_r\right) \cdot t_r} \tag{3.20}$$

$$C_r = \frac{1}{\rho_r \cdot cp_r\left(T_r\right) \cdot t_r} \tag{3.21}$$

where:

r: Reflector cell number 0,1,2,...,n

L_r: Length of the reflector cell, [m]

t_r: Reflector thickness, [m]

T_∞: Air temperature, [K]

$h_{1r}\left(T_r, T_\infty\right)$: Right hand side convection coefficient, $\left[\frac{\mathrm{W}}{\mathrm{m^2 \cdot K}}\right]$

$h_{2r}\left(T_r, T_\infty\right)$: Left hand side convection coefficient, $\left[\frac{\mathrm{W}}{\mathrm{m^2 \cdot K}}\right]$

The lateral conditions for the reflector are defined as adiabatic, Equation 3.22 and Equation 3.23, due to $W_r \gg t_r$, which makes the heat exchange in those surfaces negligible in comparison with the heat exchange of the remaining surfaces.

$$\left.\frac{\mathrm{d}T}{\mathrm{d}y}\right|_{y=0} = 0 \tag{3.22}$$

$$\left.\frac{\mathrm{d}T}{\mathrm{d}y}\right|_{y=W_r} = 0 \tag{3.23}$$

Due to the horizontal movement of the machine head, the reflector is defined to have two conditions of heat exchange by convection. The first convection condition occurs over the surface opposed to the heating element, shown at the right-hand side in Figure 3.5 as h_{1r}, and the other convection condition occurs over the left-hand side surface shown as h_{2r} in Figure 3.5, which faces the heating element.

The movement of the machine head assembly is in the positive x direction while heating, Figure 3.5 so, direct airflow is directed towards the right-hand side of the reflector. The left-hand side of the reflector has no direct airflow.

For both cases, a proper correlation for computing the convection coefficient is required. For the right-hand side, a correlation for direct airflow over a plane surface is proposed by Hilpert [169], by computing a Reynolds number for a plate of length W_r, Equation 3.24, to solve and empirical correlation between the Reynolds number and the Nusselt number, Equation 3.25.

$$Re_{r1} = \frac{U \cdot W_r}{\nu\left(T_{\mathrm{film}}\right)}, \tag{3.24}$$

where U is the movement velocity of the machine head assembly in the positive x direction

$$\overline{Nu_{r1}} = 0.228 \cdot Re_{W_r}^{0.731} \cdot Pr_{\text{air}}^{1/3}\left(T_{\text{film}}\right) \tag{3.25}$$

The average convection coefficient for the right-hand side surface of the reflector is computed using Equation 3.26.

$$\overline{h_{r1}} = \frac{\overline{Nu_{r1}} \cdot k_{\text{air}}\left(T_{\text{film}}\right)}{W_r} \tag{3.26}$$

For the left-hand side, Churchill and Chu [165] proposed the correlation presented in Equation 3.27, relating the Rayleigh number and the average Nusselt number for computing the free convection coefficient for a plane vertical wall h_{2r}

$$\overline{Nu_{2r}} = \left\{ 0.825 + \frac{0.387 \cdot Ra_{2r}^{1/6}}{\left[1 + \left(0.492/Pr\left(T_{\text{film}}\right)\right)^{9/16}\right]^{8/27}} \right\}^2, \tag{3.27}$$

where the Rayleigh number is computed using Equation 3.28.

$$Ra_{2r} = \frac{g \cdot \left(1/T_{\text{film}}\right) \cdot \left(T_r - T_\infty\right) \cdot W_r^3}{\nu\left(T_{\text{film}}\right) \cdot \alpha\left(T_{\text{film}}\right)} \tag{3.28}$$

Then, the average free convection coefficient for the left-hand side surface of the reflector is computed using Equation 3.29,

$$\overline{h_{2r}} = \frac{\overline{Nu_{2r}} \cdot k_{\text{air}}\left(T_{\text{film}}\right)}{W_r}. \tag{3.29}$$

3.5. Compaction Roll

The compaction roll is a hollow aluminium cylinder, with an internal flow of cooling fluid to keep its temperature constant, and an outer layer of silicone rubber Silex GP60THT [170]. This outer layer acts as a non-adherent surface between the aluminium cylinder and the composite material. The compaction roll is used to press the incoming material, once heated, against the mould, or a substrate made from a previously laid composite material layer.

3.5.1 Compaction roll mathematical model

The modelling strategy used for simulating the heat exchange process between the compaction roll and the composite material is to use a combination of a composite hollow cylinder with 2D radial conduction for the compaction roll internal fluid. The aluminium structure and the rubber layer are modelled as 1D conduction plane wall approximation for the composite material, as presented in Figure 3.6. This plane wall approximation is possible due to the relation presented in Equation 3.30 where D_{roll} is the compaction roll diameter without the rubber layer, t_{rubber} is the thickness of the rubber layer and Δx is the thickness of the

composite material.

$$\ln\left[\frac{(D_{roll}/2) \; + \; t_{rubber} \; + \; \Delta x}{(D_{roll}/2) \; + \; t_{rubber}}\right] \approx 0 \tag{3.30}$$

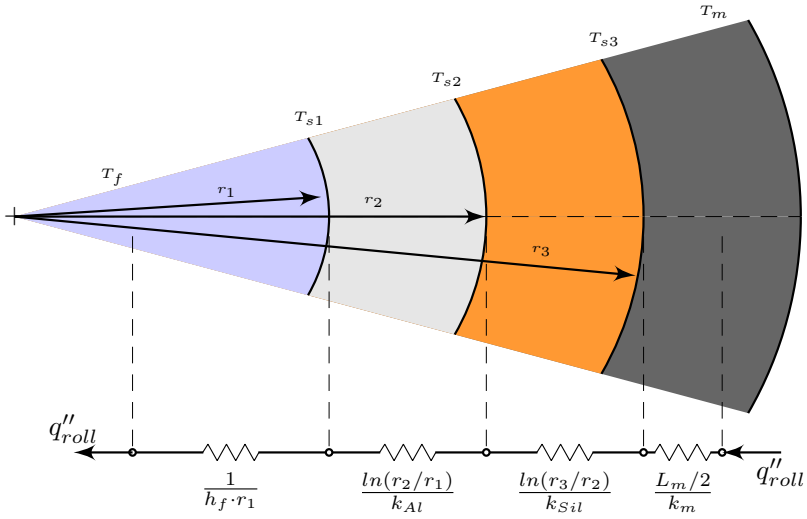

Figure 3.6: Composite wall modelling strategy for the heat conduction balance between the compaction roll and the material

The 1D model equation is obtained by making an analogy with a system of electrical resistances connected in series, as presented in Figure 3.6 then, the term R_{roll} from Equation 3.31 is deduced as the sum of all the resistors, Equation 3.32, which considers the resistance from the internal fluid of the compaction roll, the resistance of the cylinder, the resistance of the rubber layer and the resistance of the composite material.

$$q''_{roll} = \frac{(T_f - T_m)}{R_{roll}} \tag{3.31}$$

$$R_{roll} = \frac{1}{h_f \cdot r_1} + \frac{\ln(r_2/r_1)}{k_{Al}} + \frac{\ln(r_3/r_2)}{k_{Sil}} + \frac{L_m/2}{k_m}, \tag{3.32}$$

where h_f stands for the internal fluid convection coefficient, k_{Al}, k_{Sil} and k_m are the coefficient of thermal conduction of the cylinder, the rubber layer and the composite material respectively, L_m is the thickness of the composite material, r_1, r_2, r_3 and r_4 are the radius for each component of the compaction roll.

If a constant temperature is assumed for the internal fluid, Equation 3.32 can be simplified to Equation 3.33.

$$R_{roll} = \frac{\ln(r_2/r_1)}{k_{Al}} + \frac{\ln(r_3/r_2)}{k_{Sil}} + \frac{L_m/2}{k_m} \tag{3.33}$$

3.6. Mould

The mould is considered as a flat surface, made of aluminium, with a film of Polytetrafluoroethylene (PTFE) on top between the aluminium and the composite material acting as a mould-releasing agent.

3.6.1 Mould mathematical model

The mathematical model to develop for the mould is based on the composite plane wall, which main heat exchange phenomena is conduction through different material layers. Figure 3.7 represents the 1D composite wall scheme.

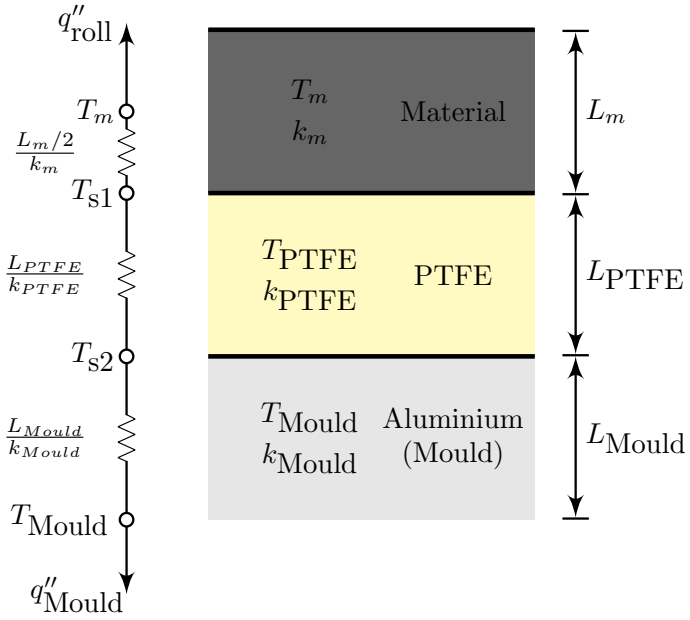

Figure 3.7: Composite wall model for the 1D mould.

The energy balance between the composite material layer and the mould is presented in Equation 3.34:

$$q''_{\text{Mould}} = \frac{T_m - T_{\text{Mould}}}{R_{\text{Mould}}}, \tag{3.34}$$

where using a modelling strategy as a group of resistors connected in series, the term R_{Mould} can be defined as in Equation 3.35:

$$R_{\text{Mould}} = \frac{L_m/2}{k_m} + \frac{L_{\text{PTFE}}}{k_{\text{PTFE}}} + \frac{L_{\text{Mould}}}{k_{\text{Mould}}} \tag{3.35}$$

3.7. Composite Material

The Automated Tape Laying process presented in Figure 3.1a shows the composite material being fed vertically towards the compaction roll. The composite material is formed by Unidirectional carbon fibres with a Polyamide 6 (PA6) thermoplastic matrix from Toray Co.®.

3.7.1 Composite Material mathematical model

As previously mentioned the entire machine assembly moves linearly at a velocity U towards the x direction on top of a mould, Figure 3.1a. This movement causes the composite material to exchange heat with its surroundings by convection, by radiation while being heated by the heating element. Once the composite material reaches the compaction roll, the heat exchange by conduction takes place.

Similarly to the reflector, section 3.4, the composite material is defined as a thin sheet with a constant temperature across its thickness. As the composite material comes from the material feeder, which in the machine assembly is placed away from the heating element, Figure 3.1, it is considered that the composite material is supplied at a constant temperature T_0. The energy balance for a cell volume V_m of the material tape is given in Equation 3.36.

$$\begin{aligned}
&\frac{\partial}{\partial t}\int_{V_m} \rho_m \cdot cp_m\left(T_m\right) \cdot T_m \cdot dV_m = \int_{V_m} k_m\left(T_m\right) \cdot \left(\nabla T_m \cdot \hat{n}\right) \cdot dS_m \\
&- \int_{V_m} \rho_m \cdot cp_m\left(T_m\right) \cdot T_m \cdot \left(U \cdot \hat{n}\right) \cdot dS_m \\
&+ \int_{V_m} q''_{\mathrm{rad},m} dS_m + \int_{V_m} q''_{\mathrm{conv},m} dS_m + \int_{V_m} q''_{\mathrm{cond},m} dS_m,
\end{aligned} \tag{3.36}$$

where:

ρ_m: Composite material density, $\left[\mathrm{kg/m^3}\right]$

T_m: Composite material temperature, [K]

$cp_m\left(T_m\right)$: Composite material specific heat, temperature dependant, $\left[\frac{\mathrm{J}}{\mathrm{kg \cdot K}}\right]$

$k_m\left(T_m\right)$: Composite material thermal conductivity, temperature dependent, $\left[\frac{\mathrm{W}}{\mathrm{m \cdot K}}\right]$

$q''_{\mathrm{rad},m}\left(T_m\right)$: Radiation heat, $\left[\mathrm{W/m^2}\right]$

$q''_{\mathrm{conv},m}\left(T_m, T_\infty\right)$: Convection heat, $\left[\mathrm{W/m^2}\right]$

$q''_{\mathrm{cond},m}\left(T_m, T_{\mathrm{mould}}\right)$: Conduction heat, $\left[\mathrm{W/m^2}\right]$

A finite volume technique, as suggested by Schaefer et. al [93], is used to represent the tape geometry, Figure 3.8, and the application of the energy balance to each tape cell gives the cell equation, Equation 3.37, for the unknown temperature using the coefficients given by Equation 3.38 through Equation 3.44.

$$\begin{aligned}
\dot{T}_m = &\left(A|_{\mathrm{Z_1,Z_2,Z_3}}\right) \cdot T_{m+1} + \left(A|_{\mathrm{Z_1,Z_2,Z_3}} + B|_{\mathrm{Z_1,Z_2,Z_3}}\right) \cdot T_{m-1} \\
&+ \left(-2\, A|_{\mathrm{Z_1,Z_2,Z_3}} - C_1|_{\mathrm{Z_1,Z_2}} - C_2|_{\mathrm{Z_1}} - D_1|_{\mathrm{Z_2}} - D_2|_{\mathrm{Z_3}}\right) \cdot T_m \\
&+ C_1|_{\mathrm{Z_1,Z_2}} \cdot T_\infty + C_2|_{\mathrm{Z_1}}\, T_\infty + D_1|_{\mathrm{Z_2}} \cdot T_{\mathrm{roll}} + D_2|_{\mathrm{Z_3}} \cdot T_{\mathrm{mould}} \\
&+ D_3|_{\mathrm{Z_1,Z_2}} \cdot q''_{\mathrm{rad}}
\end{aligned} \tag{3.37}$$

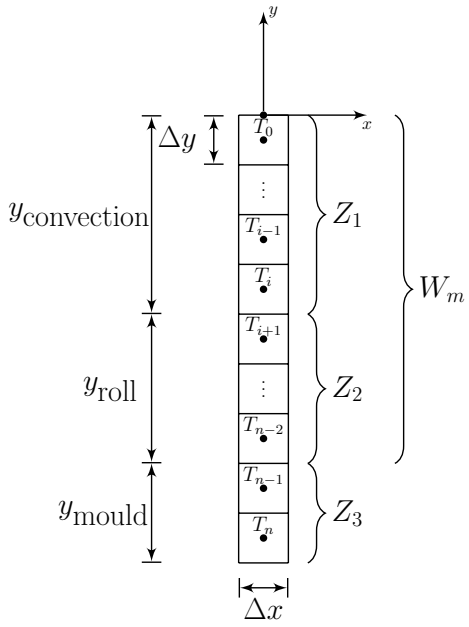

Figure 3.8: The 1.5D material model.

$$A = \frac{k_m\left(T_m\right)}{\rho_m \cdot cp_m\left(T_m\right) \cdot \Delta y^2} \tag{3.38}$$

$$B = \frac{U}{\Delta y} \tag{3.39}$$

$$C_1 = \frac{h_{2m}}{\rho_m \cdot cp_m\left(T_m\right) \cdot \Delta x} \tag{3.40}$$

$$C_2 = \frac{h_{3m}}{\rho_m \cdot cp_m\left(T_m\right) \cdot \Delta x} \tag{3.41}$$

$$D_1 = \frac{1}{\rho_m \cdot cp_m\left(T_m\right) \cdot \Delta x \cdot R_{\text{roll}}} \tag{3.42}$$

$$D_2 = \frac{1}{\rho_m \cdot cp_m\left(T_m\right) \cdot \Delta x \cdot R_{\text{mould}}} \tag{3.43}$$

$$D_3 = \frac{1}{\rho_m \cdot cp_m\left(T_m\right) \cdot \Delta x} \tag{3.44}$$

where:

m: Material cell number, 0, 1, 2, ..., n.

R_{mould}: Composite wall resistance for heat conduction between the mould and the composite material, $\left[\frac{\text{m}^2 \cdot \text{K}}{\text{W}}\right]$.

R_{roll}: Composite wall resistance for heat conduction between the compaction roll and the composite material, $\left[\frac{\text{m}^2 \cdot \text{K}}{\text{W}}\right]$.

q''_{rad}: Net radiation from the surfaces involved in the heat exchange process, $\left[\text{W}/\text{m}^2\right]$.

h_{2m}: Convection coefficient for the composite material surface facing the heat element, $\left[\frac{\text{W}}{\text{m}^2 \cdot \text{K}}\right]$.

h_{3m}: Convection coefficient for the composite material surface facing opposite the heat element, $\left[\frac{\text{W}}{\text{m}^2 \cdot \text{K}}\right]$.

The terms from Equation 3.38 through Equation 3.44 are evaluated into Equation 3.37 taking into account each material section Z_i as shown in Figure 3.8, allowing to obtain the corresponding boundary conditions for the cell. After evaluating all the terms for all the material cells, a system of differential equations is built to compute the new material temperatures.

At section Z_1 the material arrives at an initial temperature $T_0 = T_\infty$ where convection (C_1, C_2) and radiation (D_3) are the main heat exchange phenomena. At this section the convection, which relation is defined using the inside enclosure air properties (T_∞, h_{2m}), and the radiation phenomena are added to the balance to complete the relation; the radiation term comes from an energy balance further discussed in this chapter at Section 3.8.3. At section Z_2, the main heat exchange phenomena are radiation (D_3), convection (C_1) and conduction (D_1); at section Z_3 the material is located between the compaction roll and the mould, this means that conduction (D_1, D_2) is the main heat exchange phenomena occurring between the composite material, the compaction roll and the mould simultaneously. For this model, the temperature of the nip point is located at the material cell T_n, and the previously laid material temperature is modelled assuming a constant value of T_{mould}. The terms R_{roll} and R_{mould} were explained in Section 3.5 and Section 3.6 respectively.

The boundary condition related to the y axis at the first material cell is represented using Equation 3.45, and the last material cell, along the same y axis, is represented using Equation 3.46.

$$T|_{y=0} = T_0 \tag{3.45}$$

$$\left.\frac{\mathrm{d}T}{\mathrm{d}y}\right|_{y=n} = 0 \tag{3.46}$$

The terms presented in Equation 3.40 and Equation 3.41 are related to convection between the composite material and the ambient air. Due to the relative movement of the composite material with the machine assembly, the convection phenomena is defined to be an external flow in a quiescent state, the correlations for estimating the convection terms are presented from Equation 3.47 trough Equation 3.49.

$$Re_m = \frac{U \cdot W_m}{\nu\left(T_{film}\right)} \tag{3.47}$$

$$\overline{Nu_m} = \frac{0.3387 \cdot Re_m^{1/2} \cdot Pr_{air}\left(T_{film}\right)^{1/3}}{\left[1 + \left(0.0468/Pr_{air}\left(T_{film}\right)\right)^{2/3}\right]^{1/4}} \tag{3.48}$$

$$\overline{h_m} = \frac{\overline{Nu_m} \cdot k_{\text{air}}\left(T_f ilm\right)}{W_m} \tag{3.49}$$

3.8. Energy balance: Radiation

Radiation as heat transfer has been well studied when grey surfaces participate inside an enclosure. The interaction has been described in several textbooks [94, 163, 171, 172]. To model the enclosure, the general surface distribution to use is the configuration described in Figure 3.2, where the reflector, the lamp and the material are involved and, to close the enclosure, the dashed lines represent a hypothetical surface acting as the surroundings.

To simplify calculations, the radiation flux problem is modelled as a two-dimensional system, allowing to calculate the heat flux per unit of area. Equation 3.17 and Equation 3.37 can be solved using the radiation heat input expressed in [W/m^2]. It is worth mentioning that the view factors for two-dimensional problems are well studied, and analytical equations have been developed to simplify calculations [163, 171–174], these equations are discussed further in this work.

Another enclosure present in the system is the case of the heating element, which is composed, as described in Section 3.3, of a tungsten filament inside a quartz glass envelope. In this enclosure, the filament exchanges heat, mostly in the form of radiation with the inner surface of the quartz envelope. At the same time, part of this radiation is also exchanged with the external glass surface due to the glass being a transparent media, transmissivity. This characteristic is fundamental when defining the global Radiosity balance among the involved surfaces for the general enclosure.

To calculate the radiation energy of a grey surface, first, the radiation energy for an equivalent black body is calculated using the Planck's Law, presented in Equation 3.50, then a correcting factor, particular for each surface nature and temperature, is applied to transform the black body radiation into a grey body radiation. Those correcting factors are further discussed.

$$E_b = \int_0^\infty \frac{c_1}{\lambda^5 \cdot \left[e^{\left(\frac{c_2}{\lambda \cdot T}\right)} - 1\right]} d\lambda \tag{3.50}$$

with:

$$c_1 = 2 \cdot \pi \cdot h \cdot c_0^2 = 3.742 \times 10^8 \ \left[\frac{\mathrm{W} \cdot \mu\mathrm{m}^4}{\mathrm{m}^2}\right] \tag{3.51}$$

$$c_2 = \frac{h \cdot c_0}{k_b} = 1.439 \times 10^4 \ [\mu\mathrm{m} \cdot \mathrm{K}] \tag{3.52}$$

where:

λ: Wavelength, [µm]

T: Absolute temperature of the black body, [K]

h: Universal Planck constant, 6.626×10^{-34} [J · s]

k_b: Boltzmann constant, 1.381×10^{-23} [J/K]

c_0: Speed of light in vacuum, 2.998×10^8 [m/s]

The focus of the energy radiation is set upon the infrared domain of the spectrum, narrowing the calculation region between λ_1 and λ_2, 0.4 µm and 20 µm respectively, then, the total energy for a black body is obtained using Equation 3.53 from Planck's Law, Equation 3.50.

$$E_{\lambda,b} = \int_{\lambda_1}^{\lambda_2} \frac{c_1}{\lambda^5 \cdot \left[e^{\left(\frac{c_2}{\lambda \cdot T}\right)} - 1\right]} d\lambda \tag{3.53}$$

As the energy calculation depends on the wavelength, and the integration is required along a finite band of wavelengths, the numerical solution is achieved by evaluating the first 10 terms of the infinite series presented in Equation 3.54, where σ stands for the Stefan-Boltzmann Constant, $5.670 \times 10^{-8} \left[\frac{\mathrm{W}}{\mathrm{m}^2 \cdot \mathrm{K}^4}\right]$. By dividing the studied wavelength interval into 20 equally distributed evaluation domains it is possible to obtain a good approximation while improving the calculation time in comparison with numerical integration routines as suggested by Howell et al. [171].

$$\begin{aligned} E_b(T) =& \sigma \cdot T^4 \left[\frac{15}{\pi^4} \left(\sum_{n=1}^{\infty} \frac{e^{-n\cdot\xi_2}}{n} \left(\xi_2^3 + \frac{3\xi_2^2}{n} + \frac{6\xi_2}{n^2} + \frac{6}{n^3}\right)\right.\right. \\ & \left.\left. - \sum_{n=1}^{\infty} \frac{e^{-n\cdot\xi_2}}{n} \left(\xi_2^3 + \frac{3\xi_2^2}{n} + \frac{6\xi_2}{n^2} + \frac{6}{n^3}\right)\right)\right] \end{aligned} \tag{3.54}$$

with:

$$\xi_2 = \frac{h \cdot c_0}{k_b \cdot \lambda_2 \cdot T} \tag{3.55}$$

$$\xi_1 = \frac{h \cdot c_0}{k_b \cdot \lambda_1 \cdot T} \tag{3.56}$$

3.8.1 Radiative fluxes

To define the radiative balance, an identification of the surfaces involved is presented in Figure 3.9, as well as the Radiosity, J_i, and Irradiation, G_i, notation for each surface with its respective indices.

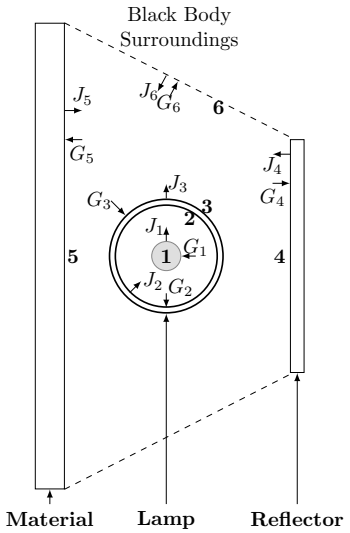

Figure 3.9: Surface identification. (1) Tungsten filament surface. (2) Internal quartz glass surface. (3) External quarts glass surface. (4) Reflector surface. (5) Material surface. (6) Equivalent surroundings surface

The boundary condition labelled as 6 is defined as a black body representing a virtual surface that closes the enclosure. This allows to determine the net radiating heat transfer with Equation 3.57 using the relation given in Equation 3.58 for each surface.

$$q_i^{''} = J_i - G_i, \tag{3.57}$$

$$J_{\lambda,i} = r_{\lambda,i} \cdot G_i + \tau_{\lambda,i} \cdot G_{\lambda,i} + \varepsilon_{\lambda,i} \cdot \sigma \cdot T_i^4 \tag{3.58}$$

The first step is consider the radiosity for each surface, giving the set of relations presented from Equation 3.59 through Equation 3.64:

$$J_{\lambda,1} = r_{\lambda,1} \cdot G_{\lambda,1} + \varepsilon_{\lambda,1} \cdot E_{\lambda,1} \tag{3.59}$$

$$J_{\lambda,2} = r_{\lambda,2} \cdot G_{\lambda,2} + \tau_{\lambda,3} \cdot G_{\lambda,3} + \varepsilon_{\lambda,2} \cdot E_{\lambda,2} \tag{3.60}$$

$$J_{\lambda,3} = r_{\lambda,3} \cdot G_{\lambda,2} + \tau_{\lambda,2} \cdot G_{\lambda,2} + \varepsilon_{\lambda,3} \cdot E_{\lambda,3} \tag{3.61}$$

$$J_{\lambda,4} = r_{\lambda,4} \cdot G_{\lambda,4} + \varepsilon_{\lambda,4} \cdot E_{\lambda,4} \tag{3.62}$$

$$J_{\lambda,5} = r_{\lambda,5} \cdot G_{\lambda,5} + \varepsilon_{\lambda,5} \cdot E_{\lambda,5} \tag{3.63}$$

$$J_{\lambda,6} = r_{\lambda,6} \cdot G_{\lambda,6} + \varepsilon_{\lambda,6} \cdot E_{\lambda,6}, \tag{3.64}$$

as suggested by Pettersson and Stenström [160] and by Lampinen et al. [173]. In generic matrix form, for n involved surfaces, the relation is given by Equation 3.65:

$$[J_{\lambda,j}]_{n\times 1} = [r]_{n\times n}\,[G_{\lambda,j}]_{n\times 1} + [\tau]_{n\times n}\,[G_{\lambda,j}]_{n\times 1} + [\varepsilon]_{n\times n}\,[E_{\lambda,j}]_{n\times 1}\,, \tag{3.65}$$

where relations from Equation 3.60 and Equation 3.61, which are related to the quartz envelope, contemplates the transmission $\tau_{\lambda,i}$ between both inner and outer surfaces due to the glass being a semitransparent medium. The term $r_{\lambda,i}$ refers to the reflectivity of the body and the term $\varepsilon_{\lambda,i}$ refers to the emissivity; all surfaces are considered diffuse grey bodies. The correlation given in Equation 3.64 refers to the surroundings, considered as a black body, acting as a heat sink as the temperature is known and kept constant over time. According to specialized literature,[160, 163, 171, 175], it is defined $r_{\lambda,6} = 0$.

The second step is to consider the irradiation balance on the different surfaces by using Equation 3.66:

$$A_i \cdot G_{\lambda,i} = \sum_{j=1}^{n} \left[A_j \cdot J_{\lambda,j} \cdot F_{j-i}\right], \tag{3.66}$$

where F_{j-i} is the view factor from surface j to surface i, A_i and A_j are the areas of surfaces i and j respectively.

From the view factor reciprocity property, presented in Equation 3.67, the expression from Equation 3.66 can be written as in Equation 3.68, or in its compact form as presented in Equation 3.69.

$$A_i \cdot F_{i-j} = A_j \cdot F_{j-i} \tag{3.67}$$

$$A_i \cdot G_{\lambda,i} = A_i \cdot J_{\lambda,1} \cdot F_{i-1} + A_i \cdot J_{\lambda,2} \cdot F_{i-2} + A_i \cdot J_{\lambda,i} \cdot F_{i-i} + \cdots + A_i \cdot J_{\lambda,n} \cdot F_{i-n} \tag{3.68}$$

$$G_{\lambda,i} = \sum_{j=1}^{n} J_{\lambda,j} \cdot F_{i-j} \tag{3.69}$$

From a computational point of view, Equation 3.69 can be written as presented in Equation 3.70 for n surfaces.

$$[G_{\lambda,i}]_{n\times 1} = [F]_{n\times n}\,[J_{\lambda,j}]_{n\times 1} \tag{3.70}$$

To solve this equation system, Equation 3.65 and Equation 3.70 are combined, leading to Equation 3.71 enabling the irradiation computation.

$$[G_{\lambda,i}]_{n\times 1} = \left([I]_{n\times n} - [F]_{n\times n}\left([r]_{n\times n} + [\tau]_{n\times 1}\right)\right)^{-1} [F]_{n\times n}\,[\varepsilon]_{n\times n}\,[E_{\lambda,i}]_{n\times 1} \tag{3.71}$$

Then, the results obtained using Equation 3.71 are used in Equation 3.65 to calculate the Radiosity $J_{\lambda,i}$. This allows the computation of the net radiative flux, leaving each involved surface per unit area defined as in Equation 3.57, which are the boundary conditions needed to solve the lamp, Equation 3.1, Equation 3.7 and Equation 3.9, the reflector Equation 3.14 and the material Equation 3.36 temperatures.

3.8.2 View factors

The view factors used in Equation 3.59 through Equation 3.64 are taken from specialized literature [88, 163, 171, 172, 176], as well as the enclosure view factor, Equation 3.72, and the reciprocity relation, Equation 3.67.

$$\sum_{j=1}^{n} F_{i-j} = 1 \tag{3.72}$$

As mentioned before, the lamp is modelled as a solid tungsten cylinder inside a quartz glass envelope (enclosure), thus, the view factor for infinitely long concentric cylinders can be expressed as Equation 3.73, Equation 3.74 and Equation 3.75, which indices refer to the notation shown in Figure 3.9.

$$F_{1-2} = 1 \tag{3.73}$$

$$F_{2-1} = \frac{d_{coil}}{d_l} \tag{3.74}$$

$$F_{2-2} = 1 - F_{2-1} \tag{3.75}$$

The view factor from an infinitely long cylinder to an infinitely long rectangle can be obtained using the scheme presented in Figure 3.10a. The case presented in Figure 3.10b is a particular case when of the view factor from Figure 3.10a when $b_1 = b/2$.

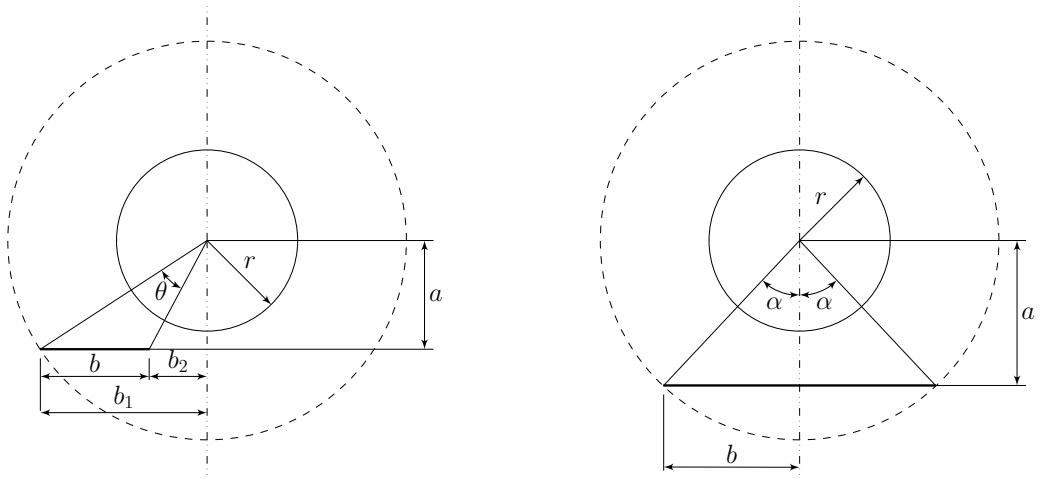

Figure 3.10: View factor between a cylindrical surface and a plane surface. **(a)** Rectangle not aligned with the cylinder vertical center line. **(b)** Rectangle symmetrically aligned with the cylinder vertical center line.

The relation to calculate the different view factor values for the case between the lamp and the reflector, and the lamp and each material cell are expressed in Equation 3.76 and Equation 3.77 respectively, where the subscript *cyl.* refers to the outer lamp surface labelled as "3" in Figure 3.9, the subscript *rect.* refers to the reflector labelled as "4" and, the material labelled as "5" in the same figure.

$$F_{cyl.-rect.} = \frac{1}{2 \cdot \pi} \left(\tan^{-1} \frac{b_1}{a} - \tan^{-1} \frac{b_2}{a} \right) \tag{3.76}$$

$$F_{rect.-cyl.} = \frac{r}{b} \left(\tan^{-1} \frac{b_1}{a} - \tan^{-1} \frac{b_2}{a} \right) \tag{3.77}$$

The view factors between two planar surfaces, in the 2D case, can be expressed using the Hottel's cross string method [172]. Figure 3.11 shows the different components of this method. The values L_1, L_2, L_3, L_4, L_5 and L_6 are lengths, being L_1 and L_2 the surfaces' involved in the view factor and the remaining values distances between the edges of the surfaces, in this case, the cells of the finite volume method.

The view factor using the Hottel's method is expressed as in Equation 3.78 for the case $F_{L_1-L_2}$ and in Equation 3.79 for the case $F_{L_2-L_1}$.

$$F_{1-2} = \frac{(L_5 + L_6) - (L_3 + L_4)}{2 \cdot L_1} \tag{3.78}$$

$$F_{2-1} = \frac{(L_5 + L_6) - (L_3 + L_4)}{2 \cdot L_2} \tag{3.79}$$

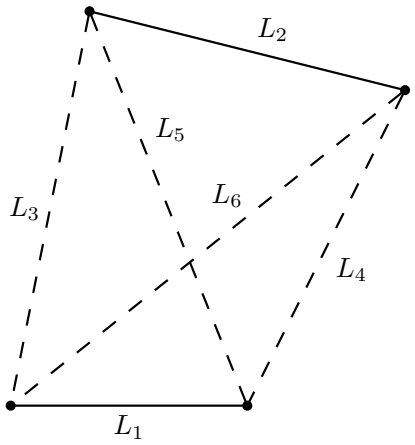

Figure 3.11: Two dimensional planar geometry. Hottel's method

3.8.3 Optical properties

The optical properties required by the system of equations, presented in Equation 3.65, for each surface type, are wavelength-dependent. For general surfaces, the relation among its optical properties is expressed by Equation 3.80, and for the case of opaque surfaces which have no transmissivity $\tau = 0$, the relation among its optical properties is expressed by Equation 3.81 [94, 167].

$$r + \alpha + \tau = 1 \tag{3.80}$$

$$\varepsilon \approxeq \alpha = 1 - r \tag{3.81}$$

To estimate the thermal-optical properties of the opaque, metallic surfaces involved in the machine assembly, the Maxwell electromagnetic wave theory gives the emissivity value as presented in Equation 3.82, that when used in Equation 3.81 leads to the reflectivity.

$$\varepsilon_{n,\lambda} = \frac{4 \cdot n_o}{n_o^2 + k_o^2 + 1 + 2 \cdot n_o}, \tag{3.82}$$

where n_o and k_o are given by Equation 3.83 and Equation 3.84 respectively:

$$n_o^2 = \frac{1}{2}\left(\sqrt{\left(\frac{\epsilon}{\epsilon_0}\right)^2 + \left(\frac{\lambda}{r_i \cdot 2 \cdot c_0 \cdot \epsilon_0}\right)^2} + \frac{\epsilon}{\epsilon_0}\right) \tag{3.83}$$

$$k_o^2 = \frac{1}{2}\left(\sqrt{\left(\frac{\epsilon}{\epsilon_0}\right)^2 + \left(\frac{\lambda}{r_i \cdot 2 \cdot c_0 \cdot \epsilon_0}\right)^2} - \frac{\epsilon}{\epsilon_0}\right) \tag{3.84}$$

with:

ϵ/ϵ_0: Relative material i permitivity.

ϵ_0: Vacuum permitivity $[\mathrm{F} \cdot \mathrm{m}^{-1}]$.

r_i: Resistivity of element i, $[\Omega \cdot \mathrm{m}]$, for the tungsten filament the resistivity value is given by Equation 3.6, for reflector the resistivity is given by Equation 3.85 [168, 177].

$$r_r = -1.1961 \times 10^{-8} + 1.5272 \times 10^{-10} \cdot T_r - 9.4257 \times 10^{-14} \cdot T_r^2 + 7.2288 \times 10^{-17} \cdot T_r^3 \quad (3.85)$$

For the tungsten filament the value of the relative permitivity is $\epsilon/\epsilon_0 = 1.000068$ and for the reflector $\epsilon/\epsilon_0 = 1.00000065$ according to Edwards and Steer [178].

The optical properties of the quartz glass envelope are gathered from specialized literature on the study of infrared dryers as from the work of Lampinen et al. [173], and from the work of Wentink and Planet [179], where the required values are reported.

The emissivity value used in Equation 3.64 is $\varepsilon_\lambda = 1$ as surroundings are considered as black bodies [94].

The optical properties related to the composite material are discussed further in this chapter in Section 3.9.4.

3.9. Composite Material characterization

As a case of study for the ATL process, the employed material is a carbon fibre reinforced Polyamide 6 (PA6) tape from Toray® with the commercial denomination Cetex TC910®, it is 50 mm width, 0.16 mm thickness, and has a fibre content of 60% [180].

3.9.1 Heat capacity

Equation 3.36, requires the material heat capacity as a function of temperature, $cp_m(T_m)$. An experimental procedure was performed according to norm ASTM E 1269-9901 [156] to three material samples, which weights are reported is Table 3.2. The test apparatus used was a TA Instruments Q20, which characteristics are shown in Table 3.3.

Table 3.2: Composite material test specimens for the Differential Scanning Calorimetry experimental procedure.

Specimen number	Weight
1	17.2 mg ± 0.21 mg
2	13.1 mg ± 0.22 mg
3	10.1 mg ± 0.22 mg

The results of the experimental tests for the three composite material samples are shown in Figure 3.12a, Figure 3.12b and Figure 3.12c for a temperature range of 300 K < T < 508 K.

Figure 3.12d shows the average specific heat of the three tested specimens, along the temperature range of 300 K < T < 508 K, indicating an approximate melting temperature of 495 K (221.85 °C).

3.9.2 Density

Another parameter required for the composite material model Equation 3.36 is the material density. The material density is measured according to the ASTM D 792-07 standard [155].

Table 3.3: Test apparatus characteristics for the Differential Scanning Calorimetry.

Characteristic	Value
Temperature range	-180 °C to 725 °C
Temperature accuracy	± 0.1 °C
Calorimetric reproducibility	± 1%
Calorimetric precision	± 0.1 %
Dynamic measurement range	± 350 mW
Baseline reproducibility	< 0.04 mW
Sensitivity	1.0 µW

The results of measuring 10 composite material samples are presented in Table 3.4.

Table 3.4: Composite material test specimens for the density measurements experimental procedure.

Specimen	Weight (dry) [g]	Weight (in water) [g]	Density [g/cm^3]
1	2.125	0.541	1.338
2	1.684	0.483	1.398
3	1.516	0.405	1.361
4	1.964	0.586	1.421
5	1.558	0.361	1.298
6	1.992	0.491	1.324
7	1.826	0.480	1.357
8	2.160	0.523	1.319
9	1.553	0.367	1.309
10	1.625	0.449	1.382
Mean	1.800	0.469	1.350
STD	0.246	0.074	0.040

3.9.3 Thermal conductivity

The thermal conductivity is another parameter required for solving Equation 3.36. This composite material parameter is temperature dependent. The most common procedure to determine this parameter is using the flash method described in the ASTM E1461-13 [157] standard, which requires the preparation of a specimen of 10-25 mm in diameter. As the required thermal conductivity parameter for the model is parallel to the alignment of the fibres, in an Uni-directional composite material, it arises a problem related to the cost of producing the specimens according to the standard.

To address the problem, an in-house procedure is designed to determine the thermal conductivity property as a function of temperature, based on theoretical and practical works proposed by Zhai et al. [109], Villière et al. [103], Betta et al. [102] and Yang [101]. The in-

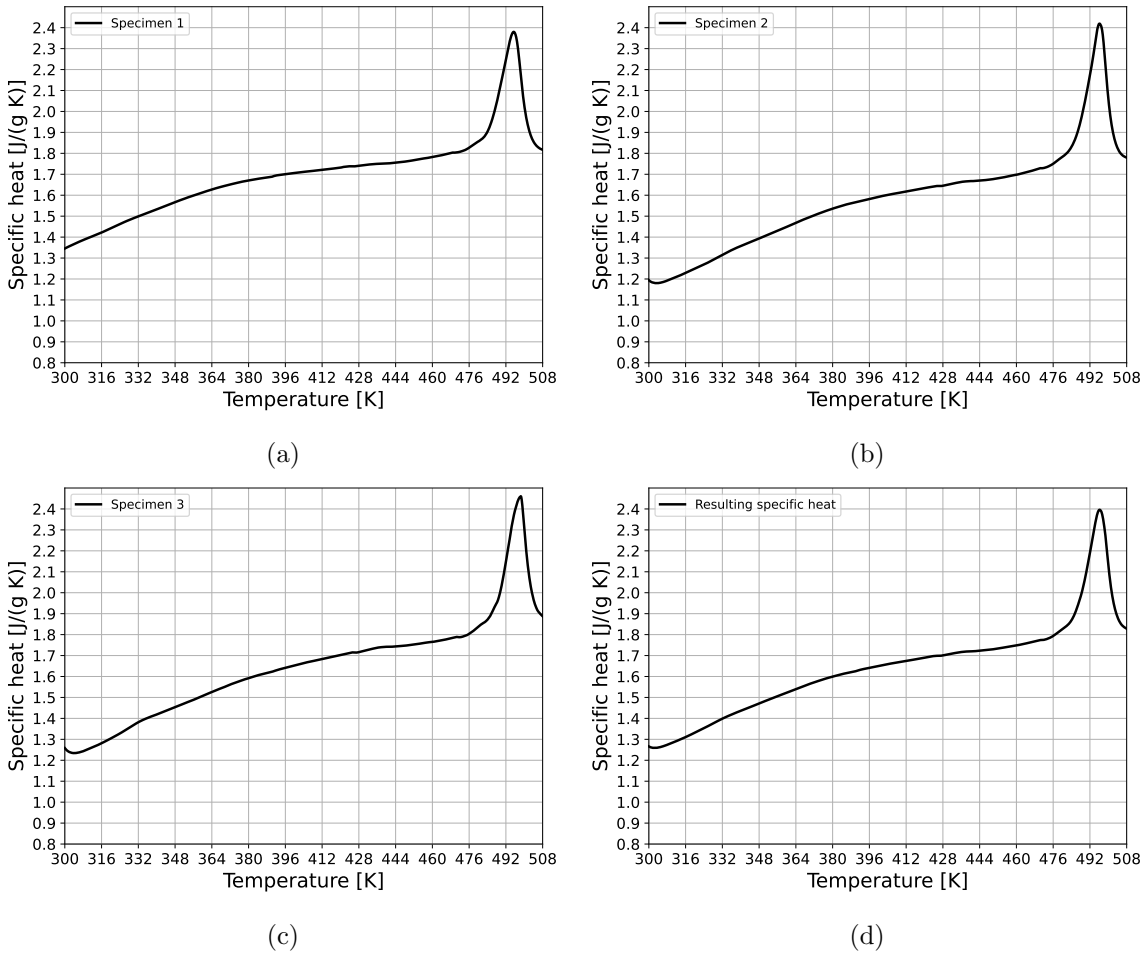

Figure 3.12: Test results for the Differential Scanning Calorimetry test. **(a)** Specimen 1. **(b)** Specimen 2. **(c)** Specimen 3. **(d)** Mean value for Specimens 1, 2 and 3.

house procedure aims to calculate the thermal conductivity along one direction. It consists on simultaneously measuring the temperature variation over time at three aligned and equally separated locations. Figure 3.13 shows a general disposition of three temperature sensors. The test specimen is designed to be narrow, compared with its length, minimizing the effect of 2-dimensional thermal conduction. The specimen is heated at one end and left free at the opposite end.

The test uses a finite difference approach, Equation 3.86, to use the three measured temperatures, at a sampling time p, to compute a thermal conductivity as a function of temperature.

$$k_m(T_i^p) = \left(\frac{T_i^{p+1} - T_i^p}{\Delta t} \right) \cdot \left(\frac{\rho_m \cdot cp(T_i^p) \cdot \Delta x^2}{T_{i+1}^p - 2 \cdot T_{i+1}^p + T_{i-1}^p} \right) \tag{3.86}$$

The heating element, shown in Figure 3.13, is an aluminium plate with an attached electrical resistance, being the main objective to effectively distribute heat to the composite material specimen due to the mass difference.

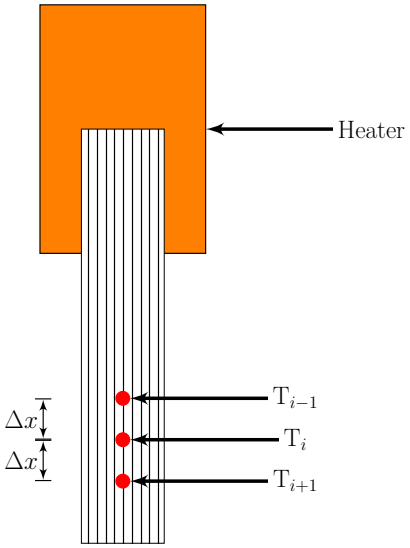

Figure 3.13: Temperature sensors location along the test specimen.

The temperature sensors used are type-T thermocouples, which temperature range covers from -270.0 °C to 370.0 °C with an accuracy of ±1.0°C according to a standard tolerance class as indicated by ASTM E230 standard [181] and specialized literature Holmsten et al. [182], Kee et al. [183]. This thermocouple type is suitable for the test considering the melting point of the composite material matrix is around 220 °C according to the results presented in Figure 3.12d. The output signal from the type-T thermocouple is measured by a NI-9211 data acquisition card.

To minimize interferences due to heat exchanges by external radiation sources and convection, the test is performed inside a vacuum chamber. The vacuum chamber is capable of reaching internal pressures lower than 1.0×10^{-3} mbar. Figure 3.14 shows the general assembly, that will be placed inside the vacuum chamber, of a composite material specimen mounted on an aluminium structure, with three thermocouples for the thermal conductivity calculation, the heating element and a fourth thermocouple for monitoring the heating element temperature. This last thermocouple is placed for safety reasons.

The test specimens' geometrical characteristics are presented in Table 3.5. The procedure is performed using a 1000 W electrical heater connected to a 60 V direct current power source. The thermocouples' separation is defined as $\Delta x = 5$ mm. Once the vacuum chamber is closed, and the interior temperature stabilizes as a result of the generated vacuum, the test starts until a target temperature is reached. Figure 3.15a, Figure 3.15b and Figure 3.15c shows the results of the temperature evolution of one hour test for the three tested specimens.

Table 3.5: Test specimens for the in house thermal conductivity test

Specimen	Length [mm]	Width [mm]	Thickness [mm]
1	100.21	4.98	0.14
2	100.35	5.07	0.14
3	100.19	5.11	0.15

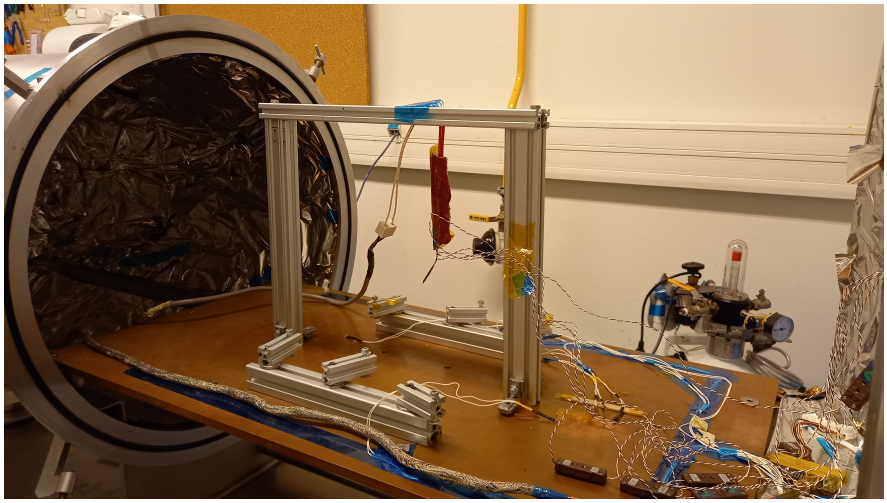

Figure 3.14: In house thermal conductivity test. General view of the test assembly.

Using the data collected from the composite material specific heat test, Figure 3.12d, the thermal conductivity is computed using Equation 3.86, resulting in the data shown in Figure 3.15d.

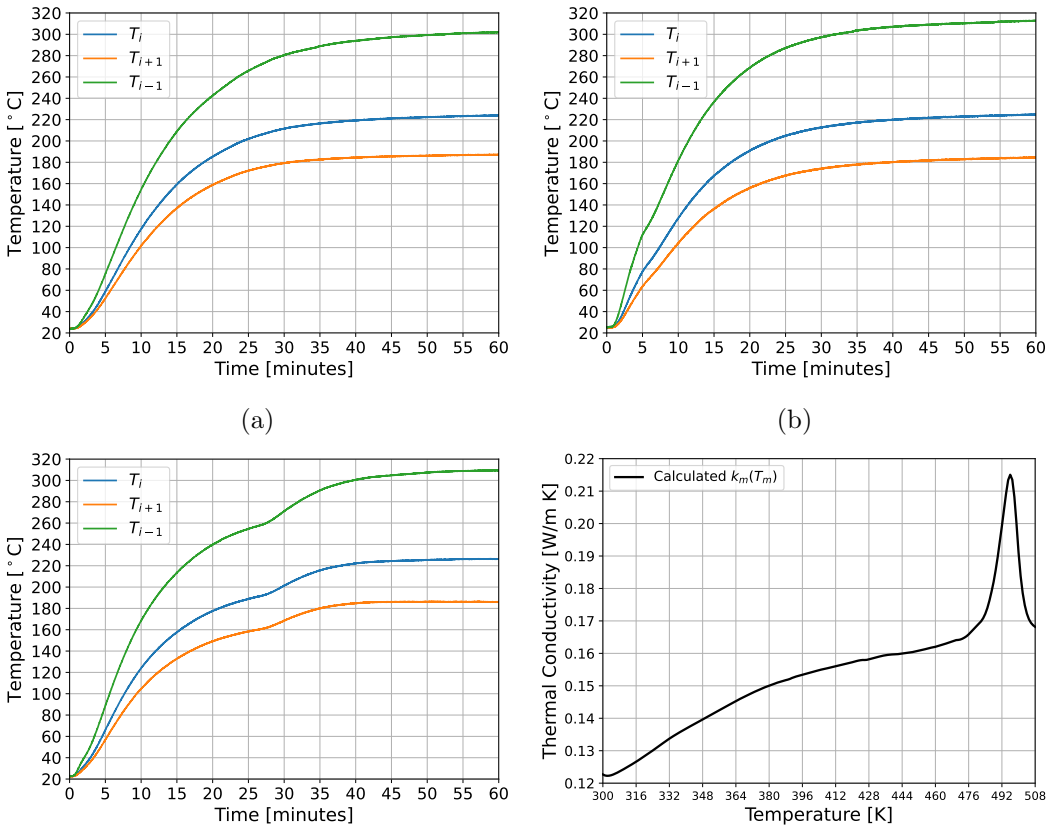

Figure 3.15: Results of the temperature measurements for the three thermal tests based on the in house designed test for thermal conductivity determination. **(a)** specimen 1. **(b)** specimen 2. **(c)** specimen 3. **(d)** computed thermal values.

3.9.4 Thermal optical properties

To obtain the emissivity, $\varepsilon_m(T_m)$, and reflectivity, $r_m(T_m)$ of the composite material as a function of temperature, an in-house test was designed based on the procedure indicated by pyrometer manufacturers to determine the emissivity of the object being measured [184]. The procedure states that the pyrometer emissivity value has to be set manually until it matches the value measured by a contact sensor located at the same target object.

The in-house test consists of heating the composite material sample, inside a closed enclosure preventing interferences due to convection and radiation from external sources, and measuring its temperature using two types of sensors. The composite material sample is a single layer of the PA6 tape. The composite material is placed on top of a aluminium flat plate, which mass is greater than the composite material sample to ensure a better heat distribution. The aluminium plate is heated using an electrical resistance connected to a regulated 60 V direct current power source. The sample surface temperature is measured simultaneously using a set of three T-type thermocouples and a pyrometer from Optris®, model CS LT [184] which characteristics are presented in Table 3.6, with an attached focus lens that can be used to adjust the measured area, as shown in Figure 3.16.

Table 3.6: Optris® pyrometer model CS LT technical specifications

Specification	Value
Temperature range	-50 °C to 1030 °C
Spectral range	8 to 14 µm
System accuracy at 23 ± 5 °C	± 1.5%
Repeatibility at 23 ± 5 °C	± 0.75%

The pyrometer is configured to read the target object as a black body, $\varepsilon = 1$. The sample is heated until it reaches the required temperature. The collected data is used in Equation 3.87 and Equation 3.88 to compute an emissivity and reflectivity value as a function of temperature respectively.

$$\varepsilon_{\text{real}}(T_{\text{material}}) = \frac{\varepsilon_{\text{optical}} \cdot T^4_{\text{optical}} - T^4_{enclosure}}{T^4_{\text{material}} - T^4_{\text{enclosure}}} \tag{3.87}$$

$$r_{\text{real}} = 1.0 - \varepsilon_{\text{real}} \tag{3.88}$$

where:

$\varepsilon_{\text{optical}}$: emissivity value defined at the pyrometer.

T_{optical}: temperature reported by the pyrometer with $\epsilon_{\text{optical}} = 1$, [K].

$T_{\text{enclosure}}$: enclosure walls temperature, [K]

T_{material}: mean temperature measured by the thermocouples, [K].

ϵ_{real}: corrected emissivity value.

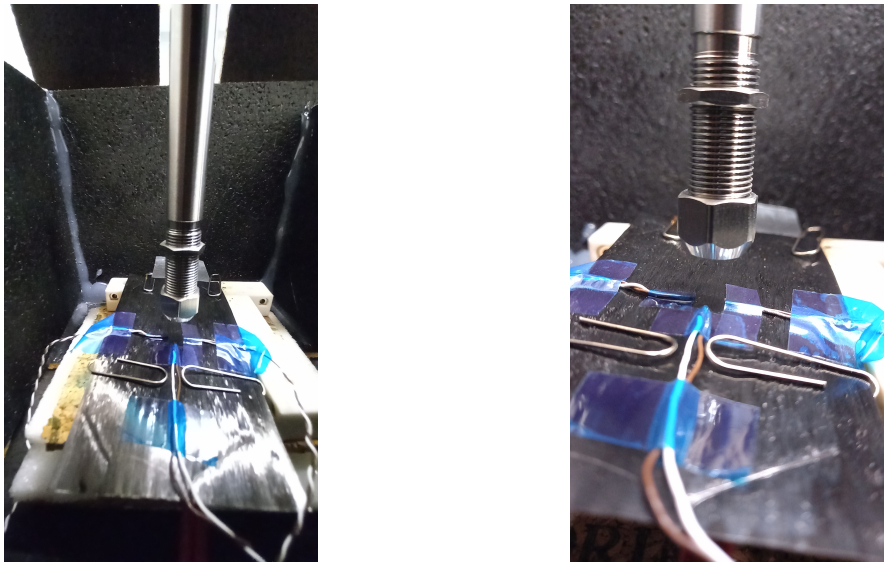

(a) (b)

Figure 3.16: Test apparatus for the in house designed test to determine optical properties as function of temperature. **(a)** general view of the composite, the pyrometer and the enclosure. **(b)** closed view of the placement of the thermocouples and the pyrometer distance from the objective for a measuring area of 5 mm diameter.

The results of testing three composite material samples are presented in Figure 3.17a, Figure 3.17b and Figure 3.17c, which shows the emissivity and reflectivity values based on the composite surface temperature.

3.10. Methods

3.10.1 Time Integration Scheme

The mathematical model involves a set of non-linear ordinary differential equations (ODE) for the temperature time derivative of the different components, namely the tungsten filament, Equation 3.1, the quartz lamp, Equation 3.9, the reflector cell temperature, Equation 3.17, and the material cell temperature, Equation 3.37. To solve this ODE system, the initial conditions are set to be at ambient temperature for all the components. The implicit solver Radau IIA is selected from the Scientific Python library as proposed by Hairer and Wanner [185], to avoid time-step limitations due to equation stiffness.

The ODE equation system is structured in an array-like way as an explicit function of the given trial temperature suitable for the external solver. To evaluate the ODE system, the following steps are performed:

Step 1. Set the given trial temperature.
Step 2. Evaluate all material properties at the trial temperature.
Step 3. Solve the radiation heat flux system for the trial temperature.
Step 4. Evaluate the ODE system array with the temperature derivatives.
Step 5. Update the trial temperatures for all the elements involved in the system.
Step 6. Repeat from step 2 for the next time step.

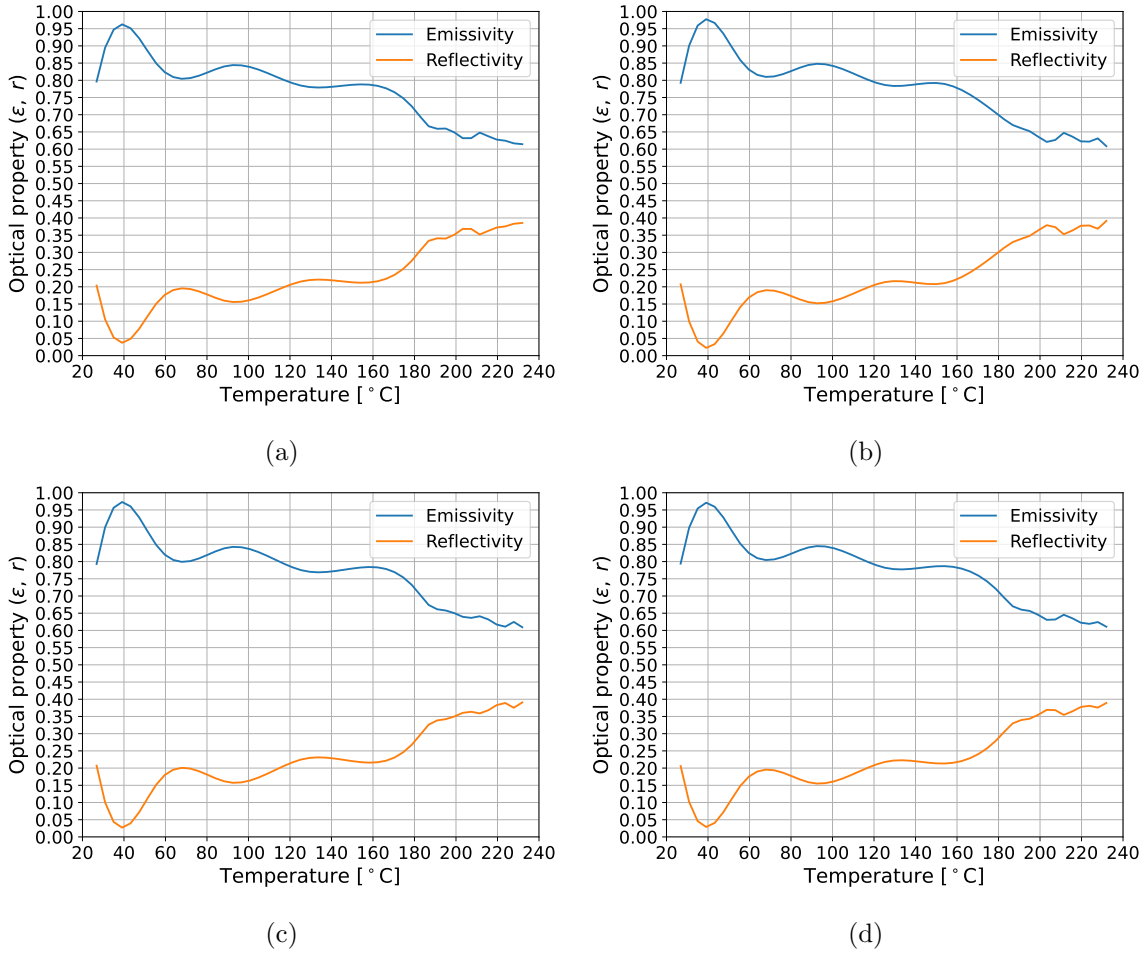

Figure 3.17: Results of the tests for emissivity and reflectivity. **(a)** specimen 1. **(b)** specimen 2. **(c)** specimen 3. **(d)** mean value.

The model solver consists of two parts, the first one being the calculation of the net radiation flux using the current temperature as a reference to determine all the properties required. The second part consists of implementing the result of the net radiation flux as an input to predict the process component temperature at the next time step. Finally, the new temperatures are used to calculate a new net heat flux then, the cycle repeats until a defined stop time. The relative error tolerance for the solver is set to 10^{-4} and the absolute error tolerance to 10^{-6}.

3.10.2 Convergence Analysis

A convergence analysis is performed to define a proper cell size for the material simulation to lower the required computational resource consumption using the lowest mesh size. Mesh sizes from 11 cells up to 239 cells were tested for the material. The mesh for the reflector was defined using the same cell size used for the material, regardless of the number of cells, to preserve stability during computation. Taking into account the temperature percentage variation using three selected points as a reference namely, the first cell at which the material has its first interaction with the heat exchange process, the middle cell along the length of

the material and, the last cell of the material. The mesh size is selected based on the lowest number of cells giving a temperature variation under 0.5% concerning a mesh size of 239 cells. The number of cells defined using odd values is intended to guarantee a central cell along the mesh at the same position regardless of the mesh size.

3.10.3 Measures and Instrumentation

To measure the process parameters and the variables needed to feed the mathematical model, two types of data acquisition cards from National Instruments were used. A NI 9234 for voltage measurements and a NI 9211 for temperature measurements. The NI 9234 data acquisition card allows high sampling rates, making it adequate for measuring the 50 Hz frequency mains voltage that feeds the heating element.

Electrical power

To compute the electrical power delivered to the heating element, the applied voltage and the current consumption must be measured. A ferrite voltage transformer is used to step down the mains voltage sine wave to a safer range for the data acquisition card, as well as to provide galvanic isolation for the measurement equipment. For the current measurement, a non-invasive current transformer is placed around one of the lines powering the heating element. The output of this transformer is a voltage signal, read by the same data acquisition card reading the mains voltage signal. The measurement strategy used for the voltage and current is presented in Figure 3.18.

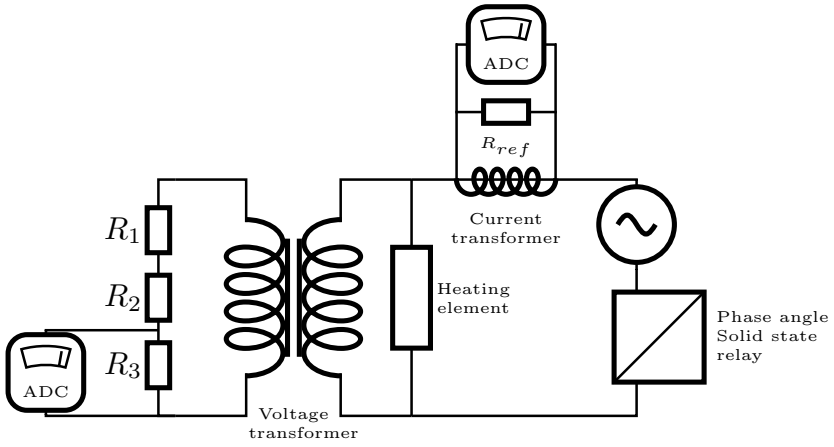

Figure 3.18: Voltage and current measurement strategy for electrical power consumption calculation.

Temperatures

To measure the temperatures involved, a set of T-type thermocouples are placed at the following locations: the compaction roll fluid inlet and outlet, on the top surface of the mould and another at the top of the machine assembly to measure the ambient temperature. The composite material temperature is measured using a pyrometer model PyroNFC K from CALEX [186], which specifications are presented in Table 3.7, facing the composite material

at a point "h" above the centre line of the compaction roll, as presented in Figure 3.19. The output of the pyrometer is a thermocouple-like signal that can be read by the same data acquisition card, NI 9211, as the other thermocouples.

Table 3.7: Calex® PyroNFC K pyrometer technical specifications

Specification	Value
Temperature range	0 °C to 1000 °C
Spectral range	8 to 14 µm
Accuracy	±1.5% of reading
Repeatability	±1.5% of reading

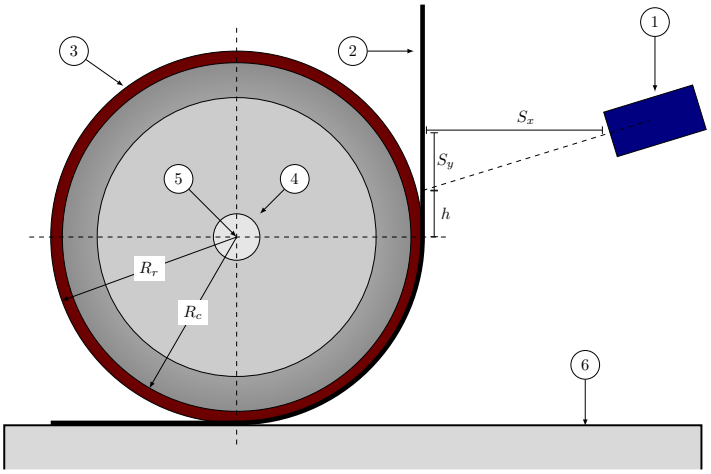

Figure 3.19: Composite material temperature measurement scheme. (1) Pyrometer PyroNFC-K. (2) Incoming composite material. (3) Compaction roll. (4) Compaction roll axis; fluid inlet/outlet ports. (5) Inlet fluid temperature sensor; outlet temperature sensor located at the other end of the axis. (6) Mould temperature sensor.

Process speed

The last parameter to measure is the process speed. This value is obtained directly as a voltage signal from the analogue output of the servo motor driver OMROM R88D-KN08H-ECT controlling the process. This value is read by the NI 9234 data acquisition card.

3.11. Process model validation

The experimental validation is performed in two parts. The first part consists of validating the temperature dynamics of the material at the measuring point, as shown in Figure 3.19, using a constant set of parameters: process speed, compaction roll temperature, and mould temperature, and imposing changes in the voltage applied to the heating element. This voltage variation is conducted using a solid state relay that, taking advantage of a phase angle strategy to reduce the delivered root mean square voltage, controls the electrical power delivered to the heating element.

The compaction roll temperature and the mould temperature are kept constant because any change to their respective reference generates a slow response in comparison with changes in the reference for the voltage delivered to the heating element.

The process speed is kept constant throughout the experiment because the driver controlling the servo motor only has signal outputs to monitor its value. Any change in the defined speed value implies stopping the process and changing it manually over the drivers' software. To see the influence of the speed upon the process, two sets of tests were carried out with different speed values, as presented in Table 3.8.

Table 3.8: Values for the process parameters.

Parameter	Set 1	Set 2
Compaction roll temperature	55 °C	55 °C
Mould temperature	22 °C	22 °C
Process speed	5 mm/s	15 mm/s

To understand the machine parameters' influence on the operation of the ATL, regarding the consolidation temperature of the material tape at the nip point, the proposed test cases presented in Table 3.9 will be simulated.

Table 3.9: Values for the process simulation.

Simulation	Parameters	Value
1	Compaction roll temperature	55 °C
	Mould temperature	22 °C
	Speed	5 mm/s
	Voltage	100 V
	Voltage	150 V
	Voltage	200 V
2	Compaction roll temperature	55 °C
	Mould temperature	22 °C
	Voltage	150 V
	Speed	5 mm/s
	Speed	10 mm/s
	Speed	15 mm/s

3.12. Results

3.12.1 Mesh Convergence

The results obtained for the convergence analysis are shown in Figure 3.20, for a speed value of 5 mm/s in Figure 3.20a, and for a speed value of 15 mm/s in Figure 3.20b, both with a simulation time of 30 seconds and, the same process conditions of initial temperature and electrical power delivered to the heating element, as well as compaction roll, mould, and

ambient temperature.

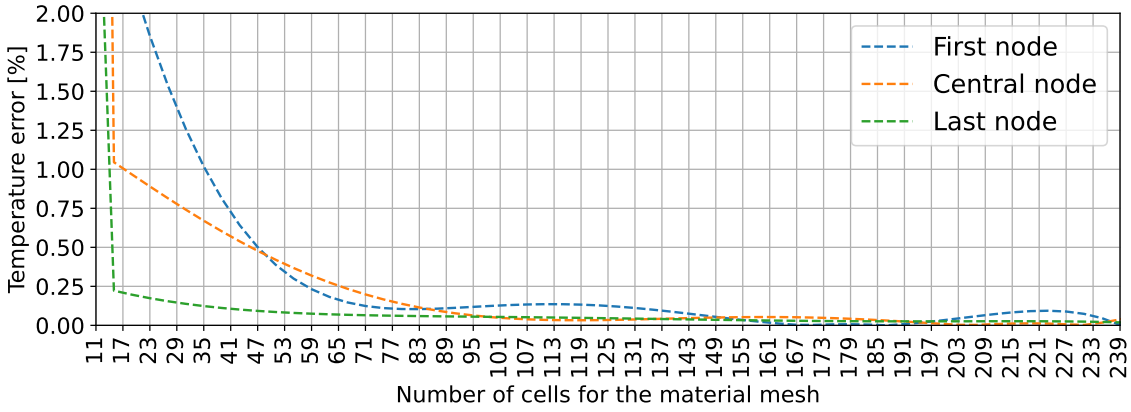

(a)

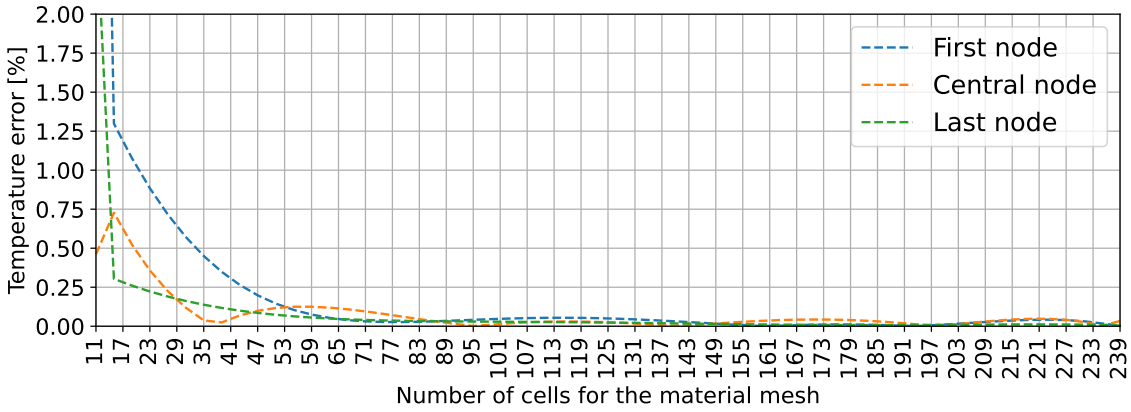

(b)

Figure 3.20: Temperature error as a function of the mesh size for the material. **(a)** speed value 5 mm/s. **(b)** speed value 15 mm/s.

The data presented in Figure 3.20a show that, for a process speed of 5 mm/s, the material temperature value, at the selected locations, tends to stabilize with a relative error below 0.5% for mesh sizes above 47 cells, and for the case of a process speed of 15 mm/s, the error below 0.5% is achieved with a mesh size above 35 cells. From these results, the selected mesh size is 51 cells, corresponding to the scenario presented in Figure 3.20a, with a cell size of $\Delta y = 2.87$ mm.

The reflector cell size is fixed to have the same size as the material, although the reflector mesh size should have less influence.

3.12.2 Process model Validation

To compare the dynamic response of the ATL machine with the predicted response of the proposed numerical model, different tests in which parameters were defined according to the values presented in Table 3.8 as Set 1 and Set 2. Multiple random changes in the voltage supplied to the heating element were performed.

The results for the parameters Set 1 are presented in Figures 3.21 and 3.22, and for Set 2 in Figures 3.23 and 3.24. This was carried out to simulate a possible control action over the heating element and to analyse the transient response of the ATL machine and the composite material.

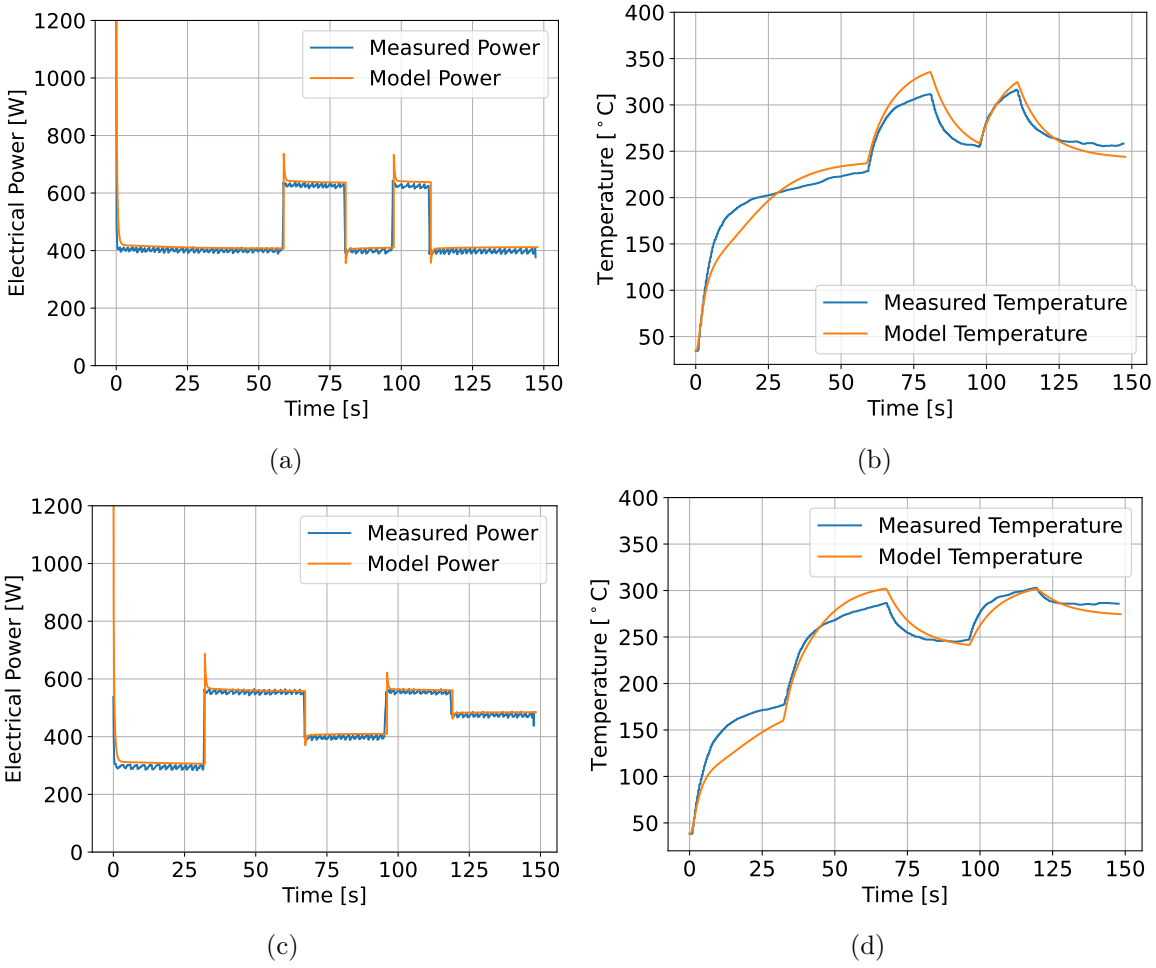

Figure 3.21: Results of Power consumption and temperature variation at the measuring point according to parameter Set 1 from Table 3.8. **(a)** test 1, electrical power. **(b)** test 1, composite temperature response. **(c)** test 2, electrical power. **(d)** test 2, composite temperature response.

First, the predicted power consumption agrees with the experimentally measured response, as shown in Figure 3.21a and Figure 3.21c. This means that the proposed model is capable of predicting the overall energy flow of the system, which is a desirable result because it is based on energy conservation laws.

Comparing the measured temperature with the predicted temperature at the corresponding "machine measurement point", it is verified that the proposed model can predict the heating and cooling dynamics of the system, as shown in Figure 3.21b and Figure 3.21d, using the process speed value, compaction roll temperature, and mould temperature presented in Table 3.8 as Set 1.

The prediction of the material temperature was adjusted by defining a compensation factor for the convection coefficient of the heating element of 5.5, Equation 3.13, and a com-

pensation factor of 2.5 for the convection coefficient of the material, Equation 3.49, to adjust the convection correlations and approximations related to geometry and relative movement [94].

Additionally, the corresponding measurements for the compaction roll temperatures, mould temperature, and process speed for test Set 1 are shown in Figure 3.22a and Figure 3.22b.

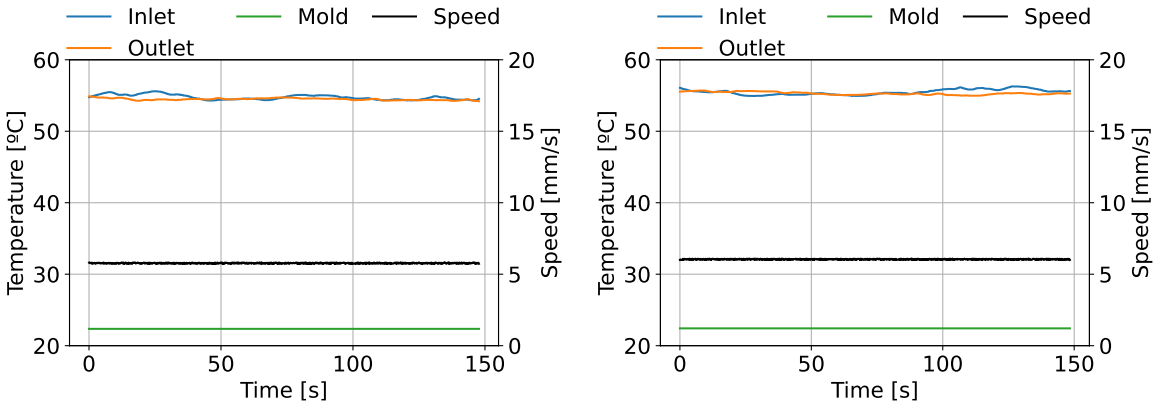

Figure 3.22: Inlet and outlet compaction roll temperatures and speed measurements for two test runs, Set 1 from Table 3.8. **(a)** first test, referring to Figure 3.21a and Figure 3.21b. **(b)** second test, referring to Figure 3.21c and Figure 3.21d.

The test and simulation results for the process parameters presented in Table 3.8 as Set 2 are presented in Figure 3.23, showing the predicted and measured power consumption for the heating element, Figure 3.23a and Figure 3.23c, and predicted and measured temperature for the material at the measuring point, Figure 3.23b and Figure 3.23d.

The model used to predict the composite material temperature at the machine measuring point shown in Figure 3.23b and Figure 3.23d includes the same compensation factors in the convection coefficient for the heating element as well as in the material convection coefficient, showing an acceptable geometrical and relative movement compensation for those values.

The corresponding measurements for the compaction roll temperature, mould temperature, and process speed, for this set of tests, are shown in Figure 3.24.

Comparing the measured temperatures at the same machine measuring point for both process speeds, it is noticed that when defining a machine speed of 15 mm/s, temperatures at this point are lower than the temperatures at the same point when tests are performed with a machine speed of 5 mm/s, showing the influence of the transport phenomena on the temperature evolution over time.

It can be seen that the compaction roll inlet and outlet temperatures are similar in both tests. This fact, added to an internal fluid flow through the compaction roll of 40 l/min produced by a temperature control unit Tool-Temp 137BP, indicates that the internal flow is sufficient to guarantee a constant temperature along the compaction roll, validating the

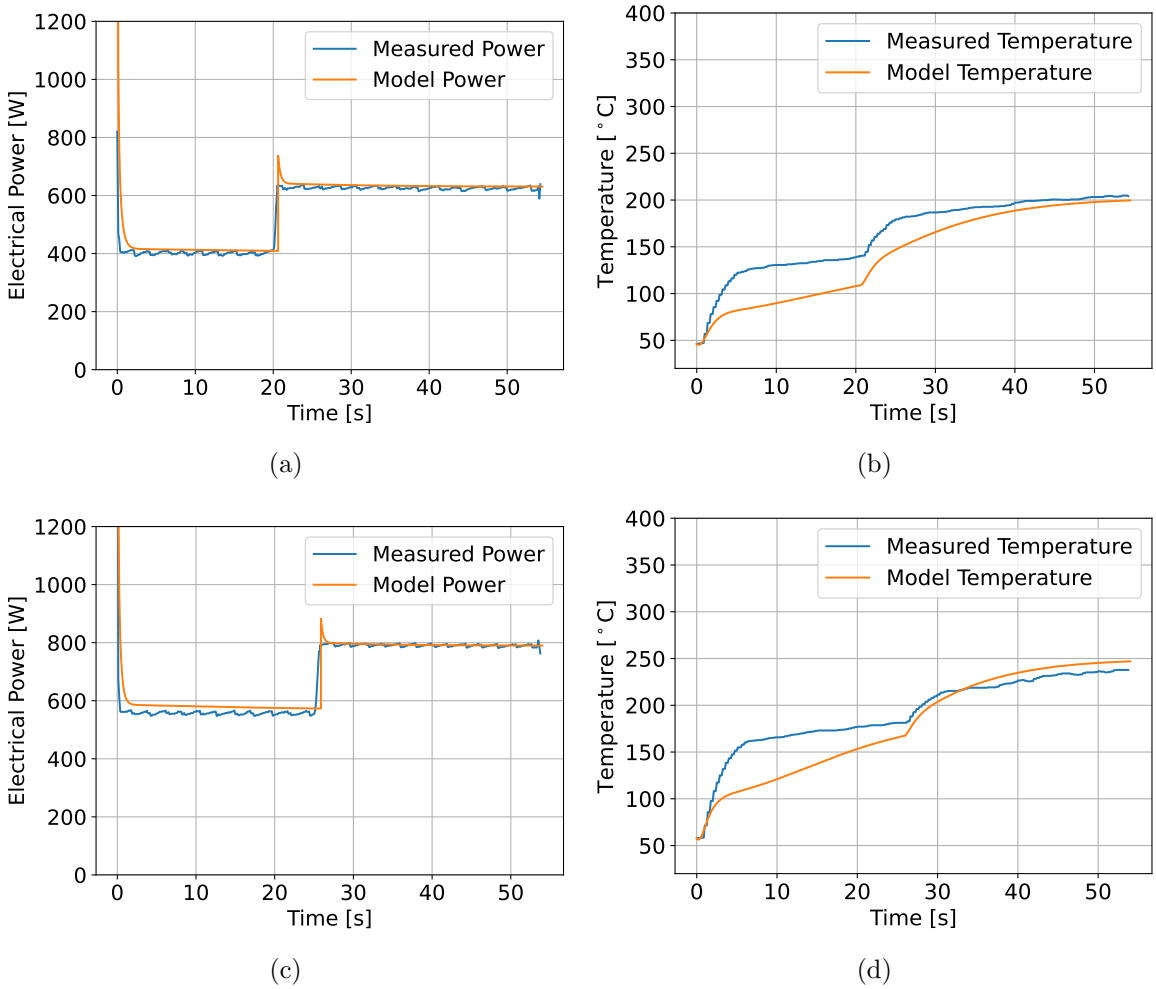

Figure 3.23: Results of power consumption and temperature variation at the measuring point according to parameter Set 2 from Table 3.8. **(a)** Test 1, electrical power. **(b)** Test 1, composite temperature response. (c) Test 2, electrical power. (d)Test 2, composite temperature response.

proposed model assumption of constant temperature given in Section 3.5. So, the need of estimating an overall convection coefficient for the compaction roll internal fluid flow is avoided.

Sensitivity Analysis

The results obtained for the simulations described in Table 3.9 are presented in Figure 3.25 for the simulation in which the speed of the process is kept constant, 5 mm/s, and in Figure 3.26 for the simulation in which the voltage applied to the heating element is kept constant, 150 V. For both simulations, a nip point temperature is estimated to understand the heat propagation as a function of the applied voltage variation and the set speed variation.

For the case presented in Figure 3.25, the simulated temperature at the nip point presents a delay with respect to the temperature at the measured point as expected. This is affected by ambient losses and, heat that is transferred to the compaction roll and the substrate by conduction. Despite of the delay, the value of the simulated temperature at the nip point

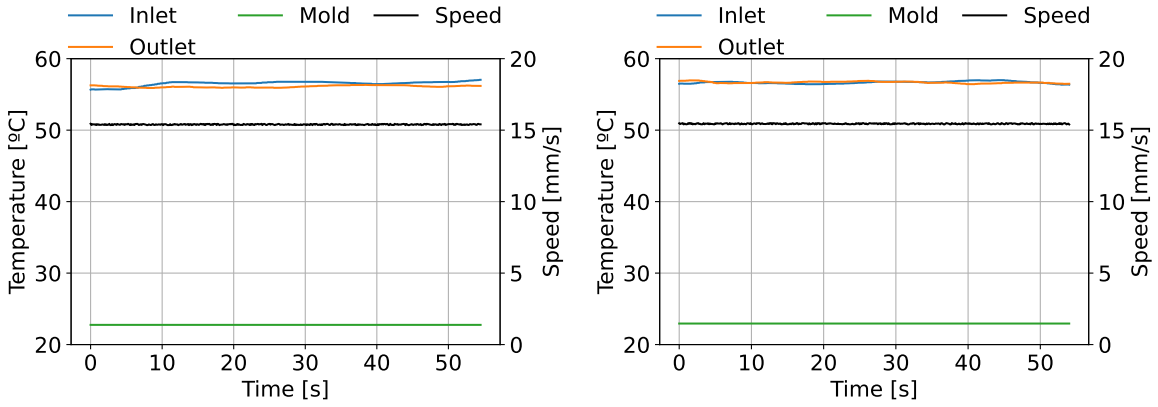

Figure 3.24: Inlet and outlet compaction roll temperatures and speed measurements for two test runs, Set 2 from Table 3.8. **(a)** First test, referring to Figure 3.23a and Figure 3.23b. **(b)** Second test, referring to Figure 3.23c and Figure 3.23d.

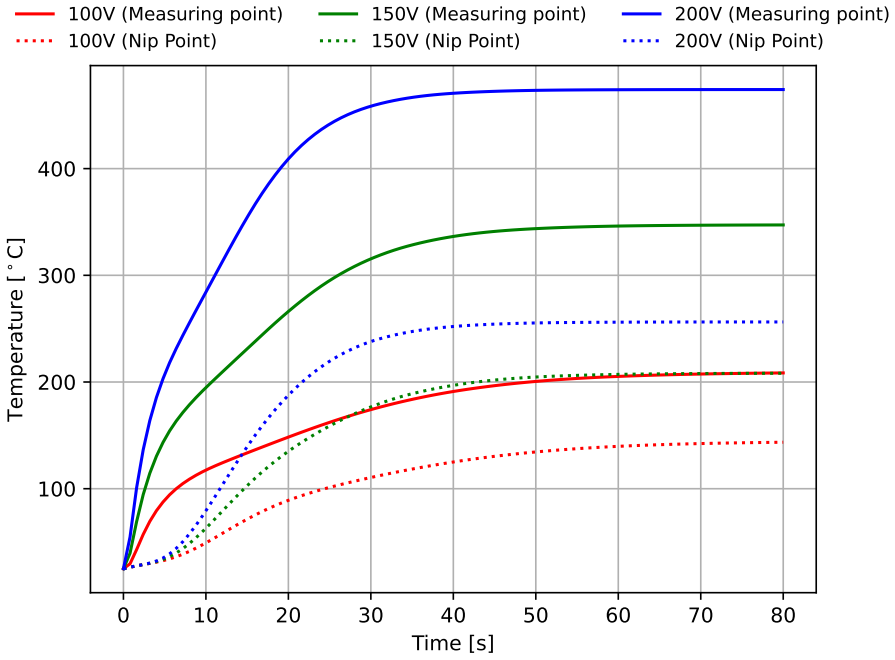

Figure 3.25: Results obtained for the simulations according to the first simulation proposed in Table 3.9. Constant process speed 5 mm/s.

increases as the applied voltage to the heating element is incremented, behaviour that is expected due to the heat losses by convection are strongly dependent on the process speed, that in this case is made constant.

Figure 3.26 also shows a delay in the estimated temperature at the nip point as expected. The main difference, is the amount of time for such delay, meaning that the process speed has a relevant influence over the nip point temperature as its value increases. This effect can be noticed for the simulated speed of 10 mm/s, when after the nip point temperature

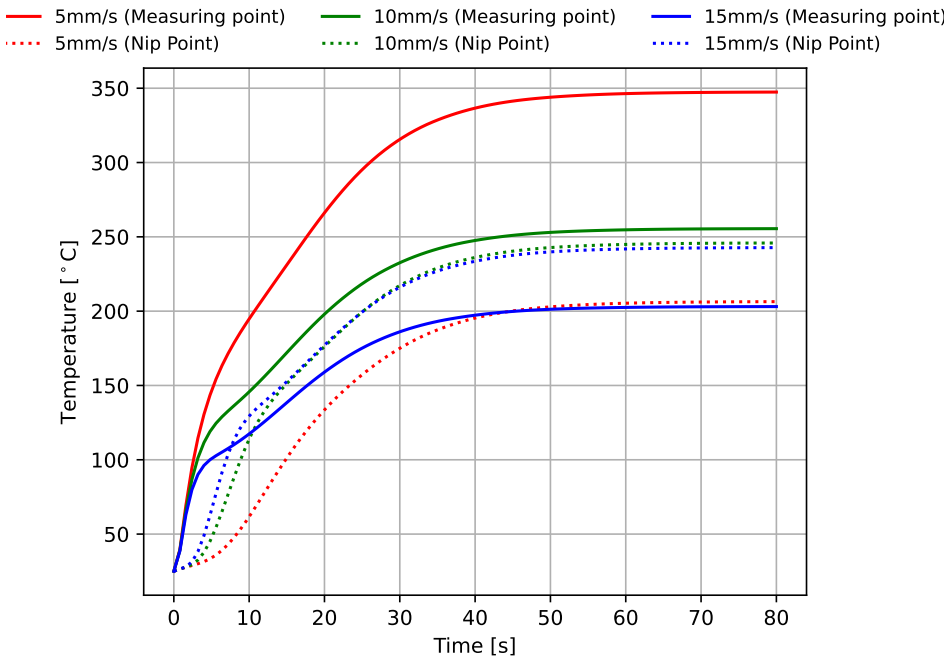

Figure 3.26: Results obtained for the simulations according to the second simulation proposed in Table 3.9.

starts to rise, it almost matches the temperature of the measuring point and, for the case of a speed of 15 mm/s, the temperature experiences an initial delay and rapidly reaches higher values with respect to the measuring point. This behaviour demonstrates the high sensitivity of the system to the feed speed, meaning that the transport phenomena dominate over the conduction and convection losses.

3.13. Concluding remarks

The energy balance model proposed for the heating element can replicate the dynamics of its electrical energy consumption, taking into account its components' properties and geometrical parameters. It is also capable of predicting the outgoing energy flux towards the material being processed, causing the temperature to rise along the material length.

Due to the temperature measurements in both inlet and outlet of the compaction roll, it can be modelled assuming isothermal conditions along its internal fluid section, by ensuring a sufficient fluid flow, causing a temperature gradient along the compaction roll thickness. This assumption simplifies the heat transfer model for this element.

The proposed 1.5D heat transfer model for the ATL machine head can be used to simulate the temperature distribution along the processed material and its dynamics upon changes in the heating element input voltage and process speed, predicting the temperature along the heating zone domain. This feature is desirable for computational efficiency, by not having to calculate a 3-dimensional composite material temperature distribution when the heating element is wider than the composite material width. It is also worth mentioning that the thickness of the pre-impregnated composite material makes possible its simulation with only

one element in that direction. On the other hand, the proposed DT in this work takes into account the effect of the radiation fluxes, which implies solving the inverse of a matrix at each calculation iteration that, for models with a significant amount of elements, can be computationally expensive.

The most relevant parameters that influence the machine behaviour are the input voltage of the heating element, which increases the temperature of the processed composite material by directly heating its surface using radiation, and the process speed, which influences the material temperature through the transport effects.

With this model, which takes into account the thermal and optical properties of the materials involved and their changes with temperature, a DT of the process can be formulated, allowing to develop and implement model-based control strategies, that could use the available actuation elements of the process to control the nip point temperature.

The process DT, conceived as a detailed process model, can be used for selecting the best machine elements by evaluating their capabilities. This applies to the heat source, the required process speed, and the mould temperature. This study can be performed as a function of the composite material being processed in order to guarantee the quality requirements of the final structure. Thus, the study of those effects on an already-built machine can be avoided by minimizing the design time and maximizing economic benefits.

This model not only allows estimating the composite temperature at the measuring point but, an entire temperature profile along the heating zone. This characteristic could be further used by a model-based control strategy as a supervisory function due to maximum restriction at any of the ATL process machine components specially upon the composite material.

Chapter 4

State Estimation

This chapter presents an overview of different methods used for solving the state estimation problem for linear and non-linear systems. It is included in the concept of the Digital Twin as the main process model for highly detailed and complex processes. This chapter also proposes a state estimation strategy, for the ATL process Digital Twin, using an optimization algorithm based on the hybridization of a zero-order and a first-order technique.

This chapter is organized as follows: Section 4.1 introduces the concept of Digital Twin into the state estimation problem. An overview of commonly used algorithms for linear and non-linear systems is described in Section 4.2. The original zero-order optimization technique is described in Section 4.3 and its hybridization is referred to in Section 4.4. Section 4.5 presents the case of study in which the proposed hybrid optimization method is used. The results are presented in Section 4.6 and finally, the concluding remarks are presented in Section 4.7.

4.1. Introduction

The Automated Tape Laying (ATL) process is an out-of-autoclave composite material manufacturing process, requiring lower energy and time consumption to produce a composite structure compared with autoclave processes. ATL contributes to minimizing the scrap material and maximizing the quality of the produced structure by ensuring repeatability.

The ATL process requires the implementation of a proper control technique, allowing to achieve the desired composite material temperature. The implemented control technique requires knowing the temperature of the composite material structure at a specific location, allowing it to compute a decision and perform the corresponding actions. The required temperature location cannot be measured directly, so a state estimator is required to estimate the temperature at the desired location. An example of this implementation was developed in the work of Ali and Zafiriou [187], where the researchers used this strategy to estimate states inside a chemical reactor, where states could not be directly measurable, allowing to implement a Model Predictive Controller (MPC) to compute the optimal control action at each sampling time.

According to how the dynamical response of a system is mathematically defined, linear or non-linear, some state estimation methods have been developed. For linear systems, some of the most popular methodologies are the Kalman Filter and the Luenberger observer, where the equations representing the dynamical responses are used to determine the system states, and using the available state measurements, correct those estimations. For non-linear systems, a commonly used strategy is the Extended Kalman Filter (EKF), which uses a linearized system representation, or a combination of linear representations, allowing to apply the methodologies developed for linear systems.

Another strategy to solve the state estimation problem for linear systems, non-linear systems, or any combination of them [188, 189], involves the use of optimization algorithms to solve a convex objective function [190–192]. The strategy can be defined in two forms, Full Information Estimation (FIE) and Moving Horizon Estimation (MHE). The main difference is that the former includes all measurements in the optimization problem while the second method, only includes a finite number of recent measurements.

With the appearance of the Industry 4.0 tendency, the concept of Digital Twin (DT) has been introduced, which involves the use of highly detailed process models to digitally represent a system, including the component's interactions among each other and its surroundings [52]. This type of system model can be deduced from physical correlations or from a considerable amount of gathered data measured from the process, as suggested by Jin et al. [128]. The concept of DT has been used by Shang et al. [193] to be included in a state estimation methodology, for further control of an irrigation system, estimating different states such as temperature and moisture, taking into account weather forecasts and their respective uncertainties.

The work of Jiang et al. [63] and González et al. [64], also take advantage of the DT concept for state estimation purposes, by using it for what has been denominated as Soft

Sensors, Virtual Sensors, Software sensors, Soft sensing or Physical/Hardware-based sensors. The use of this type of sensor is justified for processes where it may be neither economic nor beneficial to install physical sensors beyond requirement because calibration and maintenance will lead to unnecessary workload and cost. The work of González et al. [64] describes a vertical transportation system by a DT, and uses a EKF to estimate its states. The use of a DT for state estimation has also been included in state estimation strategies using a MHE methodology [131–133].

As industrial processes increase their complexity, their mathematical representation also increases in complexity, motivated by the requirement of having detailed information about the interactions among the elements involved, resulting in more complex DT models, which difficult the application of the former state estimation methods. This tendency has led to the development of other types of state estimation methods, which are based on system simulations and heuristic algorithms applied to a convex cost function [194]. The work of Conejo et al. [195] and Tungadio et al. [194], used a Particle Swarm Optimization (PSO) algorithm to optimize a cost function derived from the state estimation problem of unavailable measurements in a power grid distribution centre. Another heuristic method, Genetic Algorithms (GA), has also been used to solve the state estimation problem in power systems [135, 137, 196–198].

A recent popular choice for optimization technique is the Artificial Bee Colony (ABC), first proposed by Karaboga [144], where the search for food sources of a honeybee hive is mimicked. The search mainly consists of two parts: the exploration of the search domain and the exploitation of the proposed solutions.

The ABC optimization technique has been used, in its original form, for filtering strategies as proposed by Kaba and Kiyak [159] and Raghav et al. [199]. Other authors have used the original ABC for advanced control techniques [150, 200], maximizing problems such as the Direction-Of-Arrival in sonar technologies, as proposed by Zhang et al. [201], for parameter identification in systems where parameters are not constant, and no information is available in literature related to such parameters as in the work of Oliva et al. [202].

The original ABC technique has been adapted by different authors to adjust the method to specific problems. Omkar et al. [203] proposed a Vector Evaluated Artificial Bee Colony (VEABC) for multi-objective design optimization in composite materials, where correlations of failure criteria are used in the exploitation phase to determine how those honeybees are defined. Another modification was proposed by Gao et al. [153], where the Powell's method is used in localized search enhancing the exploitation phase but, despite the increase in speed towards the solution, it won't prevent the oscillation effect around the optimal solution. The work of Hu et al. [136] describes an ABC modification for the exploration phase for defining initial solutions in a hyper-chaotic system and a simulated annealing algorithm for the exploitation phase.

Other authors used another modification of the original ABC technique for solving harmonic estimation problems. This modification involves using the original ABC technique for the first part, the exploration phase, and for the second part, the exploitation phase, using the

least square algorithm, as presented in the work of Biswas et al. [204]. Another modification of the original ABC technique is to implement a multi-hive approach, as suggested by Arslan and Ozturk [205], where the authors assigned a decision tree structure per hive, and all the results are evaluated in the exploitation phase to define a new structure and to continue the search.

This chapter presents a modification to the original ABC technique, where a new strategy for defining the different types of honeybees at the exploration and exploitation phase is presented and, taking advantage of a first-order minimization algorithm, improves the exploitation of the selected solution, improving the convergence and minimizing the oscillation effect around the optimal solution. This modification is implemented as part of a discrete-time state estimation algorithm. The state estimation algorithm is used in an ATL manufacturing process, whose goal is to estimate the temperature distribution along the composite material, with most interest at a location where a temperature sensor cannot be placed. The algorithm uses the information gathered from a temperature sensor located in a more convenient location and the information gathered from sensors measuring the input signals at each sampling time.

4.2. State Estimation of Dynamical Systems

The state estimation problem consists of determining the states of a system, at present instant, from all the available information on the inputs and outputs of the system. State estimation emphasizes the fact that data is incomplete, uncertain or noisy and so, the values obtained for the states of the system will not be exact. The state estimation results are usually used to control a system so, the stability of the entire control loop has to be guaranteed when the state estimator is coupled to a controller. Estimating a state, or a set of states, with a significant error with respect to the real values, may destabilize the control scheme.

There are two approaches for dealing with the state estimation problem, the stochastic and the deterministic approach. The stochastic approach explicitly considers the uncertainty of the data, enabling a quantitative description of the uncertainty of the computed estimates. The most widely used methods for state estimation considering a stochastic approach are the Kalman Filter [112], the minimum variance estimator [123, 124] and the least-squares filter [127]. On the other hand, the deterministic approach disregards the uncertainty of the data when computing the estimates, considering it implicitly as the uncertainty in the data does not have a great influence on the obtained values.

4.2.1 Linear estimation

The state estimation problem for linear systems has been widely studied. Some of the most popular estimation strategies developed are the Kalman Filter (KF), being an efficient solution of the Least-Squares estimator, and the Luenberger observer.

Kalman Filter

The Kalman filter [112] is derived from the Bayesian approach, providing true conditional state estimate in a linear Gaussian setting. It can be defined as the optimal estimator in a least-squares sense since it minimizes the Mean-Sum-Squared-Error of the state estimation error. Consider the discrete-time system presented in Equation 4.1 and Equation 4.2.

$$x\,(k) = A\,x(k-1) + B\,u(k) + w(k) \tag{4.1}$$

$$y(k) = C\,x(k) + D\,u(k) + v(k), \tag{4.2}$$

where k is the discrete time, $x(k) \in \mathbb{R}^s$ is the state of the system, $u(k) \in \mathbb{R}^n$ is the known input, $w(k) \in \mathbb{R}^n$ is the input disturbance, $y(k)$ is the output, $v(k)$ is the measurement noise, all at the k-th time. A, B, C, and D are real matrices with appropriate dimensions that define the dynamics of the system.

When the system is linear and both the input disturbances and measurement noises are Gaussian, $\mathrm{E}\,[w] = \mathrm{E}\,[v] = 0$, and mutually uncorrelated, $w(k) \sim \mathcal{N}(0, Q)$ and $v(k) \sim \mathcal{N}(0, R)$, it leads to a recursive filter. The KF predicts the states at the k-th time-instant and corrects these estimations at the $k+1$-th time instant when obtaining the feedback from the noisy output measurements. Therefore, the KF algorithm comprises two steps: a time update based on equations, and a measurement-based update.

The time update projects forward, in time, the current states $\hat{x}(k|k)$ and the error covariance estimates, $\mathrm{P}(k|k)$, to obtain *a-priori* estimates for the next time step. The measurement-based update includes the new measurements into the *a-priori* estimates to obtain improved *a-posteriori* estimates according to an observer gain, $\mathrm{K}_{obs}(k+1|k)$. The time update is also known as the predictor equations, while the measurement update is known as the corrector. This 2-step process is summarized in Algorithm 1, and the block diagram presented in Figure 4.1.

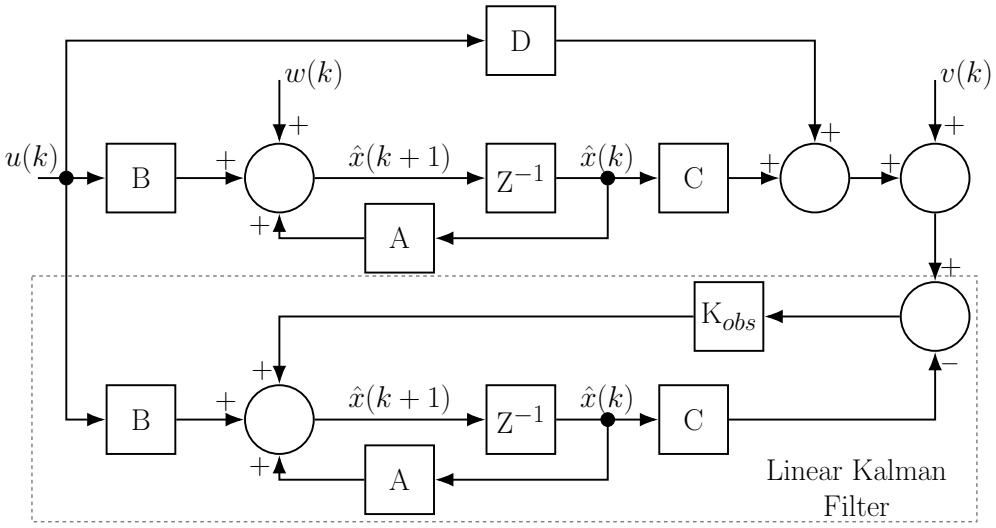

Figure 4.1: Linear Kalman Filter block diagram.

Algorithm 1 Estimation algorithm of a linear Kalman Filter

Estimate at the k-th time instant:

1: $\hat{x}\,(k+1|k) = A\,x\,(k|k) + B\,u\,(k|k)$ (4.3)

2: $\mathrm{P}\,(k+1|k) = A\,\mathrm{P}\,(k|k)\;A + Q$ (4.4)

Correct at the $k+1$-th time instant:

3: $\mathrm{K}_{obs}\,(k+1|k+1) = \mathrm{P}\,(k+1|k)\;C^T\;\left(C\,\mathrm{P}\,(k+1|k)\;C^T\right)^{-1} + R$ (4.5)

4: $\hat{x}\,(k+1|k+1) = \hat{x}\,(k+1|k) + \mathrm{K}_{obs}\,(k+1|k+1)\,(y\,(k+1) - C\,\hat{x}\,(k+1|k))$ (4.6)

5: $\mathrm{P}\,(k+1|k+1) = \mathrm{P}\,(k+1|k) - \mathrm{K}_{obs}\,(k+1|k+1)\;C\,\mathrm{P}\,(k+1|k)$ (4.7)

where:
$\hat{x}(0) = \hat{x}_0$
$\mathrm{P}(0) = \mathrm{P}_0$
$\mathrm{E}[(w-0)\,(w-0)^T] = Q$
$\mathrm{E}[(v-0)\,(v-0)^T] = R$

Luenberger observer

The Luenberger observer has a relatively simple design that can be applied as a general estimation technique [127, 206–208]. As well as the Kalman filter, the Luenberger observer objective is to correct the estimation made by the model with the feedback from the measured signal. The Luenberger observer uses a time-invariant gain vector L that can be chosen to place the eigenvalues of the observer state estimation matrix at a specified location in the unit circle. This observer framework is deterministic but, if uncertainties are considered small and their variation being around zero, their effects can be neglected and the observer can provide reasonable results when tracking the state of the stochastic system. A general block diagram of the Luenberger observer is presented in Figure 4.2.

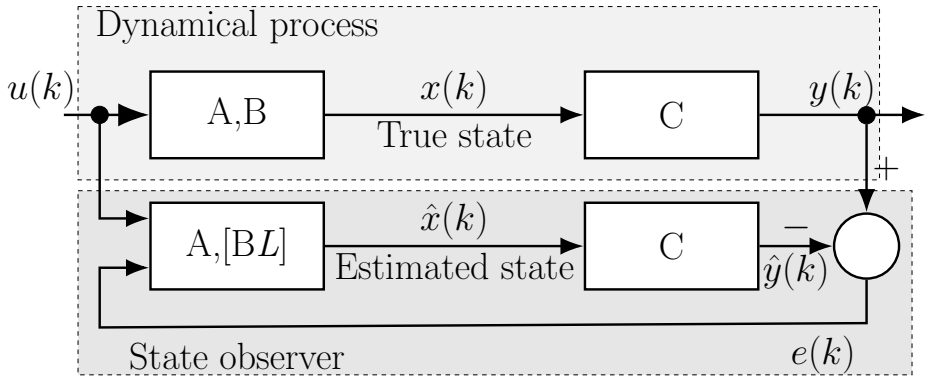

Figure 4.2: Luenberger observer block diagram.

Based on Figure 4.2, let's assume a process model presented in Equation 4.8 and Equation 4.9. The correction of the state observer, which involves the state estimation and the real state value coming from the feedback measurement is presented in Equation 4.10.

$$x\,(k+1) = A\,x(k) + B\,u(k) \tag{4.8}$$
$$y(k) = C\,x(k) \tag{4.9}$$
$$\hat{x}(k+1) = A\hat{x}(k) + Bu(k) + L\,[y(k) - \hat{y}(k)] \tag{4.10}$$

From Figure 4.2, the error between the estimate and the real value, can be defined as in Equation 4.11.

$$e(k+1) = x(k+1) - \hat{x}(k+1) \tag{4.11}$$
$$e(k+1) = Ax(k) + Bu(k) - A\hat{x}(k) - Bu(k) - L\,[y(k) - C\hat{x}(k)] \tag{4.12}$$
$$e(k+1) = Ax(k) - A\hat{x}(k) - LCx(k) + LC\hat{x}(k) \tag{4.13}$$
$$e(k+1) = [A - LC]\,x(k) - [A - LC]\,\hat{x}(k) \tag{4.14}$$
$$e(k+1) = [A - LC]\,e(k) \tag{4.15}$$

This result allows, if the pair (A, C) is observable, to place the eigenvalues of $[A - LC]$ at a convenient location turning it into a stable Hurwitz system then, the state estimation error tends to zero as time tends to infinity $e(k) \longrightarrow 0$ as $t \longrightarrow \infty$ [209].

4.2.2 Non-linear estimation

The non-linear estimation methods are heavily dependent on the system model considered, where the linear methods cannot be applied. Researchers have proposed different strategies whose goal is to implement the developed linear theory, by using a linearized process model, use a combination of linear models or use a full simulation of the non-linear model in order to compare their results with measured data. A brief introduction to some of the most used methods is given below.

Approximation, non-linear methods

The most used methods for this group are the Extended Kalman Filter (EKF) and the Second Order Filter (SOF) [210], which require a continuous and differentiable dynamical function. The EKF method, uses the Taylor series approximation, considering the first-order term and neglecting the higher-order terms, allowing to apply the KF linear techniques, while the SOF method, takes into account the second order term of the Taylor expansion, requiring more computational time but giving a more precise result [211].

Multiple model methods

This method consists of combining a set of filters, namely the KF, the EKF or the SOF, and a hypothesis testing algorithm that weights the estimates from each filter to generate a global state estimate [129]. A widely used technique is the Takagi-Sugeno which predicts the

states of the system using different models with the same number of dimensions. Recently the work of Orjuela et al. [212], proposed a decoupled multiple model technique where the different models could have different dimensions.

Numerical simulation methods

There are basically two types of numerical simulation methods for state estimation of non-linear systems, the Sequential Monte Carlo [213–216], and the Point-Mass method [217, 218]. The main difference between those two methods is while in the first, the state estimation is governed by the concentration of particles at a specific region, the second method uses piecewise linear functions.

Moving Horizon Estimation

This methodology bases its estimation on a finite cluster of past measured data, and current measurements, to solve the state estimation problem. To minimize the computational cost of minimizing the objective function, a *forgetting term* is defined so that the most recent measured data can have a most relevant influence over old data, as stated in the work of Hernández Rodríguez et al. [131]. The objective function could also include a penalty term for the change in those measurements. The stability is ensured if the system is incrementally observable, and its robustness is achieved by using a sufficiently long horizon, as stated in the work of Allan and Rawlings [189]. More recently, Zou et al. [132] proposed an alteration of the original MHE method for cases where some inputs are not available or incomplete, consisting of a two-step strategy, the first step estimates the best parameters for the estimator under certain assumptions related to the physical problem and, the second step, consists on evaluating the convergence of the MHE method using those estimated parameters.

4.3. Artificial Bee Colony

The original Artificial Bee Colony (ABC) algorithm is a zero-order optimization technique first proposed by Karaboga [144, 219], which mimics the behaviour of a honeybee swarm looking for food sources. Once a food source is found, the honeybees communicate their respective information to the hive. The food source information is related to a quality evaluation of each food source. With this information, other honeybees can decide which food source to explore in search of better food sources in its surroundings.

The ABC algorithm is a method with basically two phases: exploration and exploitation. The exploration phase covers a wide range of possible solutions, which maximizes the probabilities of finding the global minimum. The other phase, exploitation, is based on exploring the found solution's surroundings.

From a mathematical point of view, food sources are intended to represent solutions for the optimization problem, and the source quality is related to the fitness function, allowing to select the most appropriate solution by optimizing an objective function.

The solutions may be defined by one or more parameters, referred to as "dimensions" for the ABC algorithm. The algorithm proposes that the solutions for the problem are initialized by defining a set of honeybees, whose dimension values are randomly selected from a search domain. The search domain can be constrained or unconstrained.

The problem is then evaluated using the initialized honeybees, the information from each food source evaluation is processed and the best food sources are selected. Once the best food sources have been selected, another set of honeybees is initialized and sent to explore their surroundings. These new honeybees are also initialized using a random function which defines their dimensions.

The new honeybees will evaluate their respective solutions and will retrieve their information to the hive. At the hive, the solutions are analysed to find improvements and to evaluate convergence conditions. If the convergence conditions are satisfied, the algorithm stops. Otherwise, a new set of honeybees is created around the best food source found so far and the cycle repeats until convergence conditions are satisfied.

4.3.1 Honeybee types

The ABC algorithm defines three types of honeybees namely: *Employed* bee, *Onlooker* bee and *Scout* bee, each with a specific function within the algorithm.

Employed bees

The *Employed* bees are the first population of solutions, x_{ij}, that the ABC algorithm uses to initialize the search. The *Employed* bees population are initialized by using Equation 4.16.

$$x_{ij} = x_{j_{\min}} + \omega_i \left(x_{j_{\max}} - x_{j_{\min}} \right), \tag{4.16}$$

where index i represents the i-th solution of the problem, with $i = \{1, 2, 3, \ldots, SN\}$, being SN the total number of food sources. The index j represents the j-th dimension of the i-th solution, $j = \{1, 2, 3, \ldots, D\}$ being D the total number of dimensions which define the entire solution vector and, ω_i is a constant whose value is randomly chosen between 0 and 1.

The *Employed* bees evaluate their respective food source, problem solution, and then the information about each food source evaluation is used to determine their respective fitness, that for a minimization problem is computed by Equation 4.17.

$$fit_i = \begin{cases} \frac{1}{1+f(x_i)} & f(x_i) \geq 0 \\ 1 + |f(x_i)| & f(x_i) < 0 \end{cases} \tag{4.17}$$

The fitness of each solution found by the *Employed* bees are used in Equation 4.18, this equation determines the probability of a solution to be selected for solving the problem, allowing to select the solution, or solutions, with the highest probability. This process is called *greedy selection*.

$$p_i = \frac{fit_i}{\sum_{i=1}^{SN} fit_n} \tag{4.18}$$

Onlooker bees

After a solution or set of solutions are selected, another type of honeybees is defined, called *Onlooker* bees, v_{ij}, whose dimensions are selected using Equation 4.19. The *Onlooker* bees' main objective is to explore the surroundings of the selected *Employed* bees' solution in search of an improvement for the optimization problem.

$$v_{ij} = x_{j_{\min}} + \lambda_i \left(x_{ij} - x_{kj} \right), \tag{4.19}$$

where i and k are the i-th and k-th *Onlooker* solution respectively, taken from all the *Employed* bees x_{ij}, and computed with respect to the same dimension j. The index condition that needs to be satisfied while defining the *Onlooker* bees is $k \neq i$. λ_i is a constant whose value is chosen between -1 and 1.

Scout bees

Parallel to the *Onlooker* bees definition, the non-selected *Employed* bees are replaced with a set of a third type of bee, called the *Scout* bees. The *Scout* bees are defined using Equation 4.16 and sent to explore for new solutions along the search domain while the former *Employed* bees solutions are kept in memory as failed attempts.

After evaluating the *Onlooker* bees and *Scout* bees, their respective fitness is calculated using Equation 4.17, and convergence conditions are evaluated. The convergence conditions can be established based on the Karush–Kuhn–Tucker (KKT) conditions for convex optimization [220], or any other convergence condition which satisfies the particular problem requirements. If the convergence conditions are met, the algorithm stops. Otherwise, a new set of *Onlooker* bees is defined, as well as another set of *Scout* bees replacing the non-selected bees when the probability condition is applied, and the process repeats until the convergence conditions are satisfied. A representation of the ABC algorithm is shown in Algorithm 2.

4.4. Hybrid Artificial Bee Colony Algorithm

The hybrid Artificial Bee Colony (hABC) algorithm is based on the original ABC algorithm, being a stochastic search for a near-optimal solution by defining a set of initial solutions and, based on the problem result obtained after evaluation, making a decision on which direction to continue the search.

Let's assume a process where the dynamic relation and observation relation are defined by Equation 4.20 and Equation 4.21 respectively. The process has n states variables and m inputs.

Algorithm 2 Artificial Bee Colony algorithm

1: Initiate the *Employed* bees population $x_{ij},\ i = \{1, 2, \ldots, SN\}$ using Equation 4.16
2: Evaluate the population $f(x_i)$
3: cycle = 1
4: **repeat**
5: Produce a population of *Onlooker* bees using Equation 4.19
6: Calculate the probability values p_i for the solutions x_i using Equation 4.18
7: Apply a *greedy selection* for the *Employed* bees to select the best *Employed* bee
8: Produce new solutions v_i, *Onlooker* bees, from the selected *Employed* bee using Equation 4.19
9: Generate a new population of *Scout* bees using Equation 4.16
10: Evaluate the new created *Onlooker* and *Scout* bee population
11: Apply the *greedy selection* for the *Onlooker* and the *Scout* bees
12: Memorize the best solution achieved so far
13: cycle = cycle + 1
14: **until** convergence condition **or** cycle = max iteration

$$\dot{x} = f(x, u) \tag{4.20}$$

$$y = g(x, u) \tag{4.21}$$

Let's also assume that for a sampling period T_s, all the inputs can be measured M times at a sampling rate R_s.

The objective of the proposed algorithm is to minimize a convex cost function J, Equation 4.22, subjected to constraints related to all the input variables and the available outputs, Equation 4.23 and Equation 4.24 respectively.

$$J = [\Delta U]\,[Q]\,[\Delta U]^T + [\Delta Y]\,[W]\,[\Delta Y]^T \tag{4.22}$$

s.t.

$$u_m^- \leq \bar{u}_m \leq u_m^+ \tag{4.23}$$

$$y_n^- \leq \bar{y}_n \leq y_n^+ \tag{4.24}$$

where $[\Delta U]$ is a vector of dimension m containing the difference between the measured input values and the values proposed by the hABC algorithm, and $[\Delta Y]$ is a vector of dimension n containing the difference between the measured output variables value and the calculated values by solving the problem using the solution proposed by the hABC algorithm. The matrices $[Q]$ and $[W]$ are diagonal weight matrices for the input variables and the output variables respectively. u_m^- and u_m^+ are the lower and upper limits respectively for the m-th input, and y_n^- and y_n^+ are the lower and upper limits respectively for the n-th measurement.

hABC Employed bees

The *Employed* bees are defined by performing a measurement for all the input variables to determine a central point composed by all the dimensions of the problem. Assuming the hypothesis that the measurements can be represented as a normal Gaussian distribution, the

central value for each dimension is the mean of each dimension measurement.

To define the constraints around the mean of each dimension, Equation 4.23, the concept of the confidence interval is used. The confidence interval is defined with an α level of confidence for the measurements of each dimension, leading to Equation 4.25 and Equation 4.26 for the upper and lower limits, respectively.

$$u_m^+ = \bar{u}_m + \alpha \cdot \sqrt{\frac{\sigma_m}{M}}, \tag{4.25}$$

$$u_m^- = \bar{u}_m - \alpha \cdot \sqrt{\frac{\sigma_m}{M}}, \tag{4.26}$$

where $\bar{u}_m$ stands for the mean of the input m of length M, and σ_m stands for the input m variance. The value of α is determined based on the probability density function of a normal distribution.

Once the confidence intervals are defined for each measured input, those dimensions are divided into d divisions equally spaced by Δu_m. The total number of *Employed* bees is the number of dimension divisions to the power of total dimensions, $SN = d^m$. For the measurable output variables, Equation 4.25 and Equation 4.26 are also used to calculate the confidence interval.

For example, if the problem from Equation 4.20 and Equation 4.21 has two dimensions on the input side, u_1 and u_2, and it is determined to use the same number of divisions for each dimension, 5, the number and definition of *Employed* bees, in a grid-like pattern, should look as presented in Figure 4.3, giving a total number of bees of $SN = 5^2 = 25$.

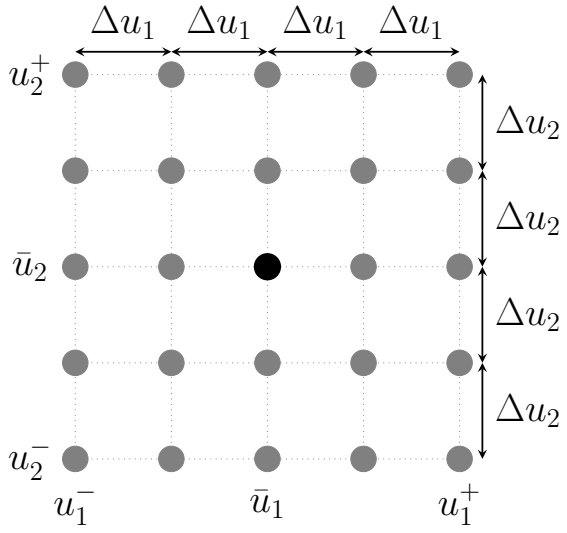

Figure 4.3: *Employed* bees grid-like distribution for a two-dimensional input problem. Black circle as central initial value (mean). Gray circles as the distributed solutions based on Equation 4.25 and Equation 4.26

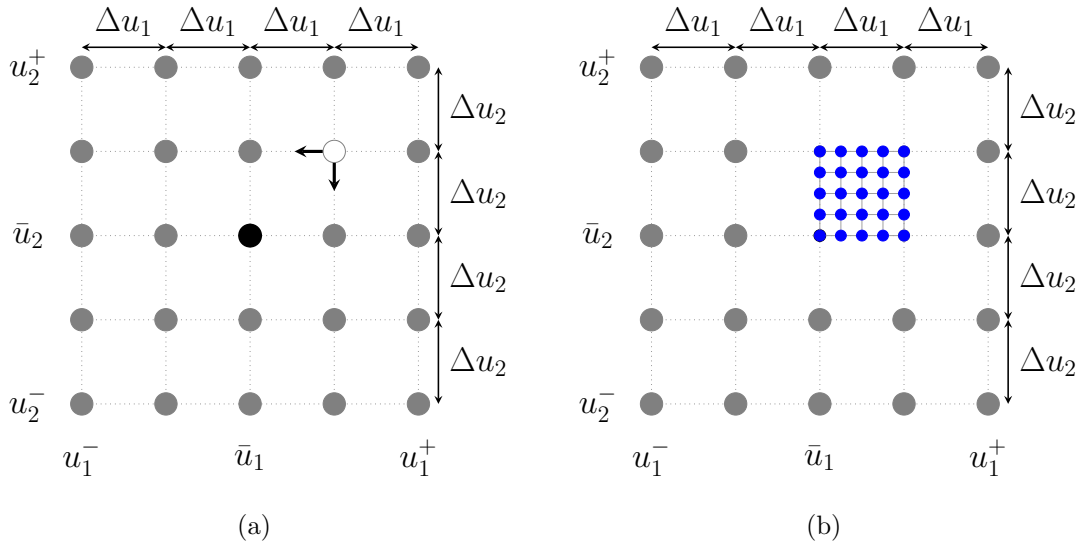

Figure 4.4: **(a)** Selected *Employed* bee, white circle, and its descent direction for each dimension. **(b)** *Onlooker* bees defined, in a grid-like pattern, between the selected *Employed* bee and the central *Employed*

The *Employed* bees are then evaluated using Equation 4.20, Equation 4.21 and Equation 4.22, and their respective fitness are calculated using Equation 4.17. Using the *Employed* bees fitness their respective probabilities are calculated using Equation 4.18. Then, the best *Employed* bee is selected.

hABC Onlooker bees

The *Onlooker* bees are the next set of bees to be defined according to the ABC algorithm from Section 4.3.1. The goal of the *Onlooker* bees is to explore the surroundings of the selected *Employed* bee. The hABC proposal for the *Onlooker* bees definition is to understand where to send the *Onlooker* bees to explore to reduce the search domain and then minimize the number of failed evaluations. This definition is dependent on computing the descent direction from the selected *Employed* bee using Equation 4.27.

$$g = -\left[\frac{\partial f(x,u)}{\partial u_1} \quad \frac{\partial f(x,u)}{\partial u_2} \quad \frac{\partial f(x,u)}{\partial u_3} \quad \cdots \quad \frac{\partial f(x,u)}{\partial u_{m-1}} \quad \frac{\partial f(x,u)}{\partial u_m}\right]^T \tag{4.27}$$

Once the descent direction is computed, a set of SN *Onlooker* bees are defined towards the descent directions for each problem dimension in a grid-like pattern similar to the definition of the *Employed* bees. Figure 4.4a shows the descent direction per dimension calculated at the selected *Employed* bee for a two-dimensional input problem.

The bounds for each direction are defined between the value of the selected *Employed* bee and the value of the central *Employed* bee, then the resulting length is divided. Following the same example, the two dimensions are divided into 5 parts each. The *Onlooker* bees are then distributed in a grid-like pattern, evenly spaced, as presented in Figure 4.4b.

If any of the descent directions are pointing away from the central *Employed* bee, as shown

in Figure 4.5a, to define the *Onlooker* the search domain for such dimension is taken from the distance between the selected *Employed* bee and the dimension bound in which the descent direction is pointing towards. Figure 4.5 shows a case in which both descent directions are pointing away from the central *Employed* bee, then the *Onlooker* bees are defined using the bounds of each dimension, as shown in Figure 4.5b.

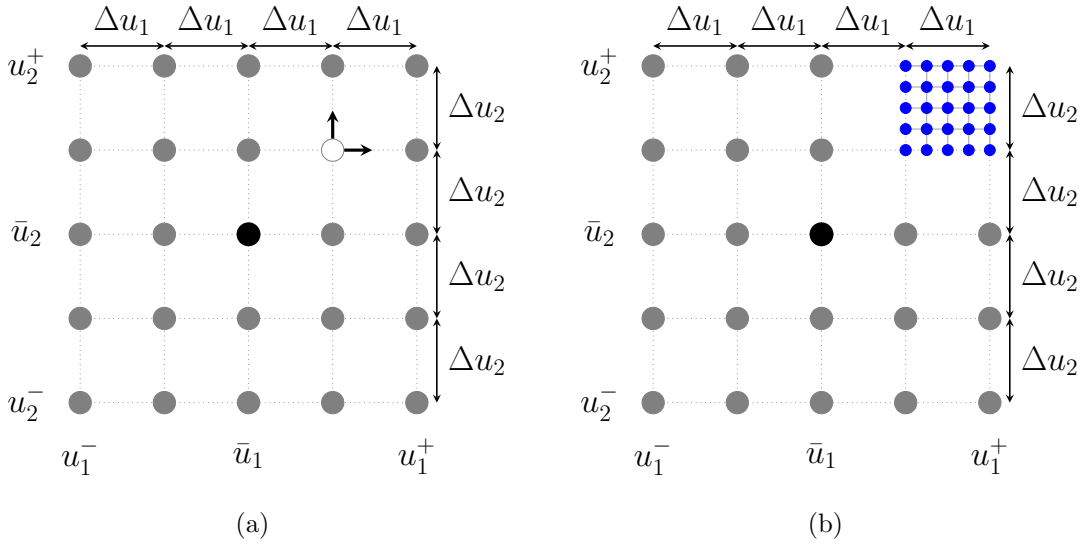

Figure 4.5: **(a)** Selected *Employed* bee and its descent direction for each dimension. **(b)** *Onlooker* bees defined as a grid-like pattern between the selected *Employed* bee and the bounds of each dimension

Once the *Onlooker* bees have been defined, the result of the problem is obtained from evaluating Equation 4.20, Equation 4.21 and Equation 4.22. Their respective fitness and probabilities are calculated according to Equation 4.17 and Equation 4.18, respectively. The best bee is selected based on the highest probability.

At this stage, the convergence condition is evaluated based on the convex cost function, Equation 4.22. If the convergence conditions are satisfied, the algorithm stops, otherwise the gradient towards the descent direction is calculated at the selected *Onlooker* bee.

The search continues with a new set of *Onlooker* bees, defined in a grid-like pattern towards the descent direction computed at the selected *Onlooker* bee, dividing each dimension into 5 parts. The newly created *Onlooker* bees are evaluated, and their respective fitness and probability are calculated to evaluate the convergence conditions until these are satisfied.

Figure 4.6 presents the state estimator structure using the proposed optimization algorithm, where the error between the measured and the predicted output is evaluated into the *Optimizing algorithm* as well as the constraints related to the degrees of freedom of the input variables and the output variables, to compute an input value $\hat{u}$ that minimizes such error.

The proposed hABC does not contemplate the use of any form of *Scout* bees, as their original goal is to replace the non-selected *Employed* bees which were defined randomly.

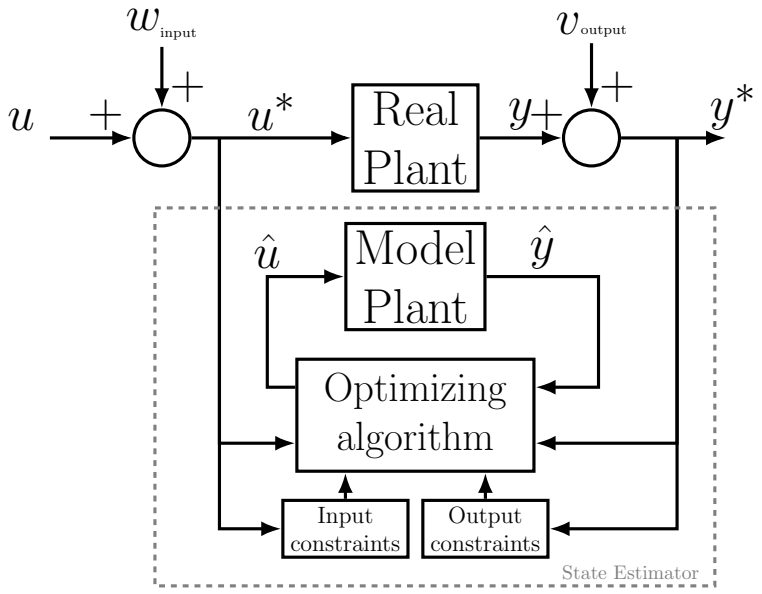

Figure 4.6: Block diagram of the proposed hABC estimation loop

4.5. Materials and Methods

4.5.1 Manufacturing process

The manufacturing process that will serve as a case of study is the ATL process presented in Chapter 3. For this case of study, an additional temperature sensor is placed, facing the composite material to validate the temperature distribution at two different locations. The method is described below.

4.5.2 Material

The ATL process uses a carbon fibre reinforced Polyamide 6 tape from Toray® with the commercial denomination Cetex TC910®, it is 50 mm wide, 0.16 mm thick, and has a fibre content of 60% [221]. A complete thermal characterization of the composite material can be found in Section 3.9.

4.5.3 Measurements and instrumentation

To measure the process input variables needed to feed the mathematical model, the strategy used is the same as described in Chapter 3, Section 3.10.3.

For the output variables, in this case, the composite material temperature, both are measured at two different locations as presented in Figure 4.7a. The upper location measurements, Figure 4.7a (6a), are performed using a primary pyrometer, PyroNFC K from CALEX®, facing the composite material at a point above the centre line of the compaction roll. This measurement characteristic was referred to in Chapter 3, Section 3.10.3.

The lower location measurements, Figure 4.7a (6b), are performed with another pyrometer, placed facing the composite material, under the centre line of the compaction roll and is

defined as the secondary pyrometer. The secondary pyrometer is an Optris® model CS LT with serial communication. The secondary pyrometer was selected to fit the narrow space between the machine assembly and the process mould, as shown in Figure 4.7b, to avoid suffering from mechanical damages and to not interfere with the process.

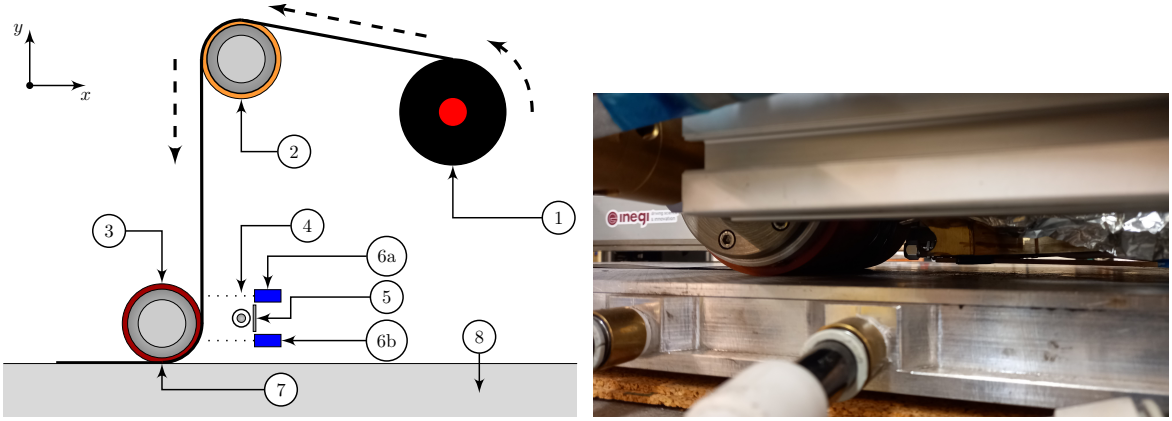

(a) (b)

Figure 4.7: **(a)** ATL machine assembly spatial disposition scheme for: (1) Material unwind mechanism. (2) Material Guide. (3) Compaction roll. (4) Heating element. (5) Reflector. (6a) Primary Pyrometer. (6b) Secondary Pyrometer. (7) Nip Point. (8) Mould. **(b)** Secondary Sensor assembly

The tests for the hABC algorithm are performed by measuring the process speed, the voltage and current applied to the heating element, the ambient temperature, the mould temperature, the compaction roll temperature and the composite material temperature, at two different locations according to Figure 4.7a.

4.5.4 Methods

The hABC algorithm computes both the state variables and the output variable of the composite material, based on information gathered from measuring the voltage of the heating element, the process speed, the compaction roll temperature, the mould temperature and, using the primary pyrometer, compares the composite material temperature with the computed output variable. The secondary pyrometer measurements, Figure 4.7b, are not used in the hABC algorithm. This measurement is used only to compare the real composite material temperature with the estimation made by the hABC algorithm at a different location. The hABC algorithm is defined to have a sampling period of 2 seconds.

As stated in the *Sensitivity analysis* from Chapter 3 Section 3.12.2, the heating element voltage and the process speed are the inputs with the most significative impact over the composite material model dynamics, being the process speed the most influential of both inputs because it is directly coupled with the composite material.

The heating element voltage and the process speed are used by the hABC algorithm as degrees of freedom. Those degrees of freedom are used to define two of the dimensions for the different types of bees. The remaining dimensions, such as the compaction roll, mould and surrounding temperatures, are defined using their respective mean sampled values. Those

three last dimension definitions are made due to limitations of their respective real actuation mechanisms to change their states, having slower dynamics when compared to the dynamics of the voltage change at the heating element and the speed change at the servo driver thus, having a slower influence upon the composite material change in temperature.

The tests for the hABC algorithm are performed using different operating conditions, making emphasis on the process speed, by defining the machine controller with a fixed value for the voltage of the heating element and a fixed value for the process speed for the entire process. Those values are presented in Table 4.1.

Table 4.1: Values for the hABC Test

Test	Voltage [V]	Speed [mm/s]
1	115.0	5.50
2	130.0	6.00
3	120.0	11.00
4	140.0	20.00

Figure 4.8 shows a block diagram for the hABC algorithm applied to the ATL process, where G(k) computes the heat flow among the involved process elements based on the input variables, as mentioned in Section 3.8.1, B(k) and A(k) are time variable matrices related to the reflector and composite material as mentioned in Section 3.4 and Section 3.7 respectively. The matrix C(k) gives the information from the primary pyrometer, Figure 4.7. The time integration strategy is described in Section 4.5.5.

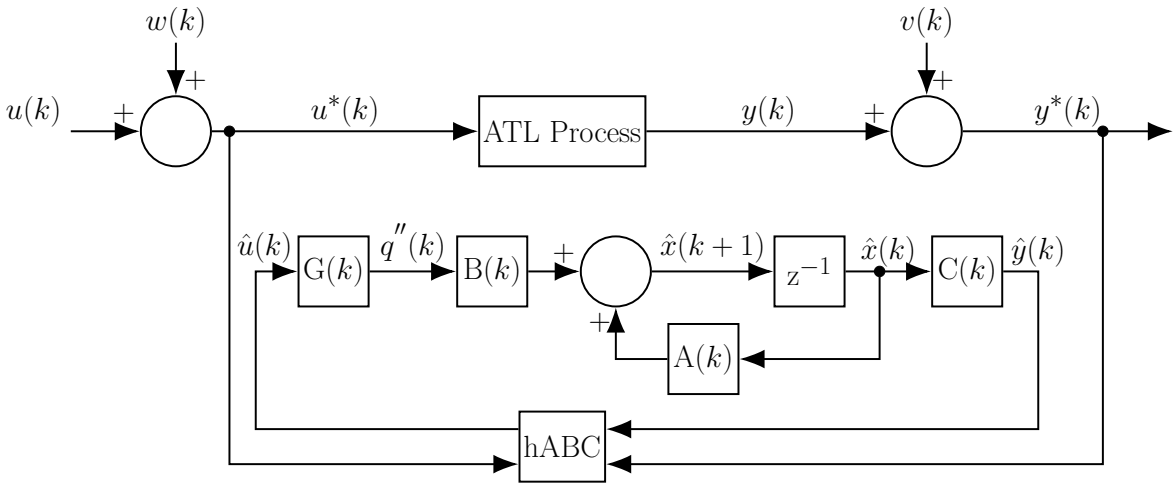

Figure 4.8: Block diagram of the proposed hABC algorithm applied to the ATL process

4.5.5 Time Integration Scheme

The mathematical model involves a set of non-linear ordinary differential equations (ODE) for the temperature time derivative of the different components involved in the machine assembly, as presented in Section 3.3 trough Section 3.7 and, for the energy balance presented in Section 3.8. To solve this ODE system, the initial condition is set to be the ambient

temperature for all the components. The implicit solver Radau IIA [185] is selected from the Scientific Python library to avoid time-step limitations due to equation stiffness.

4.6. Results

To compare the estimations made by the original model and the estimations made by the hABC algorithm, different tests results are presented in Figure 4.9 through Figure 4.15. The test results are measurements made by the primary and secondary pyrometers, as well as the computed estimations made by the original process model and the hABC algorithm at the two measuring locations. The operation conditions for each test were described in Table 4.1.

Figure 4.9 presents the composite material temperatures related to test 1 from Table 4.1. For the primary pyrometer, the original process model can predict a composite temperature with an error of up to 6% during the transient stage and up to 3% for the steady-state stage. The hABC algorithm was capable of reducing the error in both stages under 1%, by adjusting the process model inputs related to the heating element voltage and the process speed. The temperature estimations made by the hABC algorithm located at the secondary pyrometer present an average error of 2% during the transient stage, and an average error of 1% at the steady state stage.

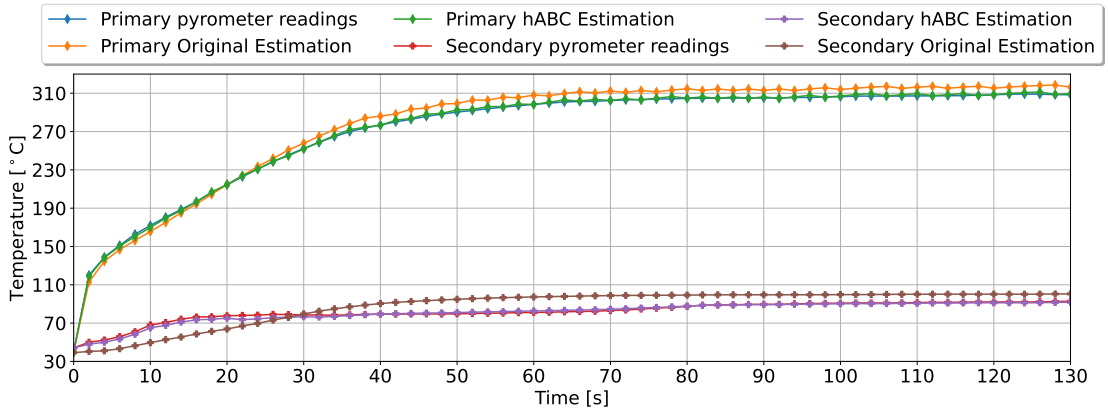

Figure 4.9: Results of Temperature prediction made using the main process model and the estimations made by the hABC algorithm, for the first test from Table 4.1

The adjustments to the heating element voltage and the process speed made by the hABC algorithm are presented in Figure 4.10a and Figure 4.10b respectively. The algorithm increases the voltage input and decreases the input speed, inside the search limits, to compensate for the underestimation of the original process model.

Figure 4.11 shows the temperature results for the second test described in Table 4.1. For this test, the reference voltage of the heating element was increased as well as the process speed, which induced a different dynamical response at the primary pyrometer location, as well as the secondary pyrometer location in comparison with test 1. For this test, the error with respect to measurements for the original process model estimation has an average of 6% along the entire process, while the estimation made by the hABC algorithm is 1% on average.

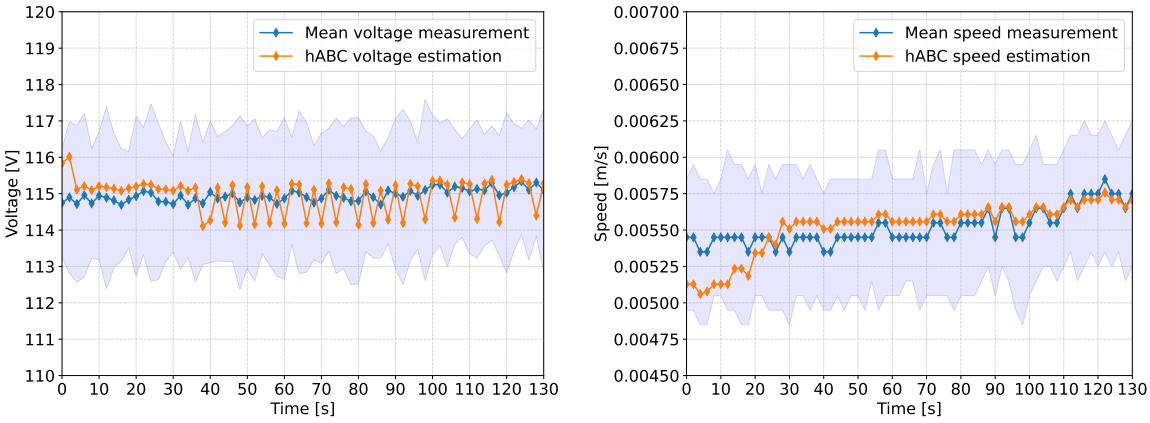

(a) (b)

Figure 4.10: Test 1 results. **(a)** Heating element voltage. **(b)** Process speed

For the location of the secondary pyrometer, a similar behaviour is obtained with respect to the results of the test 1. The temperature estimation computed for this location has an error under 1%.

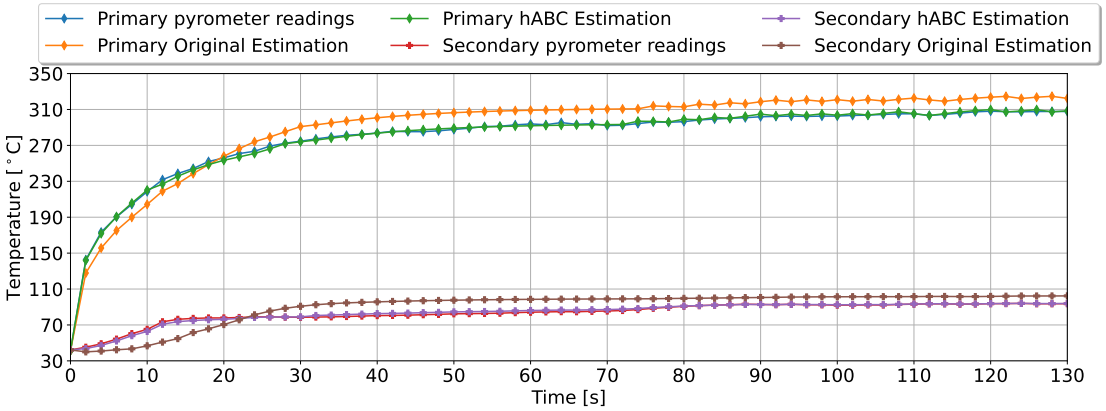

Figure 4.11: Results of Temperature prediction made using the main process model and the estimations made by the hABC algorithm, for the second test from Table 4.1

Similarly to test 1, the hABC algorithm defines a higher voltage input and a lower value for the process speed along the transient stage, Figure 4.12a and Figure 4.12b respectively, to compensate for the rapid increase in temperature along the transient stage.

At the steady state stage, the hABC algorithm oscillates the voltage input around a value, Figure 4.10a and Figure 4.12a, meaning that the algorithm is compensating minor deviations in temperature caused by perturbations on the readings or in the composite material structure, by adjusting the least sensitive input for the process model. This sensitivity is defined when the algorithm computes the descent direction at the selected solution.

The third test results for the temperature are presented in Figure 4.13, where it can be seen that, at the primary pyrometer location, the original process model has an estimation error above 15% along the transient stage, while the hABC algorithm minimizes the error

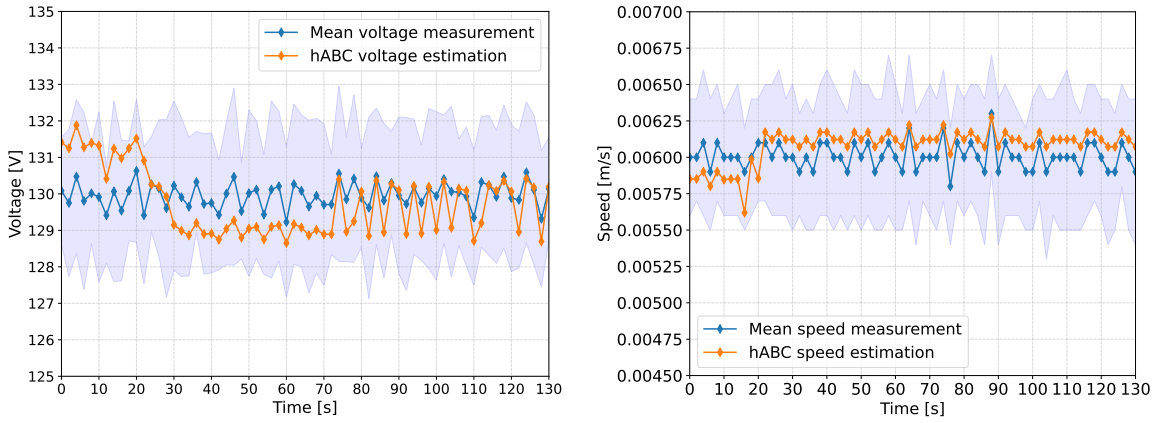

(a) (b)

Figure 4.12: Test 2 results. **(a)** Heating element voltage. **(b)** Process speed

below 1% by computing a combination of higher input voltage and lower process speed with respect to the measurements, as presented in Figure 4.14a and Figure 4.14b, respectively.

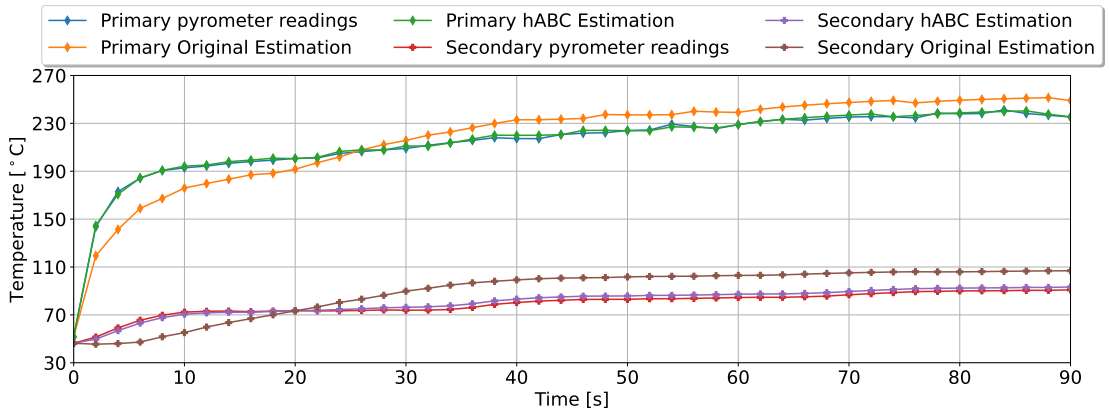

Figure 4.13: Results of Temperature prediction made using the main process model and the estimations made by the hABC algorithm, for the third test from Table 4.1

For the secondary pyrometer location, the hABC algorithm estimates a temperature closest to the measured temperature. It minimizes the transport effect computed by the original process model estimation at the same location by decreasing the input process speed, which goes accordingly with the effect presented at the primary pyrometer location.

The results related to the temperature at the primary and secondary pyrometer locations of the fourth test are presented in Figure 4.15. This test involved a higher process speed compared with tests 1, 2 and 3. This higher process speed produces a faster increment in temperature at the primary pyrometer location. This temperature is lower compared with the other three tests due to the increment in speed, which is handled by the original process model with an error over 10% at the transient stage, and an average of 6% after 30 seconds of process. As expected, the hABC minimizes the estimation error at the primary pyrometer location, under 2%, by adjusting the input values related to the heating element voltage and

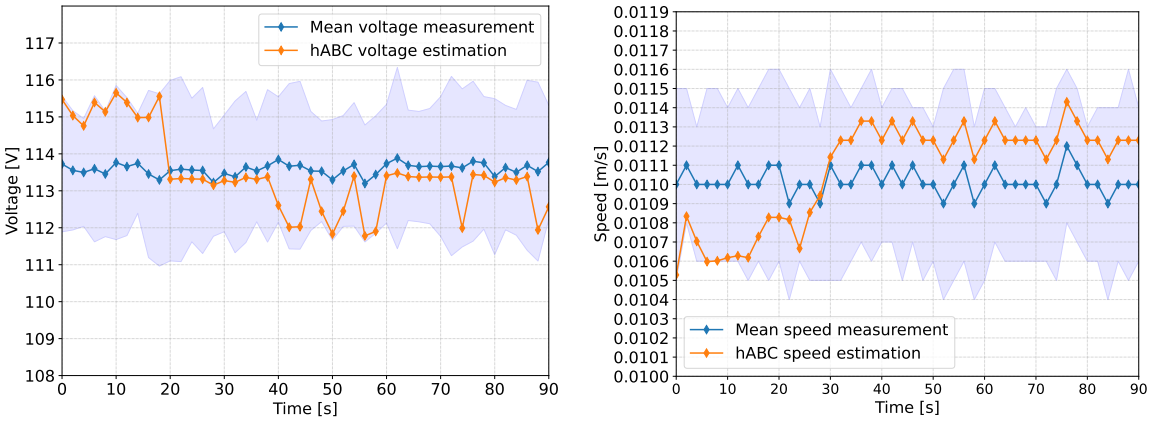

(a) (b)

Figure 4.14: Test 3 results. **(a)** Heating element voltage. **(b)** Process speed

the process speed.

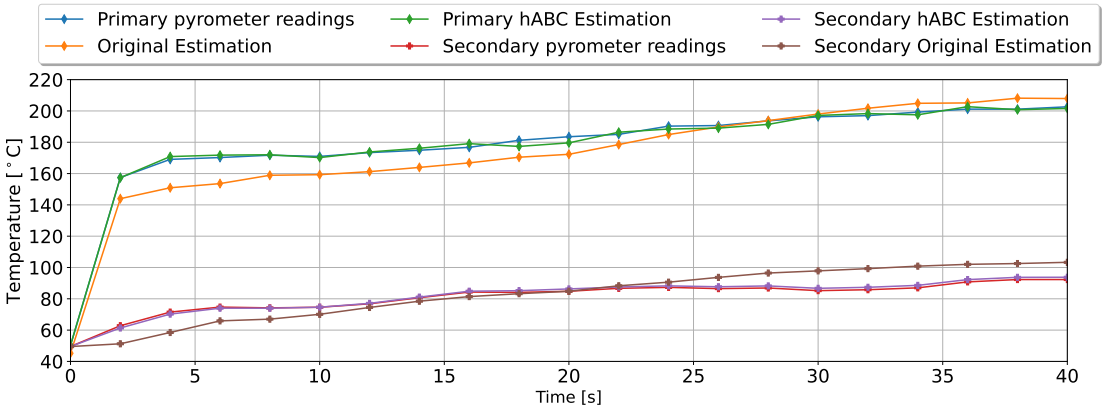

Figure 4.15: Results of Temperature prediction made using the main process model and the estimations made by the hABC algorithm, for the fourth test from Table 4.1

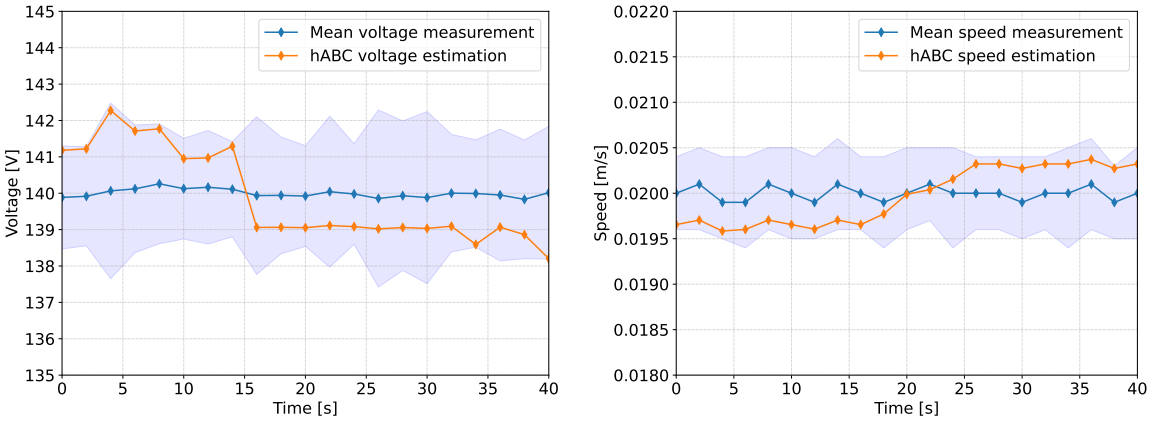

(a) (b)

Figure 4.16: Test 4 results. **(a)** Heating element voltage. **(b)** Process speed

Data presented in Figure 4.9 and Figure 4.11 shows that the original process model has lower estimation error than the data presented in Figure 4.13 and Figure 4.15. Nevertheless, the hABC algorithm is capable of converging to a solution that approximates the real measurement of the composite material during the transient and steady-state phase.

The presence of an error in the estimation made by the hABC algorithm is due to how the possible solutions are defined. As presented in Figure 4.4, the hABC algorithm searches for the optimal solution located between a set of values. If the optimal solution is located between two proposed solutions but near one of them, the algorithm will always select the closest defined solution. This selected solution is compared with the previously selected solution that minimized the problem to check convergence. If convergence is reached using solutions near the optimal solution, it means that a near-optimal solution has been reached.

4.7. Concluding remarks

The original ABC algorithm, as a zero-order method for minimization, postulates a random search by defining independent solutions. Even though this search can be computationally expensive for the time spent computing solutions away from the optimal solution, the proposed modification is suitable for minimizing the probability of stepping into a local minimum, during the exploration phase, by defining a coarse search in a structured pattern. The exploitation phase is improved by transforming the random search to an organized search, by defining a search direction using part of a first-order method. The objective of this first-order method is to lower the number of evaluations by minimizing the oscillation effect occurring in other hybridizations as mentioned by Gao et al. [153], and typical of the original ABC algorithm due to the random search.

The initial computational iterations performed by the hABC algorithm are made up of a first search domain exploration, computation of the descent direction, and a first exploitation of the descent direction. A second exploitation towards a new descent direction is performed only if the solution can be further improved. The steps required for the hABC algorithm to reach a near-optimal solution are significantly fewer than the steps required for the original ABC algorithm to reach a similar solution, due to the removal of the random exploration characteristic of the original ABC algorithm.

In contrast with the original ABC method, the proposed hABC algorithm does not define *Scout* bees to replace the non-selected solutions, as the objective function is always convex and during the exploration phase, the entire search domain is evaluated by defining a coarse grid, avoiding selecting a local minimum solution. The grid defined during the exploration phase can be refined using parallel programming algorithms, which take advantage of the multiprocessing capability of modern processor units. The non-selected solutions are completely discarded when the search direction is defined by forcing solution exploitation towards such direction, improving the solution exploitation compared with the original ABC algorithm.

The hABC algorithm used to minimize the estimation error produced by the presented process DT modified two of its inputs, inside a statistical confidence interval, to achieve a

near-optimal estimation. The error at the reference location was minimized with respect to the error in the estimation made by the original process model, as well as the error at the secondary location. On the other hand, the error at the secondary location produced by the hABC algorithm presents a greater error value compared with the primary location. This error is due to uncertainties associated with the process DT and the fact that the hABC algorithm is only adjusting two inputs and none of the process parameters.

Even though the second location measurements were not taken into account for the hABC algorithm to compute the near-optimal solution, its estimation had an acceptable maximum error of 1.72%, meaning that the hABC algorithm can be used as an estimator in processes with only one measurement location, lowering the overall machine cost by placing a single sensor and facilitating the machine design by not having to locate such sensor near the point of interest.

As the process model not only depends on the input values to estimate the different temperatures, but also on defining other parameters such as material properties and heat transfer phenomena, which are modelled with constant values or using empirical correlations, the hABC algorithm could be expanded to include those unknown parameters, or physical phenomena, as degrees of freedom as other authors have made by modifying of the original ABC algorithm like in the works of Oliva et al. [202] and Hu et al. [136].

For the case in which the hABC algorithm is intended to be used with unknown parameters, the challenge resides in how to define a proper set of physically-justified constraints for each problem dimension, in which those added degrees of freedom could fluctuate. An alternative is to define a value for the discretization of the search domain that allows to explore a significant range of the particular dimension around the value given as the first guess.

The proposed hABC requires the definition of the same hyper-parameters as the original ABC algorithm, such as the number of working honeybees per type, the maximum number of iterations per minimization process and the convergence conditions. This is an advantage facing other modifications of the original ABC algorithm, which makes it more simple to implement.

Chapter 5

Discussion

The present chapter discusses the most relevant aspects mentioned along this thesis. This chapter is organized as follows: Section 5.1 discusses the impact of the Industry 4.0 concept by digitally representing physical processes, Section 5.2 discusses the application of the DT approach to an ATL process, Section 5.3 highlights the most relevant aspects of the ABC optimization algorithm and finally, Section 5.4 makes reference to quality control as the goal for model-based control strategies.

5.1. On the State of the Art for Digital Twins

Through the state-of-the-art review, it was possible to identify that Cyber-Physical Systems are commonly used in industry for a better understanding of the complexity of systems as briefly summarized in Table 2.1, as well as to be included into advanced decision making algorithms, improving the overall performance as briefly presented in Table 2.2. The CPS has been successfully implemented in different areas non-related to engineering, meaning the system model could be of any nature. As identified in Section 2.2, the DT implementation for replicating the physical world into the digital world requires detailed knowledge of the former as well as the necessary mathematical tools.

The use of DT, allowed to prepare action strategies based on simulations, as in the field of health care and medicine, by identifying the best response facing an emergency. Allowed control of floor-level production by forecasting the management actions required in response to supply chain and machine availabilities. Those aspects indicate that the use of a DT for a manufacturing process could be accurate to better understand the behaviour of the process.

As the literature on the implementation of the DT concept in composite materials manufacturing is scarce, the idea of using the DT as a virtual sensor system, as stated in Section 2.2 and in Section 4.1, in the ATL process brings the advantage of reducing installation costs and being a non-invasive measuring strategy while processing. This last aspect is fundamental not only for allowing a decision-making system to know the temperature distribution along the composite material, as presented in Section 4.5.4 and Section 4.6, but also for not causing structural defects affecting the mechanical performance of the manufactured structure.

5.2. On the Automated Tape Laying model

The ATL as a good replacement for out-of-autoclave composite material production has been the object of study for several researchers as mentioned in Section 2.3, including the challenges this kind of production process arises. The most relevant, as identified by all researchers, is the problem of knowing the temperature distribution along the composite material.

Structures made from composite materials are a good replacement for traditional materials, such as steel, increasing structural performance while lowering the overall weight. On the other hand, due to the dimensional scale of composite raw materials during processing being smaller compared with the dimensions of a typical temperature sensor, implementing any kind of contact sensor will not only bring an added cost to the production process but, will represent a defect for the structure, making the use on non-contact sensors the best option, as already presented in Section 3.10.3 and later in Section 4.5.3.

For those reasons, and the nature of the ATL process that requires a pressing mechanism to consolidate the composite on top of a mould, it results impossible to place a sensor at the nip point, which is the location with the most important temperature to be controlled during the process. Based on the information gathered in Section 2.3, it was possible to understand that it was required to individually describe, from a mathematical point of view, all the machine assembly elements involved in the heating process.

For the mathematical model to reproduce the physical world as accurately as possible, a detailed characterization of the composite material was performed. The composite material density and its specific heat as a function of temperature did not represent a challenge due to the availability of normalized testing machines at INEGI's laboratories for such material parameters.

Although literature defines standard procedures for measuring other thermal properties of composite materials, characterising the thermal conductivity represented a challenge, due to the high cost and time-consuming process of creating the required testing samples for the most used procedure, the flash method, specifically for the thermal conductivity along the direction of the fibres. To overcome this challenge, it was designed the test procedure presented in Section 3.9.3, based on the fundamental equation for one-dimensional thermal conductivity, presented in Equation 3.86, and other similar works, also found in literature, that addressed a similar challenge. The proposed procedure resulted in a faster and cheaper alternative for measuring one-dimensional thermal conductivity for composite materials in the form of thin plies.

The other challenge to overcome while thermally characterising the composite material was referred to its thermo-optical properties as a function of temperature. This challenge was addressed by using a commercial pyrometer and an array of commercial thermocouples as stated in the calibration procedures for pyrometer manufacturers. This procedure discarded the requirement for using a black body furnace, which is used in a normalized test, or to use a calibrated laser beam, which procedure consists of measuring the laser beam refraction intensity through a pyramidal crystal as proposed by Okada et al. [222]. The proposed procedure allowed for a faster and cheaper method for estimating the thermo-optical properties of the composite material.

Once the individual machine elements were mathematically described and the thermal characterization was performed, it allowed the compilation of two mathematical systems, the first one, as described in Section 3.8, is used for understanding the energy balance due to each machine assembly element temperature and the second, as described from Section 3.3 through Section 3.7, is used to understand the heat distribution along the composite material as the result of the energy balance previously computed. Those mathematical models allowed the creation of a process Digital Twin, which is used in Chapter 4 as a case study for the state estimation strategy.

As mentioned in Section 3.10.1, the suggested method for solving the DT mathematical model is based on Radau II for stiff systems to maximize the time step used by the solving method. Solving the mathematical system by implementing an explicit method consumes a significant amount of computational effort by having to define a smaller time increment to ensure stability.

Another aspect that slows down the algorithm is that the first phase, the energy balance, implies solving the inverse of a matrix, which is an expensive task from a computational point of view. As the matrix to invert is time-dependent, it has to be numerically calculated as requested by the Radau II method. To overcome this aspect, a convergence analysis was

performed to determine the lowest number of elements that describes the system that gives the less variation when compared with the same system with a significant amount of elements, as presented in Section 3.10.2.

5.3. On the State estimation

The state estimation, as a solution for understanding the dynamics of non-measurable variables and parameters, seemed to be a good strategy for the ATL problem of temperature measurement at the nip point. According to the information reviewed in Section 2.5, the most popular approach is the Kalman Filter. This approach has two main characteristics, the first being an optimal solution based on recursivity and, the second characteristic is that it works for linear systems. As the DT developed for the ATL process is not a linear model, it is difficult to implement the Kalman filter as a solution for the state estimation problem.

A strategy studied by other authors, suggests that a linearization could be used, around the operation point, to be able to use the Kalman Filter approach, the Extended Kalman Filter, as long as the error around the operation point could be tolerated. If a significant error is not tolerated, researchers proposed applying the linearization approach with a higher frequency. This is not always feasible due to computational limitations so, alternative methods have been studied. Neither of those methods could be applied due to the model's high non-linearity, as mentioned in Section 5.2, for being a model that has to solve two different algorithms to achieve a prediction.

The requirement for a mathematical representation of the system was addressed in Chapter 3, and the requirement of an optimization method is addressed in Chapter 4 based on different methods reviewed in Section 2.6. The ABC method seemed to be the most appropriate due to its easy implementation in different engineering areas, having fewer hyper-parameters to define when compared with other stochastic methods like PSO and GA, and not depending on the nature of the problem it has to solve.

As the ABC algorithm does not depend on the nature of the problem and the estimation algorithm proposed is based on numerical simulation, the estimation process has the advantage of being parallelizable, which exploits the characteristics of modern multiprocessing programming languages and processors, speeding up the convergence to a solution.

Defining a detailed mathematical model for the ATL manufacturing process using the Digital Twin concept simplifies using the fewer hyper-parameters of the original ABC method. This simplification is related to the problem constraints for the search domain, where taking a representative amount of samples per each measurable variable can be defined using a basic statistical process as proposed in Section 4.4, a sufficient range per dimension to minimize the convex cost function, and finally estimating the required states.

As the hABC algorithm proposes a mesh refinement as the calculations go forward during the exploitation phase and, if a reasonable tolerance for the convergence conditions for the cost function is given, the proposed hABC state estimation algorithm reaches a near-optimal solution despite numerically computing the descent direction, which in the case of the ATL

process is correct due to the capability of the actuator for fine adjusting their respective actuation action. This near-optimal solution can be improved by defining a greater number of *Employed* honeybees during the exploration phase and *Onlooker* honeybees during the exploitation phase. This advantage becomes more significant when using programming parallelization methods.

Even though the proposed approach for the state estimation strategy is based on numerical simulation, the hybridization of the original ABC algorithm with a descent method, was possible and successfully validated, as shown in Section 4.6. Those results enable a model-based control strategy implementation for the ATL process.

5.4. On the control strategy for quality control

Having achieved the design of a proper DT for the ATL process, and validated a state estimator, it is now possible to implement a model-based control strategy for the composites manufacturing process based on quality control. As mentioned by some researchers as Parlevliet et al. [6], Sonmez et al. [15], Narnhofer et al. [10] and Comer et al. [81], the quality of a composite material structure is highly related to the process temperature, as the overexposure could cause matrix damage and the underexposure could cause lack of bonding and delamination.

The developed state estimator in this thesis seems to be a good option to be combined in a model-based control strategy, such as the Model Predictive Control, to not only guarantee the desired temperature but to minimize the final structure defects caused by an improper actuation, as the ATL process dynamics are susceptible to variations to the process input variables, especially to the processing speed more than any other input as already stated in Section 3.12.2.

The developed DT process presented in Chapter 3, and then used for the hABC-based state estimation algorithm as shown in Chapter 4, computes not only the temperature at the same location as the feedback temperature sensor, defined as Primary Pyrometer in Section 3.10.3 and Section 4.5.3 to compare the estimated value with the real measured value but, computes the temperature profile along the composite material.

Computing this temperature profile allows the implementation of constraints for the model-based control algorithm related to the composite material being processed, specifically with the maximum temperature the composite material can be exposed to avoid damage and the minimum temperature the composite material requires in order to achieve a proper bonding, by providing sufficient information for computing the most accurate actions then, minimizing the final structure defects.

Computing the temperature profile using the proposed state estimation algorithm allows for simplifying the ATL machine assembly, enabling the positioning of a pyrometer in a more practical place, and minimizing its exposure to direct heat from the heating element and its interference with the production process.

Chapter 6

Concluding remarks and Future Work

The present chapter concludes this thesis with some final remarks on the concepts of Industry 4.0 with state estimation problems for composite materials manufacturing processes. The present thesis raised some pertinent questions, and interesting future research topics are also proposed. This chapter is organized as follows: Section 6.1 concludes the presented developments with some final remarks and highlights contributions. Section 6.2 presents a discussion on future research topics.

6.1. Concluding remarks

The research developed with this thesis focused on solving a requirement for a composite material manufacturing process to be controlled aiming to guarantee the quality of the manufactured structure. The solution to this problem involved the use of concepts proper of the Industry 4.0 tendency, specifically the Digital Twin, presented in Chapter 3, in addition to a state estimation strategy founded on a population-based optimization algorithm, that is independent of the mathematical problem to solve and can handle complex non-linear systems, as presented along Chapter 4.

6.1.1 Digital Twin

The employment of the Digital Twin concept in the ATL process required a detailed characterization of the machine assembly elements which resulted in the following achievements:

- To develop a characterization procedure, based on fundamental equations and specialized literature, to determine the one-dimensional thermal conductivity for a single-ply composite material using a vacuum chamber and monitoring the temperature dynamics along time at three specific locations.
- To implement a characterization procedure for obtaining the thermo-optical properties of an opaque composite material as a function of temperature.

Once the elements were characterized, the mathematical model could be assembled. Using a combination of analytical and numerical solutions, it was possible to define the following:

- The 1.5-dimensional mathematical model, consisting of a two-part algorithm, is capable of reproducing the dynamics of the heat distribution for an ATL process model. The dimensionality of the model allows for consuming less computational resources compared with a three-dimensional model.
- The produced Digital Twin can be integrated into a design methodology based on an optimization algorithm for understanding the process requirements based on the product.

The main concern while solving the mathematical model of a Digital Twin, is to guarantee the stability of the solution, which was achieved through the use of a solver for stiff systems of equations, the Radau II method.

6.1.2 State estimation

State estimation for stochastic systems is possible due to the use of meta-heuristic optimization methods as the proposed hybrid Artificial Bee Colony, presented in Chapter 4. As the method is independent of the problem, the following objectives were achieved:

- The hABC algorithm can handle complex non-linear systems, as the DT for the ATL process presented in Chapter 3.
- The proposed hABC algorithm takes advantage of the sampling frequency of each variable sensor to define the search bounds for the exploration phase of the algorithm, avoiding the method for selecting variable values with no physical sense for the system.

The use of bounded input variables allows the definition of the following feature for the hABC algorithm:

- The use of the system inputs as degrees of freedom for state estimation, allowed to minimize a cost function using the output variable measured, which results in reducing the state estimation error.

Another main concern of optimization algorithms for dealing with local minimums was achieved while defining the hABC algorithm search method:

- The proposed hABC method allows to deal with local minima by performing a coarse search along the entire search domain, using a convex cost function and defining the search bounds based on the measures performed by the sensors. This guarantees the convergence to the global minimum, or a near-global minimum if a coarse tolerance is given, as was the case for the ATL DT.

From a computational point of view, the proposed hABC algorithm can take advantage of modern computational systems:

- The proposed hABC algorithm allows the use of parallel computing, as all the involved solutions do not interact or depend on each other, increasing the efficiency of the method.

Finally, once the ATL process DT is combined with the proposed hABC algorithm, it enables its implementation on model-based control strategies, allowing the following:

- To satisfy the requirement of the model-based control strategy for knowing the nip point temperature, using the integration of the developed process DT with the proposed state estimation strategy.
- As the state estimation strategy was validated, it is possible to place a temperature sensor at a more convenient location along the machine, ensuring to provide information to the control strategy about the temperature distribution of the composite material.
- Knowing the temperature profile, allows the implementation of constraints to the control strategy in order to guarantee the quality of the manufactured structure, by minimizing the damage to the composite material matrix and preventing poor bonding conditions.

The proposed hABC algorithm takes advantage of a constrained search domain to produce a solution which is to minimize a convex cost function. In the case of having an unconstrained search domain for a particular dimension, the challenge is to determine a proper interval in which those degrees of freedom could fluctuate while making physical sense. An alternative is to define a wide search domain for the exploration phase around a value given as the first guess.

6.2. Future work

For the case of study, the number of degrees of freedom was set to two but, the algorithm could be extended for more. In that sense, and attending the work of Basit et al. [223], those extra degrees of freedom could be unknown variables. The challenge resides in how to define a proper set of physically-justified constraints for each degree of freedom. Each case has to be individually studied according to the physical phenomena occurring.

A challenge that is present in every complex system, is the inversion of the process dynamics matrix, as mentioned in Section 3.8, required in the ATL DT for the energy balance calculation, which represents a significant computational load. An interesting area of study could be related to finding a surrogate model, that does not require the inverse of a matrix, such as neural networks or another type of machine learning algorithm, to solve the energy balance problem.

To enhance the developed DT, some other phenomena could be included in the model for quality control and supervision, for example to understand the bonding conditions as exposed on the work of Nasreen et al. [224] and Liu et al. [225] or even taking track of the thermal history of the composite material structure to better understand the degradation of the matrix as being exposed to a constant heating and cooling process, as mentioned in the work of Martín et al. [5].

From a systems control perspective, the state estimation algorithm allows the implementation of a model-based control strategy, as it has been successfully implemented in the work of Goldar et al. [226] with a Model Predictive Control. As the control strategy for an ATL process could be multi-objective, and to facilitate the integration of the constraints into the algorithm, it is proposed the study those constraints making use of Gaussian functions for two main reasons: the first, is that the general convexity of the cost function is kept and the second reason, is that as the Gaussian function can be inverted, meaning that it can be used for addressing the optimization problem where some variables should be away from any particular value and variables that should be closed to a particular value.

References

[1] European Commission. **Efficient Material Hybridization by Unconventional Layup and Forming of Metals and Composites for Fabrication of Multifunctional Structures**, July 2018. URL `https://cordis.europa.eu/project/id/768710`. Publication Title: Efficient Material Hybridization by Unconventional Layup and Forming of Metals and Composites for Fabrication of Multifunctional Structures.

[2] Junxia Jiang, Yuxiao He, Han Wang, and Yinglin Ke. **Modeling and experimental validation of compaction pressure distribution for automated fiber placement**. *Composite Structures*, 256(June 2020):113101, 2021. ISSN 02638223. doi: 10.1016/j.compstruct.2020.113101.

[3] Eddy Barakat and Mikhael Tannous. **Simulation of the tape laying process with steering of tapes: Bonding defects prevention using simulation**. In *2019 Fourth International Conference on Advances in Computational Tools for Engineering Applications (ACTEA)*, pages 1–7. IEEE, July 2019. ISBN 978-1-72810-130-9. doi: 10.1109/ACTEA.2019.8851111.

[4] Khaled Yassin and Mehdi Hojjati. **Processing of thermoplastic matrix composites through automated fiber placement and tape laying methods**. *Journal of Thermoplastic Composite Materials*, 31(12):1676–1725, December 2018. ISSN 0892-7057. doi: 10.1177/0892705717738305.

[5] M. I. I. Martín, F. Rodríguez-Lence, A. Güemes, A. Fernández-López, L. A. A. Pérez-Maqueda, and A. Perejón. **On the determination of thermal degradation effects and detection techniques for thermoplastic composites obtained by automatic lamination**. *Composites Part A: Applied Science and Manufacturing*, 111 (April):23–32, August 2018. ISSN 1359835X. doi: 10.1016/j.compositesa.2018.05.006.

[6] Patricia P. Parlevliet, Harald E. N. N. Bersee, and Adriaan Beukers. **Residual stresses in thermoplastic composites - a study of the literature. Part III: Effects of thermal residual stresses**. *Composites Part A: Applied Science and Manufacturing*, 38(6):1581–1596, 2007. ISSN 1359835X. doi: 10.1016/j.compositesa.2006.12.005.

[7] P. D. D. Juarez and E. D. D. Gregory. **In Situ Thermal Inspection of Automated Fiber Placement for manufacturing induced defects**. *Composites*

Part B: Engineering, 220(January):109002, September 2021. ISSN 13598368. doi: 10.1016/j.compositesb.2021.109002.

[8] Anastasios Danezis, David Williams, Michael Edwards, and Alexandros A. Skordos. **Heat transfer modelling of flashlamp heating for automated tape placement of thermoplastic composites**. *Composites Part A: Applied Science and Manufacturing*, 145(March):106381, 2021. ISSN 1359835X. doi: 10.1016/j.compositesa.2021.106381.

[9] Ralf Engelhardt, Stefan Ehard, Tobias Wolf, Jonathan Oelhafen, Andreas Kollmannsberger, and Klaus Drechsler. **In Situ Joining of Unidirectional Tapes on Long Fiber Reinforced Thermoplastic Structures by Thermoplastic Automated Fiber Placement for Scientific Sounding Rocket Applications**. *Procedia CIRP*, 85:189–194, 2019. ISSN 22128271. doi: 10.1016/j.procir.2019.09.015.

[10] M. Narnhofer, R. Schledjewski, P. Mitschang, and L. Perko. **Simulation of the Tape-Laying Process for Thermoplastic Matrix Composites**. *Advances in Polymer Technology*, 32(S1):E705–E713, March 2013. ISSN 07306679. doi: 10.1002/adv.21312. ISBN: 3100012211108.

[11] Mattia Di Francesco, Laura Veldenz, Giuseppe Dell'Anno, and Kevin Potter. **Heater power control for multi-material, variable speed Automated Fibre Placement**. *Composites Part A: Applied Science and Manufacturing*, 101:408–421, October 2017. ISSN 1359-835X. doi: 10.1016/j.compositesa.2017.06.015.

[12] Dennis Maurer and Peter Mitschang. **Laser-powered tape placement process – simulation and optimization**. *Advanced Manufacturing: Polymer & Composites Science*, 1(3):129–137, July 2015. ISSN 2055-0340. doi: 10.1080/20550340.2015.1114798.

[13] F. Chinesta, A. Leygue, B. Bognet, Ch. Ghnatios, F. Poulhaon, F. Bordeu, A. Barasinski, A. Poitou, S. Chatel, and S. Maison-Le-Poec. **First steps towards an advanced simulation of composites manufacturing by automated tape placement**. *International Journal of Material Forming*, 7(1):81–92, March 2014. ISSN 1960-6214. doi: 10.1007/s12289-012-1112-9.

[14] Fazil O. Sonmez and Mustafa Akbulut. **Process optimization of tape placement for thermoplastic composites**. *Composites Part A: Applied Science and Manufacturing*, 38(9):2013–2023, 2007. ISSN 1359835X. doi: 10.1016/j.compositesa.2007.05.003.

[15] Fazil O. Sonmez, H. Thomas Hahn, and Mustafa Akbulut. **Analysis of process-induced residual stresses in tape placement**. *Journal of Thermoplastic Composite Materials*, 15(6):525–544, 2002. ISSN 08927057. doi: 10.1177/0892705702015006207.

[16] Fazil O. Sonmez and H. Thomas Hahn. **Modeling of Heat Transfer and Crystallization in Thermoplastic Composite Tape Placement Process**. *Journal of*

Thermoplastic Composite Materials, 10(3):198–240, May 1997. ISSN 0892-7057. doi: 10.1177/089270579701000301.

[17] Hee June Kim, Sun Kyung Kim, and Woo Il Lee. **A study on heat transfer during thermoplastic composite tape lay-up process**. *Experimental Thermal and Fluid Science*, 13(4):408–418, November 1996. ISSN 0894-1777. doi: 10.1016/S0894-1777(96)00095-7.

[18] Thomas M. Moerland, Joost Broekens, Aske Plaat, and Catholijn M. Jonker. **Model-based Reinforcement Learning: A Survey**. *Foundations and Trends® in Machine Learning*, 16(1):1–118, January 2023. ISSN 1935-8237, 1935-8245. doi: 10.1561/2200000086.

[19] Roderick Murray-Smith and T Johansen. *Multiple model approaches to nonlinear modelling and control*. CRC press, 2020. ISBN 978-0-7484-0595-4.

[20] Chao Shang, Wei-Han Chen, Abraham Duncan Stroock, and Fengqi You. **Robust Model Predictive Control of Irrigation Systems With Active Uncertainty Learning and Data Analytics**. *IEEE Transactions on Control Systems Technology*, 28(4):1493–1504, July 2020. ISSN 1558-0865. doi: 10.1109/TCST.2019.2916753. Conference Name: IEEE Transactions on Control Systems Technology.

[21] Jun Cheng, Ju H. Park, Jinde Cao, and Wenhai Qi. **Hidden Markov Model-Based Nonfragile State Estimation of Switched Neural Network With Probabilistic Quantized Outputs**. *IEEE Transactions on Cybernetics*, 50(5):1900–1909, May 2020. ISSN 2168-2275. doi: 10.1109/TCYB.2019.2909748. Conference Name: IEEE Transactions on Cybernetics.

[22] Katharina Bieker, Sebastian Peitz, Steven L. Brunton, J. Nathan Kutz, and Michael Dellnitz. **Deep model predictive flow control with limited sensor data and online learning**. *Theoretical and Computational Fluid Dynamics*, 34(4):577–591, August 2020. ISSN 1432-2250. doi: 10.1007/s00162-020-00520-4.

[23] Guido Sánchez, Marina Murillo, Lucas Genzelis, Nahuel Deniz, and Leonardo Giovanini. **MPC for nonlinear systems: A comparative review of discretization methods**. *2017 17th Workshop on Information Processing and Control, RPIC 2017*, 2017-Janua(2):1–6, 2017. doi: 10.23919/RPIC.2017.8214333.

[24] Oussama Ait Sahed, Kamel Kara, Abousoufyane Benyoucef, and Mohamed Laid Hadjili. **An efficient artificial bee colony algorithm with application to nonlinear predictive control**. *International Journal of General Systems*, 45(4):393–417, 2016. ISSN 15635104. doi: 10.1080/03081079.2015.1086344. Publisher: Taylor & Francis.

[25] Oussama Ait Sahed, Kamel Kara, and Abousoufyane Benyoucef. **Artificial bee colony-based predictive control for non-linear systems**. *Transactions of the Institute of Measurement and Control*, 37(6):780–792, 2015. ISSN 01423312. doi: 10.1177/0142331214546796.

[26] E. F. Camacho, D. R. Ramirez, D. Limon, D. Muñoz De La Pen, and T. Alamo. **Model predictive control techniques for hybrid systems**. *Annual Reviews in Control*, 34(1):21–31, 2010. ISSN 13675788. doi: 10.1016/j.arcontrol.2010.02.002.

[27] Fei Tao, Qinglin Qi, Lihui Wang, and A. Y. C. C. Nee. **Digital Twins and Cyber–Physical Systems toward Smart Manufacturing and Industry 4.0: Correlation and Comparison**. *Engineering*, 5(4):653–661, August 2019. ISSN 20958099. doi: 10.1016/j.eng.2019.01.014.

[28] Li Da Xu, Eric L. Xu, and Ling Li. **Industry 4.0: State of the art and future trends**. *International Journal of Production Research*, 56(8):2941–2962, April 2018. ISSN 1366588X. doi: 10.1080/00207543.2018.1444806.

[29] Werner Kritzinger, Matthias Karner, Georg Traar, Jan Henjes, and Wilfried Sihn. **Digital Twin in manufacturing: A categorical literature review and classification**. *IFAC-PapersOnLine*, 51(11):1016–1022, January 2018. ISSN 24058963. doi: 10.1016/j.ifacol.2018.08.474.

[30] Saurabh Vaidya, Prashant Ambad, and Santosh Bhosle. **Industry 4.0 – A Glimpse**. *Procedia Manufacturing*, 20:233–238, January 2018. ISSN 2351-9789. doi: 10.1016/j.promfg.2018.02.034.

[31] Jhonny de Sá Rodrigues, Paulo Teixeira Gonçalves, Luis Pina, and Fernando Gomes de Almeida. **Modelling the Heating Process in the Transient and Steady State of an In Situ Tape-Laying Machine Head**. *Journal of Manufacturing and Materials Processing*, 6(1):8, January 2022. ISSN 2504-4494. doi: 10.3390/jmmp6010008.

[32] J Rodrigues, F Silva, and J Santos. **Automated in situ consolidation process for pre-impregnated carbon fibers : a cyber physical approach**. *Materiales Compuestos*, 3(3):80–89, 2019. ISSN 2531-0739. URL `https://revista.aemac.org/`.

[33] Jhonny de Sá Rodrigues and Paulo Teixeira. **Model for an Automated Tape Laying Process: Heat source Identification**. In *DCE21: Symposium on Mechanical Engineering: Book of Abstracts and Invited Lectures*, pages 29–31. FEUP Edições, 2021. ISBN 978-972-752-286-6.

[34] Jhonny Rodrigues, Paulo Gonçalves, and Susana Sousa. **Composite material thermal characterization with conventonal and non-conventional tests**. In *5th Meeting of the Young Researchers of LAETA*, Lisbon, May 2022. IDMEC, Instituto Superior Técnico, Universidade de Lisboa. ISBN 978-989-53-5991-2. URL `https://5ejil.tecnico.ulisboa.pt/papers/`.

[35] Jhonny de Sá Rodrigues, Luís Pina, and Fernando Gomes de Almeida. **State Estimation using a Hybrid Artificial Bee Colony Algorithm for an Automated Tape Laying Process**. *Applied Soft Computing Journal*, 2022. (To be submitted).

[36] Jhonny Rodrigues and Paulo Teixeira Gonçalves. **Design of an Optimal Automated Tape Laying Process Using Digital Twin and Artificial Bee Colony Algorithms**. In *Composites Meet Sustainability – Proceedings of the 20th European Conference on Composite Materials, ECCM20*, volume 2, pages 44–50, Lausanne, Switzerland, July 2022. Ecole Polytechnique Fédérale de Lausanne. ISBN 978-2-9701614-0-0. doi: doi.org/10.5075/epfl-298799_978-2-9701614-0-0.

[37] Jhonny Rodrigues and Alejandro Goldar. **Computational Use of an Artificial Bee Colony approach for Model Predictive Control**. In *41st Benelux Meetings on Systems and Control*, volume 1, pages 193–194, Brussels, July 2022. Université libre de Bruxelles. URL `https://beneluxmeeting.nl/2022/uploads/images/2022/boa_BeneluxMeeting2022_Web_betaV12_withChairs.pdf`.

[38] Pedro Fernandes, Rui Marques, Ricardo Pinto, Pedro Mimoso, Jhonny Rodrigues, and Nuno Correia. **Design and optimization of a self-deployable composite structure**. *Materiales Compuestos*, 3(3):15–23, 2019. ISSN 2531-0739. URL `https://revista.aemag.org/`.

[39] Paulo Gonçalves, Albertino Arteiro, Nuno Rocha, and Jhonny Rodrigues. **Numerical analysis of cure induced stress in polymeric composite materials using a micromechanics approach**. In *5th Meeting of the Young Researchers of LAETA*, Lisbon, May 2022. IDMEC, Instituto Superior Técnico, Universidade de Lisboa. ISBN 978-989-53-5991-2. URL `https://5ejil.tecnico.ulisboa.pt/papers/`.

[40] Yongxin Liao, Fernando Deschamps, Eduardo de Freitas Rocha Loures, and Luiz Felipe Pierin Ramos. **Past, present and future of Industry 4.0 - a systematic literature review and research agenda proposal**. *International Journal of Production Research*, 55(12):3609–3629, June 2017. ISSN 0020-7543. doi: 10.1080/00207543.2017.1308576.

[41] Jie Xu, Edward Huang, Liam Hsieh, Loo Hay Lee, Qing Shan Jia, and Chun Hung Chen. **Simulation optimization in the era of Industrial 4.0 and the Industrial Internet**. *Journal of Simulation*, 10(4):310–320, 2016. ISSN 17477786. doi: 10.1057/s41273-016-0037-6. ISBN: 4127301600 Publisher: Palgrave Macmillan UK.

[42] N. Jazdi. **Cyber physical systems in the context of Industry 4.0**. In *2014 IEEE International Conference on Automation, Quality and Testing, Robotics*, pages 1–4, May 2014. doi: 10.1109/AQTR.2014.6857843.

[43] Jay Lee, Behrad Bagheri, and Hung-An An Kao. **A Cyber-Physical Systems architecture for Industry 4.0-based manufacturing systems**. *Manufacturing Letters*, 3:18–23, January 2015. ISSN 22138463. doi: 10.1016/j.mfglet.2014.12.001. Publisher: Elsevier.

[44] Hervé Panetto, Benoit Iung, Dmitry Ivanov, Georg Weichhart, and Xiaofan Wang. **Challenges for the cyber-physical manufacturing enterprises of the future**. *Annual Reviews in Control*, 2019. ISSN 13675788. doi: 10.1016/j.arcontrol.2019.02.002.

[45] Benjamin Schleich, Nabil Anwer, Luc Mathieu, and Sandro Wartzack. **Shaping the digital twin for design and production engineering**. *CIRP Annals - Manufacturing Technology*, 66(1):141–144, January 2017. ISSN 17260604. doi: 10.1016/j.cirp.2017.04.040.

[46] Felipe Baena, Alvaro Guarin, Julian Mora, Joel Sauza, and Sebastian Retat. **Learning Factory: The Path to Industry 4.0**. *Procedia Manufacturing*, 9:73–80, January 2017. ISSN 2351-9789. doi: 10.1016/j.promfg.2017.04.022.

[47] Thomas H.-J. Uhlemann, Christian Lehmann, and Rolf Steinhilper. **The Digital Twin: Realizing the Cyber-Physical Production System for Industry 4.0**. In *Procedia CIRP*, volume 61, pages 335–340. Elsevier, January 2017. doi: 10.1016/j.procir.2016.11.152.

[48] S. Waschull, J. A. C. C. C. Bokhorst, E. Molleman, and J. C. Wortmann. **Work design in future industrial production: Transforming towards cyber-physical systems**. *Computers and Industrial Engineering*, pages 1–11, 2019. ISSN 03608352. doi: 10.1016/j.cie.2019.01.053. URL `https://doi.org/10.1016/j.cie.2019.01.053`. Publisher: Elsevier.

[49] Rainer Stark, Carina Fresemann, and Kai Lindow. **Development and operation of Digital Twins for technical systems and services**. *CIRP Annals*, 68(1):129–132, January 2019. ISSN 17260604. doi: 10.1016/j.cirp.2019.04.024.

[50] Florian Biesinger, Davis Meike, Benedikt Kraß, and Michael Weyrich. **A digital twin for production planning based on cyber-physical systems: A Case Study for a Cyber-Physical System-Based Creation of a Digital Twin**. In *Procedia CIRP*, volume 79, pages 355–360, 2019. doi: 10.1016/j.procir.2019.02.087. ISSN: 22128271.

[51] Enrique Ruiz Zuniga, Matias Urenda Moris, and Anna Syberfeldt. **Integrating simulation-based optimization, lean, and the concepts of industry 4.0**. In *Proceedings - Winter Simulation Conference*, volume 17, pages 3828–3839, 2018. ISBN 978-1-5386-3428-8. doi: 10.1109/WSC.2017.8248094. ISSN: 08917736 Issue: 376 2.

[52] Qinglin Qi, Fei Tao, Ying Zuo, and Dongming Zhao. **Digital Twin Service towards Smart Manufacturing**. In *Procedia CIRP*, volume 72, pages 237–242. Elsevier, January 2018. doi: 10.1016/j.procir.2018.03.103.

[53] Paulo Leitão, Armando Walter Colombo, and Stamatis Karnouskos. **Industrial automation based on cyber-physical systems technologies: Prototype implementations and challenges**. *Computers in Industry*, 81:11–25, September 2016. ISSN 01663615. doi: 10.1016/j.compind.2015.08.004. Publisher: Elsevier.

[54] Mike Shafto, Mike Conroy, Rich Doyle, Ed Glaessgen, Chris Kemp, Jacqueline LeMoigne, Lui Wang, and a. **Modeling , Simulation , Information Technology & Processing Roadmap**, 2012. URL `https://www.nasa.gov/sites/default/files/501321main_TA11-ID_rev4_NRC-wTASR.pdf`. Accessed on 2020-04-15.

[55] Fei Tao and Meng Zhang. **Digital Twin Shop-Floor: A New Shop-Floor Paradigm Towards Smart Manufacturing**. *IEEE Access*, 5:20418–20427, 2017. ISSN 2169-3536. doi: 10.1109/ACCESS.2017.2756069.

[56] Marco Macchi, Irene Roda, Elisa Negri, and Luca Fumagalli. **Exploring the role of Digital Twin for Asset Lifecycle Management**. *IFAC-PapersOnLine*, 51(11): 790–795, January 2018. ISSN 24058963. doi: 10.1016/j.ifacol.2018.08.415.

[57] Jiewu Leng, Hao Zhang, Douxi Yan, Qiang Liu, Xin Chen, and Ding Zhang. **Digital twin-driven manufacturing cyber-physical system for parallel controlling of smart workshop**. *Journal of Ambient Intelligence and Humanized Computing*, 10(3): 1155–1166, 2019. ISSN 18685145. doi: 10.1007/s12652-018-0881-5. ISBN: 0123456789 Publisher: Springer Berlin Heidelberg.

[58] Michael Grieves and John Vickers. **Digital Twin: Mitigating Unpredictable, Undesirable Emergent Behavior in Complex Systems**. In Franz-Josef Kahlen, Shannon Flumerfelt, and Anabela Alves, editors, *Transdisciplinary Perspectives on Complex Systems: New Findings and Approaches*, pages 85–113. Springer International Publishing, Cham, 2017. ISBN 978-3-319-38756-7. doi: 10.1007/978-3-319-38756-7_4.

[59] Iris Graessler and Alexander Poehler. **Intelligent control of an assembly station by integration of a digital twin for employees into the decentralized control system**. In *Procedia Manufacturing*, volume 24, pages 185–189. Elsevier, January 2018. doi: 10.1016/j.promfg.2018.06.041. ISSN: 23519789.

[60] Jiri Tupa, Jan Simota, and Frantisek Steiner. **Aspects of Risk Management Implementation for Industry 4.0**. *Procedia Manufacturing*, 11:1223–1230, January 2017. ISSN 23519789. doi: 10.1016/j.promfg.2017.07.248. Publisher: Elsevier.

[61] Volkan Gunes, Steffen Peter, Tony Givargis, and Frank Vahid. **A survey on concepts, applications, and challenges in cyber-physical systems**. *KSII Transactions on Internet and Information Systems*, 8(12):4242–4268, 2014. ISSN 22881468. doi: 10.3837/tiis.2014.12.001.

[62] Christine Schulze, Sebastian Thiede, Bastian Thiede, Denis Kurle, Stefan Blume, and Christoph Herrmann. **Cooling tower management in manufacturing companies: A cyber-physical system approach**. *Journal of Cleaner Production*, 211:428–441, 2019. ISSN 09596526. doi: 10.1016/j.jclepro.2018.11.184.

[63] Yuchen Jiang, Shen Yin, Jingwei Dong, and Okyay Kaynak. **A Review on Soft Sensors for Monitoring, Control, and Optimization of Industrial Processes**. *IEEE Sensors Journal*, 21(11):12868–12881, June 2021. ISSN 1558-1748. doi: 10.1109/JSEN.2020.3033153. Conference Name: IEEE Sensors Journal.

[64] Mikel González, Oscar Salgado, Jan Croes, Bert Pluymers, and Wim Desmet. **A Digital Twin for Operational Evaluation of Vertical Transportation Systems**.

IEEE Access, 8:114389–114400, 2020. ISSN 2169-3536. doi: 10.1109/ACCESS.2020.3001686. Conference Name: IEEE Access.

[65] Jay Lee. **Smart Factory Systems**. *Informatik-Spektrum*, 38(3):230–235, 2015. ISSN 1432122X. doi: 10.1007/s00287-015-0891-z.

[66] Henning Kagermann, Wolfgang Wahlster, and Johannes Helbig. **Recommendations for implementing the strategic initiative INDUSTRIE 4.0 - Final report of the Industrie 4.0 Working Group**. *acatech - National Academy of Science and Engineering*, (April):84, 2013.

[67] Dominik Lucke, Carmen Constantinescu, and Engelbert Westkämper. **Smart Factory - A Step towards the Next Generation of Manufacturing**. *Manufacturing Systems and Technologies for the New Frontier*, (Sfb 627):115–118, 2008. doi: 10.1007/978-1-84800-267-8_23.

[68] Xuemin Sun, Jinsong Bao, Jie Li, Yiming Zhang, Shimin Liu, and Bin Zhou. **A digital twin-driven approach for the assembly-commissioning of high precision products**. *Robotics and Computer-Integrated Manufacturing*, 61(March 2019):101839, February 2020. ISSN 07365845. doi: 10.1016/j.rcim.2019.101839.

[69] Yuqian Lu, Chao Liu, Kevin I. Kai Wang, Huiyue Huang, and Xun Xu. **Digital Twin-driven smart manufacturing: Connotation, reference model, applications and research issues**. *Robotics and Computer-Integrated Manufacturing*, 61(April 2019):101837, 2020. ISSN 07365845. doi: 10.1016/j.rcim.2019.101837.

[70] Janos Sztipanovits, Xenofon Koutsoukos, Gabor Karsai, Nicholas Kottenstette, Panos Antsaklis, Vijay Gupta, Bill Goodwine, John Baras, and Shige Wang. **Toward a science of cyber-physical system integration**. *Proceedings of the IEEE*, 100(1):29–44, 2012. ISSN 00189219. doi: 10.1109/JPROC.2011.2161529.

[71] James A. Momoh. **Fundamentals of analysis and computation for the Smart Grid**. In *IEEE PES General Meeting*, pages 1–5, July 2010. ISBN 1944-9925. doi: 10.1109/PES.2010.5589984.

[72] Kyoung-Dae Kim and P. R. Kumar. **Cyber–Physical Systems: A Perspective at the Centennial**. *Proceedings of the IEEE*, 100(Special Centennial Issue):1287–1308, May 2012. ISSN 1558-2256. doi: 10.1109/JPROC.2012.2189792.

[73] Insup Lee and Oleg Sokolsky. **Medical cyber physical systems**. In *Proceedings of the 47th Design Automation Conference*, DAC '10, pages 743–748, New York, NY, USA, June 2010. Association for Computing Machinery. ISBN 978-1-4503-0002-5. doi: 10.1145/1837274.1837463.

[74] David Arney, Sebastian Fischmeister, Julian M. Goldman, Insup Lee, and Robert Trausmuth. **Plug-and-Play for Medical Devices: Experiences from a Case Study**. *Biomedical Instrumentation & Technology*, 43(4):313–317, July 2009. doi: 10.2345/0899-8205-43.4.313. Publisher: AAMI.

[75] Wenjuan Li, Weizhi Meng, Chunhua Su, and Lam For Kwok. **Towards false alarm reduction using fuzzy if-Then rules for medical cyber physical systems**. *IEEE Access*, 6:6530–6539, 2018. ISSN 21693536. doi: 10.1109/ACCESS.2018.2794685. Publisher: IEEE.

[76] A. Crosky, C. Grant, D. Kelly, X. Legrand, and G. Pearce. **4 - Fibre placement processes for composites manufacture**. In Philippe Boisse, editor, *Advances in Composites Manufacturing and Process Design*, pages 79–92. Woodhead Publishing, January 2015. ISBN 978-1-78242-307-2.

[77] D. Saenz-Castillo, M. I. I. Martín, S. Calvo, F. Rodriguez-Lence, and A. Güemes. **Effect of processing parameters and void content on mechanical properties and NDI of thermoplastic composites**. *Composites Part A: Applied Science and Manufacturing*, 121(March):308–320, June 2019. ISSN 1359835X. doi: 10.1016/j.compositesa.2019.03.035. Publisher: Elsevier.

[78] Muhammad Amir Khan, Peter Mitschang, and Ralf Schledjewski. **Identification of some optimal parameters to achieve higher laminate quality through tape placement process**. *Advances in Polymer Technology*, 29(2):98–111, 2010. ISSN 1098-2329. doi: 10.1002/adv.20177.

[79] A. Liebsch, W. Koshukow, J. Gebauer, R. Kupfer, and M. Gude. **Overmoulding of consolidated fibre-reinforced thermoplastics - increasing the bonding strength by physical surface pre-treatments**. *Procedia CIRP*, 85:212–217, 2019. ISSN 22128271. doi: 10.1016/j.procir.2019.09.047.

[80] S. Tumkor, N. Turkmen, C. Chassapis, and S. Manoochehri. **Modeling of heat transfer in thermoplastic composite tape lay-up manufacturing**. *International Communications in Heat and Mass Transfer*, 28(1):49–58, January 2001. ISSN 07351933. doi: 10.1016/S0735-1933(01)00212-3.

[81] A. J. Comer, D. Ray, W. O. Obande, D. Jones, J. Lyons, I. Rosca, R. M. O'Higgins, and M. A. McCarthy. **Mechanical characterisation of carbon fibre-PEEK manufactured by laser-assisted automated-tape-placement and autoclave**. *Composites Part A: Applied Science and Manufacturing*, 69:10–20, 2015. ISSN 1359835X. doi: 10.1016/j.compositesa.2014.10.003.

[82] J. Colton and D. Leach. **Processing parameters for filament winding thick-section PEEK/carbon fiber composites**. *Polymer Composites*, 13(6):427–434, 1992. ISSN 1548-0569. doi: 10.1002/pc.750130605.

[83] Bruce K. Fink, Roy L. McCullough, and John W. Gillespie Jr. **A local theory of heating in cross-ply carbon fiber thermoplastic composites by magnetic induction**. *Polymer Engineering & Science*, 32(5): 357–369, 1992. ISSN 1548-2634. doi: 10.1002/pen.760320509. _eprint: https://onlinelibrary.wiley.com/doi/pdf/10.1002/pen.760320509.

[84] Aadhithya Rajasekaran and Farjad Shadmehri. **Steering of carbon fiber/PEEK tapes using Hot Gas Torch-assisted automated fiber placement**. *Journal of Thermoplastic Composite Materials*, page 08927057211067962, February 2022. ISSN 0892-7057. doi: 10.1177/08927057211067962.

[85] Mehrshad Moghadamazad and Suong V. Hoa. **Models for heat transfer in thermoplastic composites made by automated fiber placement using hot gas torch**. *Composites Part C: Open Access*, 7:100214, March 2022. ISSN 2666-6820. doi: 10.1016/j.jcomc.2021.100214.

[86] Muhammad Amir Khan, Peter Mitschang, and Ralf Schledjewski. **Tracing the Void Content Development and Identification of its Effecting Parameters during in Situ Consolidation of Thermoplastic Tape Material**. *Polymers and Polymer Composites*, 18(1):1–15, January 2010. ISSN 0967-3911. doi: 10.1177/096739111001800101.

[87] R. Pitchumani, J. W. Gillespie, and M. A. Lamontia. **Design and Optimization of a Thermoplastic Tow-Placement Process with In-Situ Consolidation**. *Journal of Composite Materials*, 31(3):244–275, February 1997. ISSN 0021-9983. doi: 10.1177/002199839703100302. ISBN: 0893-3200.

[88] Magnus Pettersson. *Heat Transfer and Energy Efficiency in Infrared Paper Dryers*. Chemical Engineering, Lund University, 1999. ISBN 978-0-12-386990-6.

[89] Omar Baho, Gilles Ausias, Yves Grohens, Marco Barile, Leonardo Lecce, and Julien Férec. **Automated fibre placement process for a new hybrid material: A numerical tool for predicting an efficient heating law**. *Composites Part A: Applied Science and Manufacturing*, 144(September 2020):106360, May 2021. ISSN 1359835X. doi: 10.1016/j.compositesa.2021.106360.

[90] Martin Römer, Johannes Bergers, Felix Gabriel, and Klaus Dröder. **Temperature Control for Automated Tape Laying with Infrared Heaters Based on Reinforcement Learning**. *Machines*, 10(3):164, March 2022. ISSN 2075-1702. doi: 10.3390/machines10030164.

[91] Christopher Mark Stokes-Griffin, Paul Compston, Timothy I. Matuszyk, and Michael J. Cardew-Hall. **Thermal modelling of the laser-assisted thermoplastic tape placement process**. *Journal of Thermoplastic Composite Materials*, 28(10):1445–1462, October 2015. ISSN 0892-7057. doi: 10.1177/0892705713513285.

[92] C. M. M. Stokes-Griffin and P. Compston. **A combined optical-thermal model for near-infrared laser heating of thermoplastic composites in an automated tape placement process**. *Composites Part A: Applied Science and Manufacturing*, 75:104–115, August 2015. ISSN 1359835X. doi: 10.1016/j.compositesa.2014.08.006. Publisher: Elsevier Ltd.

[93] P. M. Schaefer, D. Gierszewski, A. Kollmannsberger, S. Zaremba, and K. Drechsler. **Analysis and improved process response prediction of laser- assisted automated tape placement with PA-6/carbon tapes using Design of Experiments and numerical simulations**. *Composites Part A: Applied Science and Manufacturing*, 96:137–146, 2017. ISSN 1359835X. doi: 10.1016/j.compositesa.2017.02.008.

[94] Frank P. Incropera, David P. DeWitt, Theodore L. Bergman, Adrienne S. Lavine, and others. *Fundamentals of heat and mass transfer*, volume 6. Wiley New York, 2006. ISBN 978-85-216-3659-5.

[95] Anaïs Barasinski, Adrien Leygue, Eric Soccard, and Arnaud Poitou. **An improvement in thermal modelling of automated tape placement process**. *AIP Conference Proceedings*, 1315(2011):185–190, 2010. ISSN 0094243X. doi: 10.1063/1.3552438. ISBN: 9780735408715.

[96] R. Lichtinger, P. Hörmann, D. Stelzl, and R. Hinterhölzl. **The effects of heat input on adjacent paths during Automated Fibre Placement**. *Composites Part A: Applied Science and Manufacturing*, 68:387–397, January 2015. ISSN 1359-835X. doi: 10.1016/j.compositesa.2014.10.004.

[97] S. M. Amin Hosseini, Ismet Baran, Martin van Drongelen, and Remko Akkerman. **On the temperature evolution during continuous laser-assisted tape winding of multiple C/PEEK layers: The effect of roller deformation**. *International Journal of Material Forming*, June 2020. ISSN 1960-6206. doi: 10.1007/s12289-020-01568-7.

[98] Magnus Pettersson and Stig Stenström. **Modelling of an electric IR heater at transient and steady state conditions: Part I: model and validation**. *International Journal of Heat and Mass Transfer*, 43(7):1209–1222, 2000. ISBN: 0017-9310.

[99] Magnus Pettersson and Stig Stenström. **Modelling of an electric IR heater at transient and steady state conditions: Part II: modelling a paper dryer**. *International Journal of Heat and Mass Transfer*, 43(7):1223–1232, April 2000. ISSN 00179310. doi: 10.1016/S0017-9310(99)00202-1.

[100] R. C. Progelhof, J. L. Throne, and R. R. Ruetsch. **Methods for predicting the thermal conductivity of composite systems: A review**. *Polymer Engineering {&} Science*, 16(9):615–625, 1976. ISSN 15482634. doi: 10.1002/pen.760160905.

[101] Ching Yu Yang. **Estimation of the temperature-dependent thermal conductivity in inverse heat conduction problems**. *Applied Mathematical Modelling*, 23 (6):469–478, 1999. ISSN 0307904X. doi: 10.1016/S0307-904X(98)10093-8.

[102] Giampaolo Betta, Massimiliano Rinaldi, Davide Barbanti, and Roberto Massini. **A quick method for thermal diffusivity estimation: Application to several foods**. *Journal of Food Engineering*, 91(1):34–41, March 2009. ISSN 02608774. doi: 10.1016/j.jfoodeng.2008.08.003. Publisher: Elsevier Ltd.

[103] Maxime Villière, Damien Lecointe, Vincent Sobotka, Nicolas Boyard, and Didier Delaunay. **Experimental determination and modeling of thermal conductivity tensor of carbon/epoxy composite**. *Composites Part A: Applied Science and Manufacturing*, 46(1):60–68, 2013. ISSN 1359835X. doi: 10.1016/j.compositesa.2012.10.012.

[104] Yue Cong, Yan Zhang, Zhili Hu, Johan Liu, and Zhaonian Cheng. **Modeling of the effective thermal conductivity of composite materials with FEM based on resistor networks approach**. *Microsystem Technologies*, 16(4):633–639, 2010. ISSN 09467076. doi: 10.1007/s00542-009-0984-1.

[105] Ce-Wen Nan. **Physics of inhomogeneous inorganic materials**. *Progress in Materials Science*, 37(1):1–116, January 1993. ISSN 0079-6425. doi: 10.1016/0079-6425(93)90004-5.

[106] Hugo Fricke. **The Maxwell-Wagner Dispersion in a Suspension of Ellipsoids**. *American Chemical Society*, May 2002. doi: 10.1021/j150510a018.

[107] Y. Benveniste. **Effective thermal conductivity of composites with a thermal contact resistance between the constituents: Nondilute case**. *Journal of Applied Physics*, 61(8):2840–2843, April 1987. ISSN 0021-8979. doi: 10.1063/1.337877.

[108] K. Pietrak and T. Wiśniewski. **A review of models for effective thermal conductivity of composite materials**. *Journal of Power of Technologies*, 95(1):14–24, 2015. ISSN 1425-1353.

[109] Siping Zhai, Ping Zhang, Yaoqi Xian, Jianhua Zeng, and Bo Shi. **Effective thermal conductivity of polymer composites: Theoretical models and simulation models**. *International Journal of Heat and Mass Transfer*, 117:358–374, 2018. ISSN 00179310. doi: 10.1016/j.ijheatmasstransfer.2017.09.067.

[110] Ajay Kumar, Abhishek Kumar Singh, and Rajeev. **A Stefan problem with temperature and time dependent thermal conductivity**. *Journal of King Saud University - Science*, 32(1):97–101, 2020. ISSN 10183647. doi: 10.1016/j.jksus.2018.03.005.

[111] François Auger, Mickael Hilairet, Josep M. Guerrero, Eric Monmasson, Teresa Orlowska-Kowalska, and Seiichiro Katsura. **Industrial Applications of the Kalman Filter: A Review**. *IEEE Transactions on Industrial Electronics*, 60(12):5458–5471, December 2013. ISSN 1557-9948. doi: 10.1109/TIE.2012.2236994.

[112] R. E. Kalman. **A New Approach to Linear Filtering and Prediction Problems**. *Journal of Basic Engineering*, 82(1):35–45, March 1960. ISSN 0021-9223. doi: 10.1115/1.3662552.

[113] Richard Blundell, Whitney K Newey, and Torsten Persson. *Advances in Economics and Econometrics: Volume 1: Theory and Applications, Ninth World Congress*, volume 1. Cambridge University Press, 2006. ISBN 978-0-521-87152-5.

[114] Mohinder S. Grewal and Angus P. Andrews. **Applications of Kalman Filtering in Aerospace 1960 to the Present [Historical Perspectives]**. *IEEE Control Systems Magazine*, 30(3):69–78, June 2010. ISSN 1941-000X. doi: 10.1109/MCS.2010.936465.

[115] J. Woods and C. Radewan. **Kalman filtering in two dimensions**. *IEEE Transactions on Information Theory*, 23(4):473–482, July 1977. ISSN 1557-9654. doi: 10.1109/TIT.1977.1055750. Conference Name: IEEE Transactions on Information Theory.

[116] D. Salmond. **Target tracking: introduction and Kalman tracking filters**. In *IEE Target Tracking: Algorithms and Applications (Ref. No. 2001/174)*, volume Workshop, pages 1/1–1/16 vol.2, October 2001. doi: 10.1049/ic:20010245.

[117] Qiang Li, Ranyang Li, Kaifan Ji, and Wei Dai. **Kalman Filter and Its Application**. In *2015 8th International Conference on Intelligent Networks and Intelligent Systems (ICINIS)*, pages 74–77, November 2015. doi: 10.1109/ICINIS.2015.35.

[118] Michael Roth, Gustaf Hendeby, and Fredrik Gustafsson. **Nonlinear Kalman filters explained: A tutorial on moment computations and sigma point methods**. *Journal of Advances in Information Fusion*, 11(1):47–70, 2016. ISSN 1557-6418.

[119] M. Farsi and M. Dehghan Manshadi. **A State Estimation Method Based on Integration of Linear and Extended Kalman Filters**. *Chemical Product and Process Modeling*, 14(4):1–16, December 2019. ISSN 1934-2659. doi: 10.1515/cppm-2018-0051.

[120] Piotr Kaniewski. **Extended Kalman Filter with Reduced Computational Demands for Systems with Non-Linear Measurement Models**. *Sensors*, 20(6): 1584, March 2020. ISSN 1424-8220. doi: 10.3390/s20061584.

[121] Milca de Freitas Coelho, Kouamana Bousson, and Kawser Ahmed. **An Improved Extended Kalman Filter for Radar Tracking of Satellite Trajectories**. *Designs*, 5(3):54, August 2021. ISSN 2411-9660. doi: 10.3390/designs5030054.

[122] J. Mendel. **Computational requirements for a discrete Kalman filter**. *IEEE Transactions on Automatic Control*, 16(6):748–758, December 1971. ISSN 1558-2523. doi: 10.1109/TAC.1971.1099837. Conference Name: IEEE Transactions on Automatic Control.

[123] Arthur Gelb and others. *Applied optimal estimation*. MIT press, 16 th edition edition, 1974. ISBN 0-262-20027-9.

[124] Douglas C Montgomery, George C Runger, and Norma F Hubele. *Engineering statistics*. John Wiley & Sons, 2009. ISBN 978-0-470-63147-8.

[125] Yuxuan Shen, Zidong Wang, and Hongli Dong. **Minimum-Variance State and Fault Estimation for Multirate Systems With Dynamical Bias**. *IEEE Transactions on Circuits and Systems II: Express Briefs*, 69(4):2361–2365, April 2022. ISSN 1558-3791. doi: 10.1109/TCSII.2022.3142094.

[126] Prabhat K. Mishra, Girish Chowdhary, and Prashant G. Mehta. **Minimum variance constrained estimator**. *Automatica*, 137:110106, March 2022. ISSN 0005-1098. doi: 10.1016/j.automatica.2021.110106.

[127] A.H. Sayed and T. Kailath. **A state-space approach to adaptive RLS filtering**. *IEEE Signal Processing Magazine*, 11(3):18–60, July 1994. ISSN 1558-0792. doi: 10.1109/79.295229. Conference Name: IEEE Signal Processing Magazine.

[128] Xue-Bo Jin, Ruben Jonhson Robert Jeremiah, Ting-Li Su, Yu-Ting Bai, and Jian-Lei Kong. **The New Trend of State Estimation: From Model-Driven to Hybrid-Driven Methods**. *Sensors*, 21(6):2085, March 2021. ISSN 1424-8220. doi: 10.3390/s21062085.

[129] Yanjun Ma, Shunyi Zhao, and Biao Huang. **Multiple-Model State Estimation Based on Variational Bayesian Inference**. *IEEE Transactions on Automatic Control*, 64(4):1679–1685, April 2019. ISSN 1558-2523. doi: 10.1109/TAC.2018.2854897. Conference Name: IEEE Transactions on Automatic Control.

[130] Kaveh Dehghanpour, Zhaoyu Wang, Jianhui Wang, Yuxuan Yuan, and Fankun Bu. **A Survey on State Estimation Techniques and Challenges in Smart Distribution Systems**. *IEEE Transactions on Smart Grid*, 10(2):2312–2322, March 2019. ISSN 1949-3061. doi: 10.1109/TSG.2018.2870600.

[131] Tanja Hernández Rodríguez, Christoph Posch, Ralf Pörtner, and Björn Frahm. **Dynamic parameter estimation and prediction over consecutive scales, based on moving horizon estimation: applied to an industrial cell culture seed train**. *Bioprocess and Biosystems Engineering*, 44(4):793–808, April 2021. ISSN 1615-7605. doi: 10.1007/s00449-020-02488-1. URL `https://doi.org/10.1007/s00449-020-02488-1`.

[132] Lei Zou, Zidong Wang, Jun Hu, and Donghua Zhou. **Moving Horizon Estimation With Unknown Inputs Under Dynamic Quantization Effects**. *IEEE Transactions on Automatic Control*, 65(12):5368–5375, December 2020. ISSN 1558-2523. doi: 10.1109/TAC.2020.2968975. Conference Name: IEEE Transactions on Automatic Control.

[133] Xiaosong Hu, Dongpu Cao, and Bo Egardt. **Condition Monitoring in Advanced Battery Management Systems: Moving Horizon Estimation Using a Reduced Electrochemical Model**. *IEEE/ASME Transactions on Mechatronics*, 23(1):167–178, February 2018. ISSN 1941-014X. doi: 10.1109/TMECH.2017.2675920. Conference Name: IEEE/ASME Transactions on Mechatronics.

[134] Dražen Bajer and Bruno Zorić. **An effective refined artificial bee colony algorithm for numerical optimisation**. *Information Sciences*, 504:221–275, December 2019. ISSN 0020-0255. doi: 10.1016/j.ins.2019.07.022. URL `https://www.sciencedirect.com/science/article/pii/S0020025519306280`.

[135] Seid Miad Zandavi and Vera Chung. **State estimation of nonlinear dynamic system using novel heuristic filter based on genetic algorithm**. *Soft Computing*, 23(14):5559–5570, July 2019. ISSN 1433-7479. doi: 10.1007/s00500-018-3213-y. URL `https://doi.org/10.1007/s00500-018-3213-y`.

[136] Wei Hu, Yongguang Yu, and Wenjuan Gu. **Parameter estimation of fractional-order arbitrary dimensional hyperchaotic systems via a hybrid adaptive artificial bee colony algorithm with simulated annealing algorithm**. *Engineering Applications of Artificial Intelligence*, 68:172–191, February 2018. ISSN 0952-1976. doi: 10.1016/j.engappai.2017.10.002.

[137] Moritz Cramer, Philipp Goergens, Fabian Potratz, and Armin Schnettler. **Genetic Algorithm for Optimal Meter Placement and Selection in Distribution Grid State Estimation**. In *International ETG Congress 2015; Die Energiewende - Blueprints for the new energy age*, pages 1–7, November 2015. ISBN 978-3-8007-4121-2.

[138] Asegunloluwa Eunice Babalola, Bolanle Adefowoke Ojokoh, and Julius Beneoluchi Odili. **A Review of Population-Based Optimization Algorithms**. In *2020 International Conference in Mathematics, Computer Engineering and Computer Science (ICMCECS)*, pages 1–7, March 2020. doi: 10.1109/ICMCECS47690.2020.240856.

[139] Xue Rongrong, Ye Zhengyin, Ye Kun, and Wang Gang. **Composite material structure optimization design and aeroelastic analysis on forward swept wing**. *Proceedings of the Institution of Mechanical Engineers, Part G: Journal of Aerospace Engineering*, 233(13):4679–4695, October 2019. ISSN 0954-4100. doi: 10.1177/0954410018807810.

[140] Yingjie Xu, Jihong Zhu, Zhen Wu, Yinfeng Cao, Yubo Zhao, and Weihong Zhang. **A review on the design of laminated composite structures: constant and variable stiffness design and topology optimization**. *Advanced Composites and Hybrid Materials*, 1(3):460–477, September 2018. ISSN 2522-0136. doi: 10.1007/s42114-018-0032-7.

[141] S. Nikbakt, S. Kamarian, and M. Shakeri. **A review on optimization of composite structures Part I: Laminated composites**. *Composite Structures*, 195:158–185, July 2018. ISSN 0263-8223. doi: 10.1016/j.compstruct.2018.03.063.

[142] S. Nikbakht, S. Kamarian, and M. Shakeri. **A review on optimization of composite structures Part II: Functionally graded materials**. *Composite Structures*, 214: 83–102, April 2019. ISSN 0263-8223. doi: 10.1016/j.compstruct.2019.01.105.

[143] P. Fernandes, R. Pinto, and N. Correia. **Design and optimization of self-deployable damage tolerant composite structures: A review**. *Composites Part B: Engineering*, 221:109029, September 2021. ISSN 1359-8368. doi: 10.1016/j.compositesb.2021.109029.

[144] Dervis Karaboga. **An idea based on honey bee swarm for numerical optimization**, 2005. URL `https://abc.erciyes.edu.tr/pub/tr06_2005.pdf`. Accessed on 2021-12-10.

[145] Nenavath Ravi Kumar and E. Nagabhooshanam. **An Extended Kalman Filter for Low-Cost Positioning System in Agricultural Vehicles**. In *2016 International Conference on Wireless Communications, Signal Processing and Networking (WiSPNET)*, pages 151–157. IEEE, March 2016. ISBN 978-1-4673-9338-6. doi: 10.1109/WiSPNET.2016.7566110.

[146] Behzad Nozohour-leilabady and Babak Fazelabdolabadi. **On the application of artificial bee colony (ABC) algorithm for optimization of well placements in fractured reservoirs; efficiency comparison with the particle swarm optimization (PSO) methodology**. *Petroleum*, 2(1):79–89, March 2016. ISSN 24055816. doi: 10.1016/j.petlm.2015.11.004. Publisher: Elsevier.

[147] Quan Ke Pan, M. Fatih Tasgetiren, P. N. Suganthan, and T. J. Chua. **A discrete artificial bee colony algorithm for the lot-streaming flow shop scheduling problem**. *Information Sciences*, 181(12):2455–2468, 2011. ISSN 00200255. doi: 10.1016/j.ins.2009.12.025.

[148] Abyson Scaria, Kiran George, and Jobin Sebastian. **An Artificial Bee Colony Approach for Multi-objective Job Shop Scheduling**. *Procedia Technology*, 25 (Raerest):1030–1037, 2016. ISSN 22120173. doi: 10.1016/j.protcy.2016.08.203.

[149] Xinyu Li, Shengqiang Xiao, Cuiyu Wang, and Jin Yi. **Mathematical modeling and a discrete artificial bee colony algorithm for the welding shop scheduling problem**. *Memetic Computing*, 11(4):371–389, 2019. ISSN 18659292. doi: 10.1007/s12293-019-00283-4.

[150] Majd Saied, Malak Slim, Hussein Mazeh, Clovis Francis, and Hassan Shraim. **Unmanned Aerial Vehicles Fleet Control via Artificial Bee Colony Algorithm**. In *2019 4th Conference on Control and Fault Tolerant Systems (SysTol)*, pages 80–85. IEEE, September 2019. ISBN 978-1-72810-380-8. doi: 10.1109/SYSTOL.2019.8864752. ISSN: 21621209.

[151] Weifeng Gao and Sanyang Liu. **Improved artificial bee colony algorithm for global optimization**. *Information Processing Letters*, 111(17):871–882, 2011. ISSN 00200190. doi: 10.1016/j.ipl.2011.06.002.

[152] Wei Feng Gao and San Yang Liu. **A modified artificial bee colony algorithm**. *Computers and Operations Research*, 39(3):687–697, March 2012. ISSN 03050548. doi: 10.1016/j.cor.2011.06.007.

[153] Wei-feng Gao, San-yang Liu, and Ling-ling Huang. **A novel artificial bee colony algorithm with Powell's method**. *Applied Soft Computing*, 13(9):3763–3775, September 2013. ISSN 1568-4946. doi: 10.1016/j.asoc.2013.05.012.

[154] K. Vanchinathan and N. Selvaganesan. **Adaptive fractional order PID controller tuning for brushless DC motor using Artificial Bee Colony algorithm**. *Results in Control and Optimization*, 4(February):100032, September 2021. ISSN 26667207. doi: 10.1016/j.rico.2021.100032. Publisher: Elsevier B.V.

[155] ASTM D 792-07. **Standard Test Methods for Density and Specific Gravity (Relative Density) of Plastics by Displacement**. Technical report, 2007. PA, USA.

[156] ASTM E 1269-9901. **Standard Test Method for Determining Specific Heat Capacity by Differential Scanning Calorimetry**. Technical report, 2001. PA, USA.

[157] ASTM E1461-13. **Standard Test Method for Thermal Diffusivity by the Flash Method**. Technical report, 2013. PA, USA.

[158] R. Srinivasa Raghav, Kalaipriyan Thirugnanasambandam, Vijayakumar Varadarajan, Subramaniyaswamy Vairavasundaram, and Logesh Ravi. **Artificial Bee Colony Reinforced Extended Kalman Filter Localization Algorithm in Internet of Things with Big Data Blending Technique for Finding the Accurate Position of Reference Nodes**. *Big Data*, November 2021. ISSN 2167-6461. doi: 10.1089/big.2020.0203.

[159] Aziz Kaba and Emre Kiyak. **Artificial bee colony–based Kalman filter hybridization for three–dimensional position estimation of a quadrotor**. *Aircraft Engineering and Aerospace Technology*, 92(10):1523–1532, August 2020. ISSN 1748-8842. doi: 10.1108/AEAT-01-2020-0015. ISBN: 0120200015.

[160] Magnus Pettersson and Stig Stenström. **Modelling of an electric IR heater at transient and steady state conditions**. *International Journal of Heat and Mass Transfer*, 43(7):1209–1222, April 2000. ISSN 00179310. doi: 10.1016/S0017-9310(99)00201-X. ISBN: 0017-9310.

[161] J.R. R. Howell, M.P. Menguc, Siegel, J. R. Howell, M. P. Menguc, and R. Siegel. *Thermal Radiation Heat Transfer*. CRC Press, 2015. ISBN 978-1-4987-5774-4.

[162] E. S. Domalski. **NIST Chemistry WebBook**, 2011. URL `https://www.nist.gov/`. Publication Title: NIST Chemistry WebBook. Accessesd on 2019-07-05.

[163] Michael Modest. *Radiative Heat Transfer*. Academic Press, 3rd editio edition, 2013. ISBN 978-0-12-386990-6.

[164] Vincent T. Morgan. **The Overall Convective Heat Transfer from Smooth Circular Cylinders**. pages 199–264. 1975. doi: 10.1016/S0065-2717(08)70075-3.

[165] Stuart W. Churchill and Humbert H. S. Chu. **Correlating equations for laminar and turbulent free convection from a vertical plate**. *International Journal of Heat and Mass Transfer*, 18(11):1323–1329, November 1975. ISSN 00179310. doi: 10.1016/0017-9310(75)90243-4.

[166] M. W. Chase, J. L. Curnutt, J. R. Downey, R. A. McDonald, A. N. Syverud, and E. A. Valenzuela. **JANAF Thermochemical Tables, 1982 Supplement**. *Journal of Physical and Chemical Reference Data*, 11(3):695–940, 1982. ISSN 0047-2689. doi: 10.1063/1.555666.

[167] William F. Gale and Terry C. Totemeier. *Smithells metals reference book*, volume 1. Elsevier, 8th edition, 2003. ISBN 978-0-08-048096-1. Issue: 9 Publication Title: Elsevier.

[168] David R Lide. *CRC handbook of chemistry and physics*, volume 85. CRC press, 2004. ISBN 978-0-8493-0485-9.

[169] R. Hilpert. **Wärmeabgabe von geheizten Drähten und Rohren im Luftstrom**. *Forschung auf dem Gebiete des Ingenieurwesens*, 4(5):215–224, September 1933. ISSN 0015-7899. doi: 10.1007/BF02719754.

[170] Silex. **Silicone Rubber Sheeting High Temperature Solid, Datasheet**, 2019. URL `https://www.silex.co.uk/media/38087/solid-sheet-thtsilex-ntds.pdf`. Datasheet. Accessed on 2019-07-10.

[171] J.R. Howell, M.P. Menguc, and R. Siegel. *Thermal Radiation Heat Transfer*. CRC Press, 2015. ISBN 978-1-4987-5774-4.

[172] a B. Shapiro. **FACET: a radiation view factor computer code for axisymmetric, 2D planar, and 3D geometries with shadowing**. *BioTechniques*, 38, 1983. URL `https://www.osti.gov/biblio/5607653`. Accessed on 19/04/2020.

[173] Markku J. Lampinen, Kari T. Ojala, and Esai Koski. **MODELING AND MEASUREMENTS OF INFRARED DRYERS FOR COATED PAPER**. *Drying Technology*, 9(4):973–1017, August 1991. ISSN 0737-3937. doi: 10.1080/07373939108916730.

[174] N. S. Izuegbu and M. L. Adonis. **Simulation and modelling of energy efficient design of a ceramic infrared heater**. *2011 Proceedings of the 8th Conference on the Industrial and Commercial Use of Energy, ICUE 2011*, pages 69–74, 2011. ISBN: 9780981431154 Publisher: IEEE.

[175] S.P. P Venkateshan. *Heat Transfer*. Springer International Publishing, Cham, 2021. ISBN 978-3-030-58337-8. doi: 10.1007/978-3-030-58338-5.

[176] A. Feingold and K. G. Gupta. **New analytical approach to the evaluation of configuration factors in radiation from spheres and infinitely long cylinders**. *Journal of Heat Transfer*, 92(1):69–6, 1970. ISSN 15288943. doi: 10.1115/1.3449647.

[177] J. G. Hust and A. B. Lankford. **Thermal Conductivity of Aluminium, Copper, Iron, and Tungsten for Temperatures from 1 K to the Melting Point**. Technical report, U.S. Department of Commerce, 1984. URL `https://www.osti.gov/biblio/6225458`. Issue: June. Accessed on 2019-05-23.

[178] Terry C. Edwards and Michael B. Steer. *Foundations for microstrip circuit design*. John Wiley {&} Sons, fourth edi edition, 2016. ISBN 978-1-118-93619-1.

[179] Tunis Wentink and Walter G. Planet. **Infrared Emission Spectra of Quartz***. *Journal of the Optical Society of America*, 51(6):595, June 1961. ISSN 0030-3941. doi: 10.1364/JOSA.51.000595.

[180] Toray Goup. **Toray Cetex TC910**, 2021. URL `toraytac.com/product-explorer/products/r2Vf/Toray-Cetex-TC910`. Accessed on 18/10/2020.

[181] ASTM E230/E230M-17. **Standard Specification for Temperature-Electromotive Force (emf) Tables for Standardized Thermocouples**. Technical report, 2017. PA, USA.

[182] Magnus Holmsten, Jan Ivarsson, Roland Falk, Mats Lidbeck, and Lars-Erik Josefson. **Inhomogeneity Measurements of Long Thermocouples using a Short Movable Heating Zone**. *International Journal of Thermophysics*, 29(3):915–925, June 2008. ISSN 1572-9567. doi: 10.1007/s10765-008-0418-9.

[183] Yoong Yen Kee, Yutaka Asako, Tan Lit Ken, and Nor Azwadi Che Sidik. **Uncertainty of Temperature measured by Thermocouple**. *ARCHIVES OF AKADEMIA BARU ARTICLES*, 68(1):54–62, August 2021. doi: https://doi.org/10.37934/arfmts.68.1.5462. URL `https://www.akademiabaru.com/index.php/archives/article/view/738`. Number: 1.

[184] **Compact IR pyrometer for OEM applications: optris CS LT**, . URL `https://www.optris.global/optris-cs-lt-csmed-lt`. Accessed on 2020-05-12.

[185] Ernst Hairer and Gerhard Wanner. *Solving Ordinary Differential Equations II*, volume 14. Springer Berlin Heidelberg, 1996. ISBN 978-3-642-05220-0. doi: 10.1007/978-3-642-05221-7.

[186] **PyroNFC**, . URL `https://www.calex.co.uk/product/temperature-measurement/infrared-temperature-sensors/pyronfc/`. Accessed on 2020-05-12.

[187] Emad Ali and Evanghelos Zafiriou. **Optimization-based tuning of nonlinear model predictive control with state estimation**. *Journal of Process Control*, 3(2):97–107, May 1993. ISSN 0959-1524. doi: 10.1016/0959-1524(93)80005-V. URL `https://www.sciencedirect.com/science/article/pii/095915249380005V`.

[188] R. Gesthuisen, K.-U. Klatt, and S. Engell. **Optimization-based state estimation — A comparative study for the batch polycondensation of polyethyleneterephthalate**. In *2001 European Control Conference (ECC)*, pages 1062–1067, September 2001. doi: 10.23919/ECC.2001.7076055.

[189] Douglas A. Allan and James B. Rawlings. **Moving Horizon Estimation**. In Saša V. Raković and William S. Levine, editors, *Handbook of Model Predictive Control*, Control

Engineering, pages 99–124. Springer International Publishing, Cham, 2019. ISBN 978-3-319-77489-3. doi: 10.1007/978-3-319-77489-3_5. URL https://doi.org/10.1007/978-3-319-77489-3_5.

[190] F. Allgöwer, T. A. Badgwell, J. S. Qin, J. B. Rawlings, and S. J. Wright. **Nonlinear Predictive Control and Moving Horizon Estimation — An Introductory Overview**. In Paul M. Frank, editor, *Advances in Control*, pages 391–449, London, 1999. Springer. ISBN 978-1-4471-0853-5. doi: 10.1007/978-1-4471-0853-5_19.

[191] Marcello Farina, Giancarlo Ferrari-Trecate, and Riccardo Scattolini. **Distributed Moving Horizon Estimation for Linear Constrained Systems**. *IEEE Transactions on Automatic Control*, 55(11):2462–2475, November 2010. ISSN 1558-2523. doi: 10.1109/TAC.2010.2046058. Conference Name: IEEE Transactions on Automatic Control.

[192] Mahshad Valipour and Luis A. Ricardez-Sandoval. **Assessing the Impact of EKF as the Arrival Cost in the Moving Horizon Estimation under Nonlinear Model Predictive Control**. *Industrial & Engineering Chemistry Research*, 60(7):2994–3012, February 2021. ISSN 0888-5885. doi: 10.1021/acs.iecr.0c06095. URL https://doi.org/10.1021/acs.iecr.0c06095. Publisher: American Chemical Society.

[193] Chao Shang, Wei Han Chen, Abraham Duncan Stroock, and Fengqi You. **Robust Model Predictive Control of Irrigation Systems With Active Uncertainty Learning and Data Analytics**. *IEEE Transactions on Control Systems Technology*, PP:1–12, 2019. ISSN 1558-0865. doi: 10.1109/TCST.2019.2916753. Publisher: IEEE.

[194] D. H. Tungadio, B. P. Numbi, M. W. Siti, and A. A. Jimoh. **Particle swarm optimization for power system state estimation**. *Neurocomputing*, 148:175–180, January 2015. ISSN 0925-2312. doi: 10.1016/j.neucom.2012.10.049. URL https://www.sciencedirect.com/science/article/pii/S0925231214009424.

[195] Antonio J. Conejo, Sebastin de la Torre, and Miguel Canas. **An Optimization Approach to Multiarea State Estimation**. *IEEE Transactions on Power Systems*, 22(1):213–221, February 2007. ISSN 1558-0679. doi: 10.1109/TPWRS.2006.887964. Conference Name: IEEE Transactions on Power Systems.

[196] S. Naka, T. Genji, T. Yura, and Y. Fukuyama. **Practical distribution state estimation using hybrid particle swarm optimization**. In *2001 IEEE Power Engineering Society Winter Meeting. Conference Proceedings (Cat. No.01CH37194)*, volume 2, pages 815–820 vol.2, January 2001. doi: 10.1109/PESW.2001.916969.

[197] Taher Niknam and Bahman Bahmani Firouzi. **A practical algorithm for distribution state estimation including renewable energy sources**. *Renewable Energy*, 34(11):2309–2316, November 2009. ISSN 0960-1481. doi: 10.1016/j.renene.2009.03.005. URL https://www.sciencedirect.com/science/article/pii/S0960148109001086.

[198] J. Lucio, E. Espinosa-Juárez, and A. Hernández. **Voltage sag state estimation in power systems by applying genetic algorithms**. *IET Generation, Transmission & Distribution*, 5(2):223–230, February 2011. ISSN 1751-8695. doi: 10.1049/iet-gtd.2010.0148. URL `https://digital-library.theiet.org/content/journals/10.1049/iet-gtd.2010.0148`. Publisher: IET Digital Library.

[199] R. Srinivasa Raghav, Kalaipriyan Thirugnanasambandam, Vijayakumar Varadarajan, Subramaniyaswamy Vairavasundaram, and Logesh Ravi. **Artificial Bee Colony Reinforced Extended Kalman Filter Localization Algorithm in Internet of Things with Big Data Blending Technique for Finding the Accurate Position of Reference Nodes**. *Big Data*, November 2021. ISSN 2167-6461. doi: 10.1089/big.2020.0203.

[200] K. Vanchinathan and N. Selvaganesan. **Adaptive fractional order PID controller tuning for brushless DC motor using Artificial Bee Colony algorithm**. *Results in Control and Optimization*, 4(June):100032, September 2021. ISSN 26667207. doi: 10.1016/j.rico.2021.100032. Publisher: Elsevier.

[201] Zhicheng Zhang, Jun Lin, and Yaowu Shi. **Application of Artificial Bee Colony Algorithm to Maximum Likelihood DOA Estimation**. *Journal of Bionic Engineering*, 10(1):100–109, January 2013. ISSN 1672-6529. doi: 10.1016/S1672-6529(13)60204-8.

[202] Diego Oliva, Erik Cuevas, and Gonzalo Pajares. **Parameter identification of solar cells using artificial bee colony optimization**. *Energy*, 72:93–102, August 2014. ISSN 0360-5442. doi: 10.1016/j.energy.2014.05.011.

[203] S. N. Omkar, J. Senthilnath, Rahul Khandelwal, G. Narayana Naik, and S. Gopalakrishnan. **Artificial Bee Colony (ABC) for multi-objective design optimization of composite structures**. *Applied Soft Computing*, 11(1):489–499, January 2011. ISSN 1568-4946. doi: 10.1016/j.asoc.2009.12.008.

[204] Soma Biswas, Amitava Chatterjee, and Swapan Kumar Goswami. **An artificial bee colony-least square algorithm for solving harmonic estimation problems**. *Applied Soft Computing*, 13(5):2343–2355, May 2013. ISSN 1568-4946. doi: 10.1016/j.asoc.2012.12.006.

[205] Sibel Arslan and Celal Ozturk. **Multi Hive Artificial Bee Colony Programming for high dimensional symbolic regression with feature selection**. *Applied Soft Computing*, 78:515–527, May 2019. ISSN 1568-4946. doi: 10.1016/j.asoc.2019.03.014.

[206] David Luenberger. **An introduction to observers**. *IEEE Transactions on automatic control*, 16(6):596–602, 1971. doi: 10.1109/TAC.1971.1099826. Publisher: IEEE.

[207] Magdi S Mahmoud. **Observer-based control design: Basics, progress, and outlook**. In *New Trends in Observer-Based Control*, pages 143–208. Elsevier, 2019. ISBN 978-0-12-817038-0. URL `https://doi.org/10.1016/B978-0-12-817038-0.00005-6`.

[208] George Ellis. *Introduction to observers in control systems*. 2012. ISBN 0-12-237472-X.

[209] Kumpati S. Narendra and Robert Shorten. **Hurwitz Stability of Metzler Matrices**. *IEEE Transactions on Automatic Control*, 55(6):1484–1487, June 2010. ISSN 1558-2523. doi: 10.1109/TAC.2010.2045694. Conference Name: IEEE Transactions on Automatic Control.

[210] Michael Athans, Richard Wishner, and Anthony Bertolini. **Suboptimal state estimation for continuous-time nonlinear systems from discrete noisy measurements**. *IEEE Transactions on Automatic Control*, 13(5):504–514, 1968. doi: 10.1109/TAC.1968.1098986. Publisher: IEEE.

[211] Michael Roth and Fredrik Gustafsson. **An efficient implementation of the second order extended Kalman filter**. In *14th International Conference on Information Fusion*, pages 1–6, July 2011. ISBN 978-0-9824438-2-8.

[212] Rodolfo Orjuela, Benoit Marx, Jose Ragot, and Didier Maquin. **State estimation for non-linear systems using a decoupled multiple model**. *International Journal of Modelling, Identification and Control*, October 2008. doi: https://doi.org/10.1504/IJMIC.2008.021. URL `https://www.inderscienceonline.com/doi/10.1504/IJMIC.2008.021`. Publisher: Inderscience Publishers.

[213] Arnaud Doucet, Nando de Freitas, and Neil Gordon. **An Introduction to Sequential Monte Carlo Methods**. In Arnaud Doucet, Nando de Freitas, and Neil Gordon, editors, *Sequential Monte Carlo Methods in Practice*, Statistics for Engineering and Information Science, pages 3–14. Springer, New York, NY, 2001. ISBN 978-1-4757-3437-9. doi: 10.1007/978-1-4757-3437-9_1. URL `https://doi.org/10.1007/978-1-4757-3437-9_1`.

[214] Jun S. Liu and Rong Chen. **Sequential Monte Carlo Methods for Dynamic Systems**. *Journal of the American Statistical Association*, 93(443):1032–1044, September 1998. ISSN 0162-1459. doi: 10.1080/01621459.1998.10473765. URL `https://doi.org/10.1080/01621459.1998.10473765`. Publisher: Taylor & Francis _eprint: https://doi.org/10.1080/01621459.1998.10473765.

[215] S. Naka, T. Genji, T. Yura, and Y. Fukuyama. **A hybrid particle swarm optimization for distribution state estimation**. *IEEE Transactions on Power Systems*, 18 (1):60–68, February 2003. ISSN 1558-0679. doi: 10.1109/TPWRS.2002.807051. Conference Name: IEEE Transactions on Power Systems.

[216] N. Kantas, A. Doucet, S. S. Singh, and J. M. Maciejowski. **An Overview of Sequential Monte Carlo Methods for Parameter Estimation in General State-Space Models**. *IFAC Proceedings Volumes*, 42(10):774–785, January 2009. ISSN 1474-6670. doi: 10.3182/20090706-3-FR-2004.00129. URL `https://www.sciencedirect.com/science/article/pii/S1474667016387432`.

[217] M. Simandl, J. Kralovec, and T. Soderstrom. **Anticipative grid design in point-mass approach to nonlinear state estimation**. *IEEE Transactions on Automatic Control*, 47(4):699–702, April 2002. ISSN 1558-2523. doi: 10.1109/9.995053. Conference Name: IEEE Transactions on Automatic Control.

[218] Miroslav Šimandl, Jakub Královec, and Torsten Söderström. **Advanced point-mass method for nonlinear state estimation**. *Automatica*, 42(7):1133–1145, July 2006. ISSN 0005-1098. doi: 10.1016/j.automatica.2006.03.010. URL `https://www.sciencedirect.com/science/article/pii/S0005109806001403`.

[219] Dervis Karaboga and Bahriye Akay. **A comparative study of Artificial Bee Colony algorithm**. *Applied Mathematics and Computation*, 214(1):108–132, August 2009. ISSN 00963003. doi: 10.1016/j.amc.2009.03.090.

[220] Joydeep Dutta and C. S. Lalitha. **Optimality conditions in convex optimization revisited**. *Optimization Letters*, 7(2):221–229, February 2013. ISSN 1862-4480. doi: 10.1007/s11590-011-0410-3.

[221] Toray Group. **Nylon 6-Based Thermoplastic Composite**, 2019. URL `https://www.toraytac.com/media/694245aa-3765-43b4-a2cd-8cf76e4aeec5/lmhIVg/TAC/Documents/Data_sheets/Thermoplastic/UD%20tapes,%20prepregs%20and%20laminates/Toray-Cetex-TC910_PA6_PDS.pdf(a`. Accessed on 18/10/2020.

[222] Tomohiro Okada, Ryohei Ishige, and Shinji Ando. **Analysis of thermal radiation properties of polyimide and polymeric materials based on ATR-IR spectroscopy**. *Journal of Photopolymer Science and Technology*, 29(2):251–254, 2016. ISSN 13496336. doi: 10.2494/photopolymer.29.251.

[223] Abdul Basit, Muhammad Tufail, and Muhammad Rehan. **Event-Triggered Distributed State Estimation Under Unknown Parameters and Sensor Saturations Over Wireless Sensor Networks**. *IEEE Transactions on Circuits and Systems II: Express Briefs*, 69(3):1772–1776, March 2022. ISSN 1558-3791. doi: 10.1109/TCSII.2021.3109884.

[224] Adeela Nasreen, Khubab Shaker, and Yasir Nawab. **Effect of surface treatments on metal–composite adhesive bonding for high-performance structures: an overview**. *Composite Interfaces*, 28(12):1221–1256, December 2021. ISSN 15685543. doi: 10.1080/09276440.2020.1870192.

[225] Jiyang Liu, Qingdong Zhang, Boyang Zhang, and Mingyang Yu. **The Bonding Mechanism of the Micro-Interface of Polymer Coated Steel**. *Polymers*, 12(12):3052, December 2020. ISSN 2073-4360. doi: 10.3390/polym12123052.

[226] Alejandro Goldar, Raffaele Romagnoli, Luis D. Couto, Alberto Romero, Michel Kinnaert, and Emanuele Garone. **MPC strategies based on the equivalent hydraulic model for the fast charge of commercial Li-ion batteries**. *Computers & Chemical Engineering*, 141:107010, October 2020. ISSN 00981354. doi: 10.1016/j.compchemeng.2020.107010.